Meteorology and air-quality in a mega-city: application to Tehran, Iran

Hossein Malakooti

PhD thesis of École des Ponts ParisTech

Presented and publicly defended on January 21, 2010 by

Hossein MALAKOOTI

for obtaining the PhD degree of École des Ponts ParisTech / Universite Paris Est

Specialty: Science and technology environment

Meteorology and air-quality in a mega-city: application to Tehran, Iran

The defense committee was consisted of

Matthias BEEKMANN	LISA laboratory, CNRS & University Paris XII and VII	President
Alain CLAPPIER	LIVE laboratory, University of Strasbourg	Reviewer
Abbas-Ali ALI-AKBARI BIDOKHTI	Institute of Geophysics, University of Tehran	Reviewer
Bruno SPORTISSE	INRIA	Thesis Supervisor
Sylvain DUPONT	EPHYSE research unit, INRA	Referee
Maya MILLIEZ	EDF Research & Development	Referee

Abstract

The influence of a mega-city on the atmospheric boundary layer and surface conditions was examined in the complex-terrain, semi-arid Tehran region using the Pennsylvania State University/National Center for Atmospheric Research fifth-generation Mesoscale Model (MM5) during a high pollution period. In addition, model sensitivity studies were conducted to evaluate the performance of the urban canopy and urban soil model "SM2-U (3D)" parameterization on the meteorological fields and ground level air pollutant concentrations in this area. The topographic flows and urban effects were found to play important roles in modulating the wind and temperature fields, and the urbanized areas exerted important local effects on the boundary layer meteorology.

An emission inventory of air pollutants and an inventory of heat generation were developed and updated for 2005 in this work. Emissions from on-road motor vehicles constitute a major portion of the emission inventory and play the most important role in terms of contributions of air pollutants to the atmosphere in Tehran. By using a detailed methodology, we calculated spatial and temporal distributions of the anthropogenic heat flux (Q_f) for Tehran during 2005. Wintertime Q_f is larger than summertime Q_f, which reflects the importance of heating emissions from buildings and traffic during cold and warm period respectively.

Different urban parameterizations were used as a tool to investigate the modifications induced by the presence of an urban area in the area of interest. It was found that, for local meteorological simulations, the drag-force approach coupled with an urban soil model (DA-SM2-U) is preferable to the roughness approach (RA-SLAB). The comparisons indicated that the most important features of the wind, temperature and turbulent fields in urban areas are well reproduced by the DA-SM2-U configuration with the anthropogenic heat flux being taken into account (i.e., "DA-SM2-U Q_f: On" option). This modeling option showed that the suburban part of the city is dominated by topographic flows whereas the center and south of Tehran are more affected by urban heat island (UHI) forcing especially during the night.

The chemical transport modeling, including a model sensitivity study, was used to investigate the impact of the different urban parameterization on the dispersion and formation of pollutants over the Tehran region. Results show that applying DA approaches leads to significant improvements in the simulated spatial and temporal distribution of air pollutant concentrations in the city area and affects significantly the size of the urban plumes.

Acknowledgements

Contents

CHAPTER ONE

Introduction

The atmospheric boundary layer (ABL), also known as the planetary boundary layer (PBL) is the lowest portion of the troposphere. Stull (1988) defines PBL as "that part of the atmosphere that is directly influenced by the presence of the Earth's surface, and responds to surface forcings with a time scale of about an hour or less".

The majority of the global population currently lives and works in urban areas, and this urbanization is expected to increase. According to the United Nations, population projections (UN, 2006) suggest that the global proportion of urban population will increase from 49 % in 2005 to 60 % in 2030.

The urban surface morphology (presence of buildings), urban materials, vegetation differences and human activities profoundly modify the PBL structure over urban areas. This has important implications for the transport and dispersion of pollutants (most of anthropogenic effluents that are emitted from sources within the PBL), photochemical processes, urban design, energy usage studies, thermal comfort level evaluations, etc.

It is reported that in most of mega-cities, air pollution is worsening because of increased industry, vehicles and population. Managing waste, treating sewage, reducing noise, reducing pollutant emissions to control air quality have become challenges for planners and decision makers at all levels. The processes leading to urban air pollution are diverse, interrelated, complex and non-linear. Extended knowledge on the type, quantity, residence time and sources of the pollutants emitted in the urban atmosphere is necessary,

in order to reduce the human health effects in an effective manner. Special urban network of air quality and meteorology measurements and extensive emissions studies are conducted in order to give an overview of the cities situations. Associating these data to modeling tools makes it possible to provide decision-support and forecast tools to planners and governments to design pollutant emissions abatement strategies. Understanding and forecasting air quality in urban areas has emerged as an active field of research with clear socio-economics demands.

Tehran, the Capital of Iran, is faced with many socio-economic and environmental problems. The environmental problem that affects people more than any other in Tehran is air pollution.

Tehran's air quality has been deteriorated over time due to the cumulative effects of rapid population growth, a large and old vehicle fleet (mobile sources), a large number of industrial and commercial establishments (stationary sources), its geographical location , including an ensnared condition as it is surrounded by ranges of mountains, and also the lack of perennial winds. Urban transport is the leading cause of this problem. More than one decade ago, the Government of the Islamic Republic of Iran identified Tehran's air pollution problem as a high priority environmental and health issue (Global Environment Facility, 1993).

1.1 Scale and the urban surface

Meteorological phenomena can be classified as functions of their temporal and spatial scales. Urban meteorology covers phenomena with four typical ranges of spatial scales. For example, Britter (2003) used the following spatial scales to describe the major urban flow features: regional scale (up to 100 or 200 km), city scale (up to 10 or 20 km), neighborhood scale (up to 1 or 2 km), and street scale (less than 100 to 200 m). The complex urban morphology lead to various physical-chemical processes which have effects at different scales (meso-micro) and hence, a mega-cities can play quite a significant role on regional weather.

Consequently, numerical air quality models, which constitute a robust approach to manage and forecast air pollution, require an integrated approach to simulate both the

local urban scale and the mesoscale city surroundings. Here are two modeling approaches at respectively local and mesoscale:

I)   The *street canyon models* provide spatially detailed results, but they are restricted to small areas (one to a few streets) and generally decoupled from the larger scale circulation (which limits their accuracy to short time intervals and near source distance). They are adapted to study the air quality in the streets but cannot be used to simulate the development of the urban plume.

II) The *mesoscale models* cover a relatively large area (domains of the order of 100-200 km), but their spatial resolution (typically 1 to 10 km horizontally and a few tens of meters in the vertical) does not allow one to reproduce the detailed structure of the urban areas. Consequently, sub-grid surface fluxes and turbulence parameterizations are necessary in order to take into account the significant perturbations induced by the cities.

Since an integrated approach, both at the local and regional level, is necessary, a full coupling of the two approaches (insertion within each mesoscale grid cell of a street canyon model) seems to be an ideal approach. But it is computationally expensive proces. For this reason, the urban parameterization method, which consists of taking into account the effects of buildings and streets in a mesoscale model through turbulence parameterizations, represents a better compromise.

In order to develop urban canopy parameterizations, we need descriptions and classifications of urban landuse geometry. The methods that are typically used to introduce urban modifications inside meso-scale meteorological models (MMMs) are mostly based on averaging out the variations in parameters around individual buildings. The general parameters used to classify the urban surface morphology include building height h_e, the plane area density λ_P, and the frontal area density λ_F (e.g., Grimmond and Oke, 1999b) averaged over the scale of interest. Similar information on vegetation canopies is also used. These morphological parameters are illustrated in Figure 1.1.a for an array of uniform buildings. They are defined as follows: $\overline{\lambda_P} = \overline{A_P / A_T} = \overline{L_x L_y / D_x D_y}$ and $\overline{\lambda_F} = \overline{A_F / A_T} = \overline{z_H L_y / D_x D_y}$. One other method consists of using two parallel buildings, that are uniform in height and size with flat roofs as shown in Figure 1.1.b

(under the flow normal to the canyon axis). In this method, key morphological parameters are defined as follows: $\lambda_f = h_e / r_e$ and $\lambda_p = 1 - \omega_e / r_e$.

a)   b)
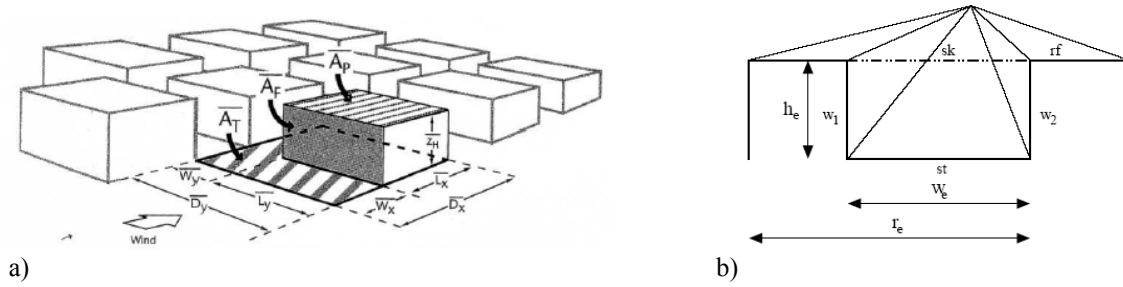
Figure 1.1: Schematic representation of the non-dimensional morphometric ratios for an array of uniform buildings (after Grimmond and Oke, 1999b).

In order to better represent the urban canopy and its effects in MMMs, one method that is often considered consists of having several layers of the model within canopies. In this method λ_P and λ_F are estimated for each kind of canopies and surfaces, and are distributed according to the fraction in each model layer within the urban canopies (adapted from Brown and Williams 1998, Martilli 2002 and Dupont et al. 2004). This method is illustrated for urban buildings in Figure 1.2.
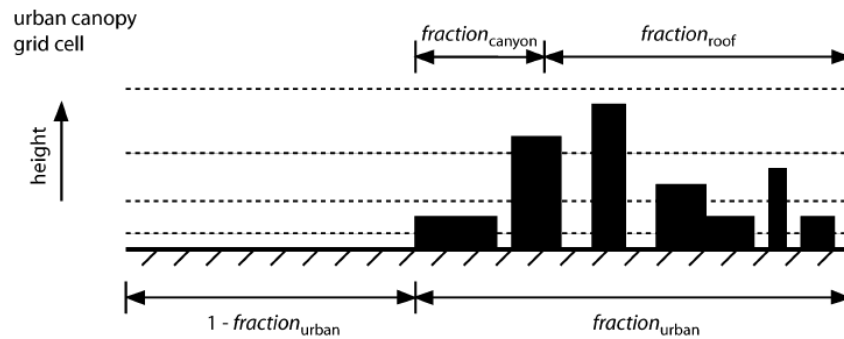
Figure 1.2: Schematic illustration of side view of an urban canopy representation. The area of interest is partitioned into areas defined as urban and nonurban. The canyon regions are defined in the areas between buildings, and the sum of the canyon areas is f_{cnyn}. The remainder of f_{urb} is defined as f_{roof}. There are several model layers (shown as dashed lines) within the urban canopy layer.

1.2 The urban boundary layer

The bottom of the boundary layer is modified by the urban surface features and the depth of this modified layer increases with distance downwind from these structure or vegetation. This modified layer is called the internal boundary layer (IBL). Above it, the air flow continues behaving as it did upwind of the structures (Stull, 1998). The internal boundary layer is influenced by, but not fully adjusted to, the structures of the new surface and it deepens with fetch.

The internal boundary layer formed over urban areas is called the urban boundary layer (UBL). When a new rural boundary layer forms at the surface downwind of the urban area, the urban boundary layer is isolated aloft and is then called the urban plume. The flow in the urban canopy layer (beneath the mean height of the buildings and trees) is highly heterogeneous spatially and subjected to a drag force (Belcher et al., 2003). The Urban Canopy Layer (UCL) is a zone of multiple effects on the PBL structure. We classify these effects into four categories: dynamic, thermodynamic, anthropogenic heating and air pollution effects. Table 1.1 summarizes the general micrometeorological effects of urban canopies. These effects alter temperature and wind fields over the urban environment and contribute to the formation of the Urban Heat Island (UHI). The UHI is typically presented as a temperature difference between the air within the UCL and that measured in a rural area outside the settlement (Mills, 2004).

UBL and urban plume are presented in Figure 1.3. The UBL is, however, a collection of successive IBLs rather than one single internal boundary layer, because of continual evolution of dynamic - thermodynamic processes across the urban area.

The UBL has a vertical structure more complex than that of the boundary layer in rural areas and it is normally partitioned into a canopy layer, a roughness sub-layer (RSL), an inertial sub-layer (ISL) and a mixed layer, depending on the characteristics of the mean and turbulent parts of the flow (e.g. Garratt, 1992).
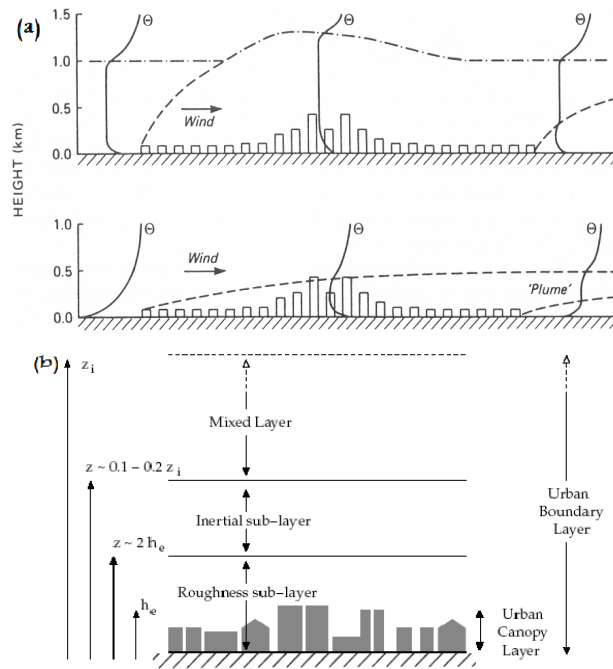
Figure 1.3: a) Schematic structure and potential temperature profiles (θ) by day (top) and at night (down) of the UBL in a large city during fine weather (after Oke, 1982) and b) Schematic of the boundary layer over an urban surface with typical depths for the sub-layers (e.g. Roth, 2000). z_i is the depth of the planetary boundary layer over an urban area.

Table 1.1 The general micrometeorological effects of urban canopies.

UCL features	Effects
Urban canopy geometry	Different spatial distribution of turbulence and wind Increased net-shortwave radiation (increased surface area and multiple reflection) Decreased net-longwave radiations (reduced sky view factor) Decreased and latent heat fluxes (reduced wind speed)
Construction materials	Increased heat storage (increased thermal admittance) Decreased latent heat flux (increased water-proofing) Increased net-shortwave radiation (reduced surface albedo)
Anthropogenic heating	Effect of heat production from fuel and electricity consumption in building and transportation sectors as well as metabolism
Air pollution	Increased sky longwave radiation (Greater absorption and re-emission)

There are several key differences in the nature of the turbulence over rural and urban sites, such as significant dispersive stresses within urban canopies (Cheng and Castro, 2002), Reynolds stress peak at or just above roof level (e.g., Rotach, 1993a), leading to an alteration of turbulent spectrum over urban areas. The peak in the energy spectrum is flattened with no single frequency dominating the power spectrum (Louka, 1998; Roth, 2000). In the RSL, in fact, the flow is influenced more by the local geometry than by a

homogeneous energy transfer between horizontal layers. The flow regimes in urban street canyons can be categorized into the isolated roughness flow, the wake interference flow, and the skimming flow, depending on the canyon aspect ratio (h_e/w_e) and uniformity of the building height. These flow regimes are determined by the degree of interaction between the vortex generated behind the upwind building and the downwind building (Hussain and Lee 1980; Oke 1988; Hunter et al. 1992; Sini et al. 1996). Three flow regimes may form depending on the ratio (h_e/w_e). The inherent features of the three flow regimes are schematically drawn in Figure 1.4.

The RSL extends from the surface up to a height at which the influence of individual roughness elements on the flow is 'mixed up' by turbulence (Raupach et al., 1991), and the flow can be considered horizontally homogeneous if the density, height and distribution of roughness elements do not vary over the upwind area of influence. The depth of RSL is estimated to be 1.8–5 building heights and it has been shown to depend on the stability, separation of the buildings and building shape (Raupach et al., 1980; Oke, 1987; Rafailidis, 1997; Roth, 1999; Roth, 2000; Cheng and Castro, 2002).
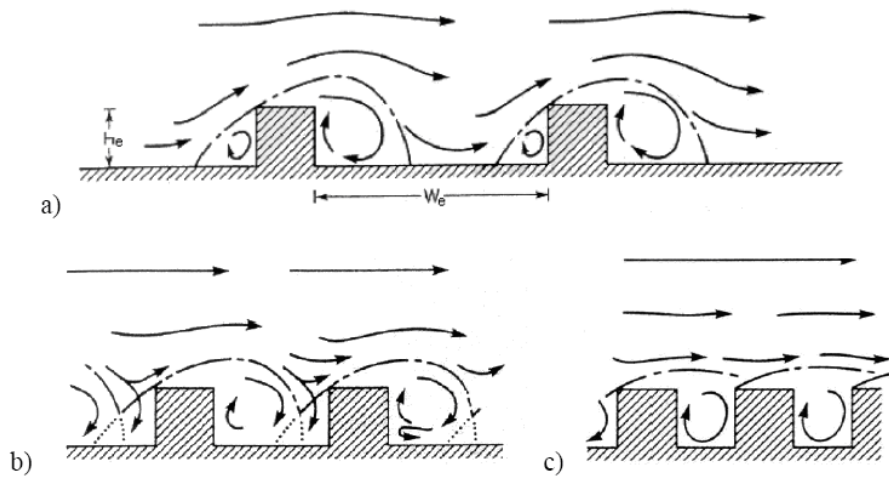
Figure 1.4: Flow regimes in UCs: (a) isolated roughness flow ($h_e/w_e \leq 0.3$), (b) wake interference flow (h_e/we intermediate), and (c) skimming flow ($h_e/we \geq 0.7$) from Oke (1987).

The classical techniques used to represent surface effects in mesoscale models are based on the Monin-Obukhov Similarity Theory (MOST) and aerodynamic characteristics of the urban surface are often represented using various approaches:

I)   The roughness approaches (RA) uses an area-specific roughness length and a displacement height (Roughness approach: RA) (e.g. Venkatram, 1980; Bottema, 1997), which assumes stationary conditions and spatial homogeneity.

II) The empirical models are based on observations of the urban surface energy balance (Grimmond et al., 1998; Grimond and Oke, 1999a). These models use extremely simple schemes, but they need many measurements data and are limited to the range of those data conditions (city, land cover, climate, season, etc).

III) The schemes adapted from plant canopies are the most common way to simulate the urban surface energy balance. This approach is based on the adaptation of the thermal and mechanical properties of a rural area in a soil vegetation transfer scheme (Todhunter and Werner, 1988 ; Dupont et al., 2002).

IV) For radiative effects and the energy balance, surface albedo is generally decreased, the ground is "dried", the soil heat capacity is modified and anthropogenic fluxes are sometimes prescribed as additional energy source (Makar et al., 2006).

These approaches are not able to take into account the geometry of the buildings and do not reproduce the radiative transfers between the different urban surfaces.

Furthermore, the MOST profiles are not valid below the displacement height (the lowest model level at which RA applies) and RA does not reproduce the turbulent kinetic energy (TKE) maximum observed just above the urban canopy. Also field measurements (e.g., Rotach, 1993b) have shown that RA is not able to reproduce the vertical structure of the turbulent fields in urban RSL.

Recently, in order to better represent realistic 3D urban canopy effects (urban canopy parameterization: UCP), the drag force approach has been applied to account for the drag induced by the buildings, as well as comprehensive canopy surfaces (wall, roof, road) energy balance inside MMMs. This UCP can be either single layer (Masson, 2000) or a multi-layer buildings parameterization (Vu et al., 1999; Martilli et al., 2002; Kondo et al., 2005). The *single-layer* parameterization concerns only the first level of MMMs, whereas

the multi-layer parameterization can impact all levels directly influenced by the buildings. In this study we use a multi-layer UCP developed by Martilli et al. (2002) and Dupont et al. (2004).

The flow and potential temperature in the inertial sub-layer are horizontally homogeneous and MOST may be applicable in this sub-layer. The mixed layer is normally covered by an inversion layer at the top of UBL and during the day, flow and potential temperature are rapidly mixed resulting in horizontally homogeneous, vertically uniform profiles in the mixed layer, during the night this sub-layer may be further partitioned into a residual mixed layer of the previous day overlying a stable surface layer which has been cooled from below (Roth, 2000).

1.3 Urban canopy parameterization in MMMs

Brown (2000) has reviewed some methods in order to improve the representation of urban RSL characteristics in mesoscale models. The improvement of the urban canopy representation in mesoscale models requires knowledge of various parameters that can be divided into three categories:

I)   The empirical parameters, which are deduced from calibration of the models,

II) The "material parameters", which correspond to the physical properties of the surface materials of the canopy elements,

III) The morphological parameters, which depend on the structure and on the 3D arrangement of the canopy elements (buildings, vegetation, etc).

The morphological parameters are variable from one city to another and need to be averaged over a few 100 m^2 with a vertical resolution of a few meters to be used at neighborhood scales. Thus, these parameters may be the most difficult parameters to estimate.

The recent UCPs based on the drag-force approach take into account the dynamic, thermodynamic and turbulent effects of urban canopies by adding terms in the conservation equations:

I) in the dynamic equation, a friction force induced by horizontal surfaces of buildings, and a pressure and viscous drag force induced by the presence of buildings and vegetation;

II) in the temperature equation, the sensible and latent heat fluxes from buildings and vegetation and the anthropogenic heat flux parameterized following Taha (1999);

III) in the specific humidity equation, the humidity sources coming from the evapotranspiration of the vegetation and the evaporation of the water intercepted by buildings;

IV) in the turbulent kinetic energy equation, a shear and buoyant production terms induced by buildings and vegetation, turbulent kinetic energy sources induced by the presence of buildings and vegetation.

Furthermore, soil and water budget models are developed for urban area because of multi cover fractions such as bare, paved, vegetated and mixed (i.e., combination of those) surfaces, lakes, irrigation areas, etc. Those models are important to improve the evaporation, since the urban latent heat flux may have a large influence on micro scale phenomena.

In these models, the lower level of the computational domain corresponds to the real level of the ground. The volume of buildings is considered in each cell and additional vertical layers are included within the canopy to allow more detailed meteorological fields within the RSL.

1.4 Urban air quality

High levels of pollution adversely affect most of the populated regions. Air pollution is one of several important environmental hazards alongside with water contamination, hazardous waste, noise and others. It is currently an important environmental concern of large cities.

Swelling urban populations and increased concentration of industry and automobile traffic in and around cities have resulted in severe air pollution. Emissions from traffic, factories, domestic heating, cooking and refuse burning are threatening the health of city dwellers, imposing not just a direct economic cost by impacting human health but also threatening long-term productivity.

Basic urban pollutants (Fenger, 1999) include sulphur dioxide (SO_2), nitrogen oxides (NO_x), carbon monoxide (CO), volatile organic compounds (VOC), ozone (O_3), particulate matter (PM) and lead (Pb).

Exposure to air pollution is associated with numerous effects on human health, including pulmonary, cardiac, vascular and neurological impairments. High-risk groups such as the elderly, infants, pregnant women and sufferers from chronic heart and lung diseases are more sensitive to air pollution than the general population. Exposure to air pollution can cause both acute (short-term) and chronic (long-term) health effects. Acute effects are usually immediate and often reversible when exposure to the pollutant ends. Some acute health effects include eye irritation, headaches and nausea. Chronic effects are usually not immediate and can be irreversible. Some chronic health effects include decreased lung capacity and lung cancer. Table 1.2 summarizes the sources, health and welfare effects for selected pollutants. Hazardous air pollutants may cause other less common but potentially hazardous health effects, including cancer, damage to the immune system, and neurological, reproductive and developmental problems. Acute exposure to some hazardous air pollutants can cause immediate death. Human health effects associated with indoor air pollution are: headaches, tiredness, dizziness, nausea, and throat irritation. More serious effects include cancer and exacerbation of chronic respiratory diseases, such as asthma. Asthma, particularly for children, can result from poor indoor air quality. Air

pollutants can also enter into our body by drinking and eating following deposition on to an ecosystem and subsequent bioaccumulation. There are many harmful welfare effects of air pollution: acid rain, climate change, depletion of stratospheric ozone, damage to agricultural crops, and decreased visibility.

Air pollutants are classified into two categories. Primary pollutants are directly emitted into the atmosphere, such as NO_x and VOCs and secondary pollutants are formed in the atmosphere as a result of chemical transformation of the primary pollutants. Secondary pollutants include tropospheric ozone (O_3) created in a reaction cycle involving NO_x, CO and VOC and which occurs in the presence of solar energy.

Primary pollutants act in situ, i.e., mainly in the cities where traffic and industrial activities are the highest, while secondary pollutants often affect the environment (as in the case of ozone) in rural areas. For example, ozone formation occurs relatively close to the ground in the plume downwind of primary pollutant emission, usually at distances of 10 to 100 km from the sources, when VOC and NO_x are both present in relevant quantities (see Figure 1.5).

This difference leads to a difficult situation for policy makers dealing with air quality management. The problems become even more complex for pollutants such as ozone and PM that are subject to transcontinental pollutant transport, which occur in the stratosphere.

Table 1.2: Sources, health and welfare effects for selected Pollutants (Ref: US EPA website).

Pollutant	Description	Sources	Health Effects	Welfare Effects
CO	Colorless, odorless gas	Motor vehicle exhaust, indoor sources include kerosene or wood burning stoves.	Headaches, reduced mental alertness, heart attack, cardiovascular diseases, impaired fetal development, death.	Contribute to the formation of smog.
SO_2	Colorless gas that dissolves in water vapor to form acid, and interact with other gases and particles in the air.	Coal-fired power plants, petroleum refineries, manufacture of sulfuric acid and smelting of ores containing sulfur.	Eye irritation, wheezing, chest tightness, shortness of breath, lung damage.	Contribute to the formation of acid rain, visibility impairment, plant and water damage, aesthetic damage.
NO_2	Reddish brown, highly reactive gas.	Motor vehicles, electric utilities, and other industrial, commercial, and residential sources that burn fuels.	Susceptibility to respiratory infections, irritation of the lung and respiratory symptoms (e.g., cough, chest pain, difficulty breathing).	Contribute to the formation of smog, acid rain, water quality deterioration, global warming, and visibility impairment.
O_3	Gaseous pollutant when it is formed in the troposphere.	Vehicle exhaust and certain other fumes. Formed from other air pollutants in the presence of sunlight.	Eye and throat irritation, coughing, respiratory tract problems, asthma, lung damage.	Plant and ecosystem damage, climate change.
VOC	Gaseous pollutants	Vehicle exhaust, home products, industrial plants, vegetations.	Eye irritation (e.g., acrolein), cancer (e.g., benzene, formaldehyde)	
PM	Very small particles of soot, dust, or other matter, including tiny droplets of liquids.	Diesel engines, power plants, industries, windblown dust, wood stoves.	Eye irritation, asthma, bronchitis, lung damage, cancer, heavy metal poisoning, cardiovascular effects.	Visibility impairment, atmospheric deposition, aesthetic damage.
Pb	Metallic element	Metal refineries, lead smelters, battery manufacturers, iron and steel producers.	Anemia, high blood pressure, brain and kidney damage, neurological disorders, cancer, lowered IQ.	Affects animals and plants, affects aquatic ecosystems, climate change.
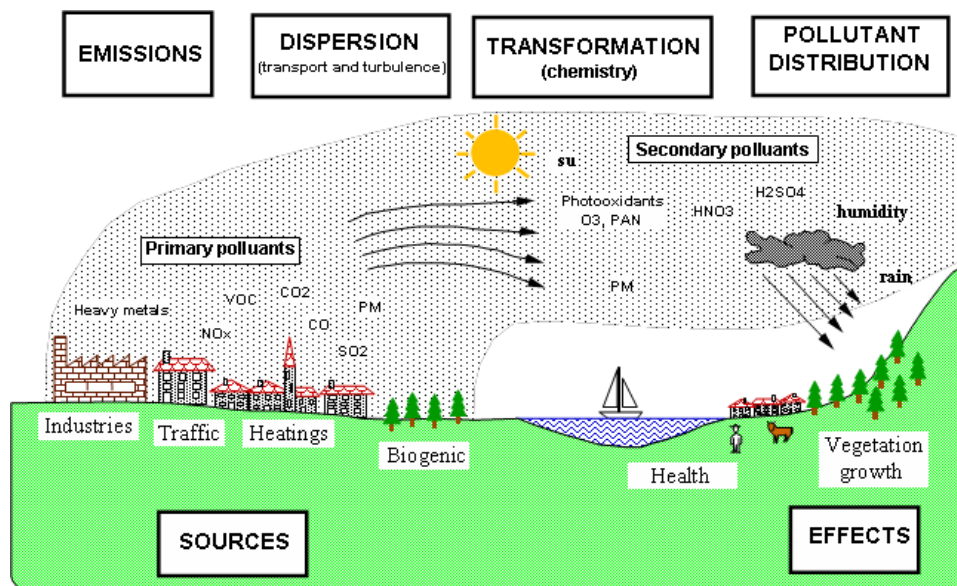
Figure 1.5: physical, chemical and environmental processes of urban plume.

The pollutants concentrations in the ambient outdoor air depend on emissions, background concentrations, chemical, transport–diffusion and deposition processes (Mayer, 1999). All these processes explicitly depend on meteorological parameters such as radiation, stability, wind, temperature, turbulence, rain, humidity, etc.

A combination of state-of-the-science measurements with state-of-the-science models is the best approach for making real progress toward understanding atmospheric processes. A model involving descriptions of emission patterns, meteorology, chemical transformations and removal processes is an essential tool for the appropriable approach. Such a model provides a link between emission changes from source control measurements and resulting changes in airborne concentrations (Seinfeld and Pandis, 1998; B. Sportisse, 2008).

Meteorological inputs constitute one of the main sources of uncertainty in chemistry transport models (CTMs), especially in urban areas, because of high influence of urbanization on local climates. Therefore, a correct treatment of meteorology is essential for accurate air quality modeling.

1.5 Overview of Tehran characteristics

With the location 35° 41' N - 51° 25' E and altitude of 1000-1800 meters above mean sea level, Tehran, capital of Iran, is located on the southern slope of the Alburz mountain chain. Its climate is generally moderate to dry. During the last 3 to 4 decades, urban expansion in Tehran resulted from a high rate of population growth and rural-urban migration combined with a strong tradition of centralization and dense urban infrastructure. As a result, there has been an over increasing trend in energy consumption in the capital. Tehran is located in valleys and is surrounded on the north, northwest, east and southeast by high to medium high (3800-1000 m) mountain ranges (see Figure 1.6). The northern part with more rainfall and vegetation is about 600-700 meter higher than the southernmost part which borders central deserts of Iran (Madanipour, 1999; Ketabi, 2004). The meteorological fields in Tehran are influenced by these geographical features.

Because of these morphological conditions, generally weak winds and urban effects such as anthropogenic heating, Tehran experiences a significant UHI. Therefore, we believe that taking into account anthropogenic heating and other urban effects within a MM model sould improve the accuracy of meteorological simulations and better represent the local climate and circulations in this area.

The resident population of Tehran is about 8.3 millions according to the 2007 census (in contrast to two hundred thousands in 1920) and its daytime population is often more than 12 millions inhabitants on workdays, reflecting the highly dynamic spatial and temporal distribution of population in the greater Tehran urban area (670 km^2). With a very large population, more than two million (often old) motor vehicles, fuel and electricity consumption and many factories (more than half of Iran's industries are based in Tehran), huge quantities of pollutants and heat are emitted in this area.

Tehran is usually enveloped in a cloud of smog and, according to a recent study, each resident inhales between 7 and 9 kilograms of dust per year. The city has been rated as one of the most polluted cities on earth, suffering from increasing acute environmental problems such as air, water, land and noise pollution. Due to these facts air pollution is reported to significantly affect the quality of urban inhabitant's life as well as to worsen urban environment and urban climate.
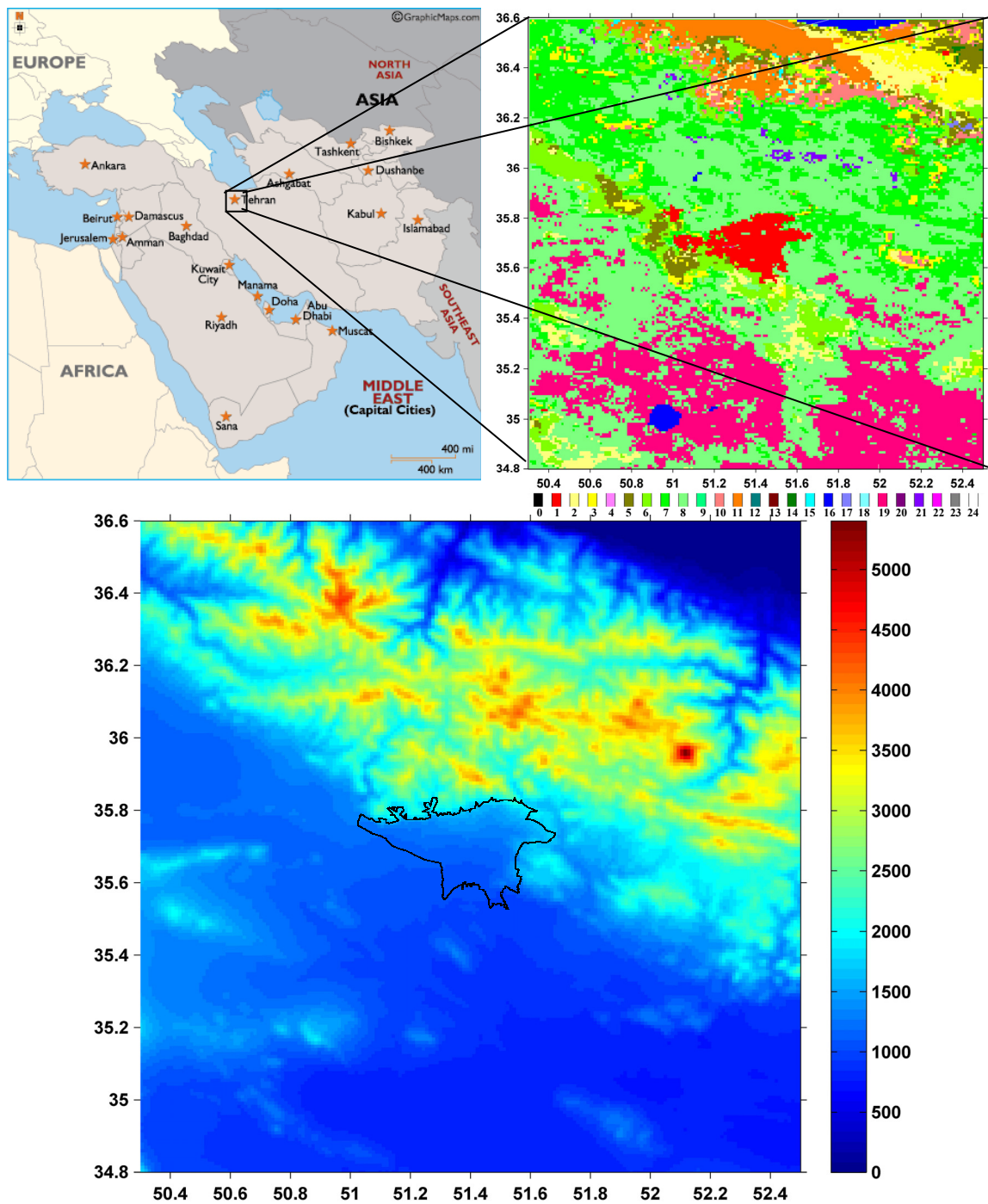
Figure 1.6: a) Geographical localization of Middle- East and Tehran, and b) landuse distribution (1: Urban, 2: Drylnd Crop. Past., 3: Irrg. Crop. Past. 4:Mix. Dry/Irrg.C.P., 5: Crop./Grs. Mosaic, 6: Crop./Wood Mosc, 7: Grassland, 8: Shrubland, 9: Mix Shrb./Grs., 10: Savanna, 11: Decids. Broadlf., 12: Decids. Needlf., 13: Evergrn. Braodlf., 14: Evergrn. Needlf., 15: Mixed Forest, 16: Water Bodies, 17: Herb. Wetland, 18: Wooded wetland, 19: Bar. Sparse Veg., 20: Herb. Tundra, 21: Wooden Tundra, 22: Mixed Tundra, 23: Bare Grnd. Tundra, 24: Snow or Ice and 0: No data) and c) topography of Tehran region.

The Pollutant Standards Index (PSI) system which was developed by the U.S.-EPA (e.g. National Air Quality and Emissions Trends Report, 1997) has been adopted by Tehran AQCC (Air Quality Control Company) for reporting daily air quality. The PSI provides a simple number on a scale of 0-500 related to the health effects of the air quality levels. Values of PSI during recent 18 years (after establishing a measurement network) show that air quality most often fell in the "moderate" category (50<PSI< 100) and had exceeded the threshold level (PSI = 100) in 75 to 169 days (20 - 46%) during one year. It is seen that carbon monoxide contributed 89% (8 hours average concentration more than 4.5 ppm) and PM 10 19% (24 hours average concentration more than 75 μgm^{-3}) of critical pollutants responsible for most of the unhealthy air quality days in Tehran. As shown in Figure 1.7, three months of August, September and October are the most polluted months in Tehran.
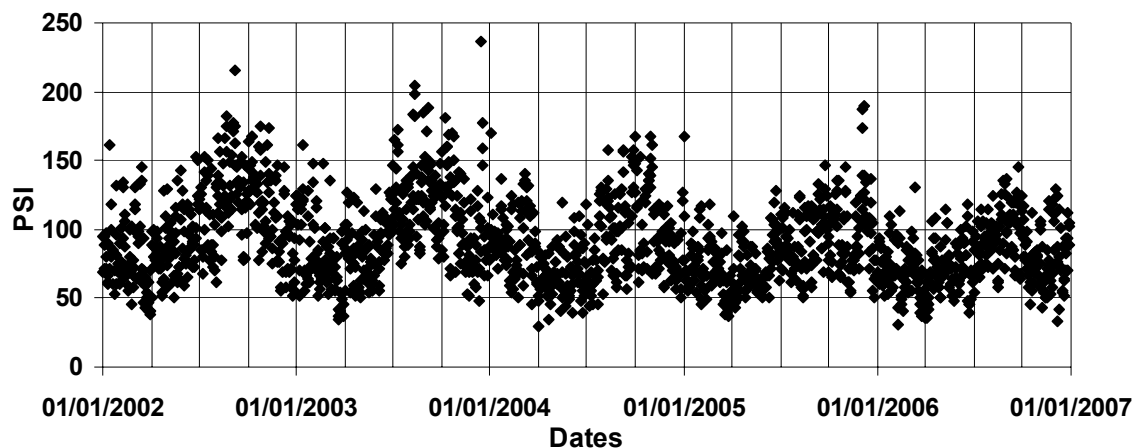
Figure 1.7: PSI distribution during 2002-2006.

1.6 Thesis outline

This study has three main parts: emission improvement, local meteorology and chemistry transport modeling and their evaluations.

In the first part a high resolution mobile emission inventory is developed in order to prepare a Dynamic Emission Database (DEB) for this episode of the study. Traffic data are obtained from the EMME/2 transportation planning database and available observations by vehicle subcategories. The emission factors are adjusted with categories

and subcategories of Tehran vehicles, and along with this, the railway and aircraft emissions are also estimated. The evaluation of spatial distribution and diurnal variation of anthropogenic heat emission in Tehran region is also developed. The methods and estimated emissions are presented in Chapter 2.

In the second part, we study the boundary layer structure and its evolution, UHI influence and interaction between topographic and UHI flows in Tehran region. The urban canopy model introduced in MM5 by Dupont et al. (2004) is adapted, modified and tested for the Tehran basin. Thus, the roughness approach and Drag force approach are evaluated in this area. The methods and results are presented in Chapter 3.

The objective of the third part is a general study of modeling gases (CO, Ozone, NO_2, etc.) and particular matters (PM_{10} and $PM_{2.5}$). Simulations are evaluated and the sensitivity to meteorological inputs with different urban options is analyzed. This part is presented in chapter 4.

The results of this work and suggestions for future works in this area are summarized and discussed in Chapter 5.

References

Belcher, S.E., Jerram, N., and Hunt, J.C.R., 2003. Adjustment of a turbulent boundary layer to a canopy of roughness elements. Journal of Fluid Mechanics 488, 369-398.

Bottema, M., 1997. Urban roughness modeling in relation to pollutant dispersion. Atmospheric Environment 31, 3059-3075.

Britter, R. and Hanna, S. R., 2003. Flow and dispersion in urban areas. Annual Review of Fluid Mechanics 35, 469-496.

Brown, M.J. and Williams, M.D., 1998. An urban canopy parameterization for mesoscale models. Preprints, Second Urban Environment symposium, Albuquerque, New Mexico, American Meteor Society, 144-147.

Brown, M., 2000. Urban parameterizations for mesoscale meteorological models, in Boybeyi (ed.), Mesoscale Atmospheric Dispersion. Wessex Press, 448 pp.

Cheng, H. and Castro, I.P., 2002. Near wall flow over an urban-like roughness. Boundary Layer Meteorology 104, 229-259.

Dupont, S., Calmet, I., and Mestayer, P.G., 2002. Urban Canopy Modeling Influence on Urban Boundary Layer Simulation, in American Meteor Society 4th Symposium on Urban Environment, Norfolk, Virginia, 20-24 May , Proceedings, pp. 151-152.

Dupont, S., Otte, T.L. and Ching, J.K.S., 2004. Simulation of meteorological fields within and above urban and rural canopies with a mesoscale model (MM5). Boundary Layer Meteorology 113, 111-158.

Environmental Protection Agency, 1998. National Air Quality and Emissions Trends Report, 1997. Washington, DC: Author.

Fenger, J., 1999. Urban air quality. Atmospheric Environment 33, 4877-4900.

Garratt, J.R., 1992. The Atmospheric Boundary Layer. chapter 8, pages 224-257. Cambridge University Press.

Global Environment Facility, 1993. Tehran Transport Emissions Reduction Project. World Bank, Washington, DC.

Grimmond, C.S.B, King, T.S., Roth, M., Oke, T.R., 1998. Aerodynamic roughness of urban areas derived from wind observations. Boundary Layer Meteorology 89, 1-24.

Grimmond, C.S.B., Oke, T.R., 1999a. Heat storage in urban areas: local-scale observations and evaluation of a simple model. Journal of Applied Meteorology 38, 922-940.

Grimmond, C.S.B. and Oke, T.R., 1999b. Aerodynamic properties of urban areas derived from analysis of surface form. Journal of Applied Meteorology 38, 1262–1292.

Harman, I.N., 2005. The energy balance of urban areas, Ph.D. thesis, Department of Meteorology, University of Reading.

Hunter, L.J., Johnson, G.T., and Watson, I.D., 1992. An investigation of three-dimensional characteristics of flow regimes within the urban canyon. Atmospheric Environment 26B, 425-432.

Hussain, M., Lee, B.E., 1980. A wind tunnel study of the mean pressure forces acting on large groups of low-rise buildings. Journal of Wind Engineering and Industrial Aerodynamics 6, 207-225.

Ketabi, M., 2004. Sustainable Development in Tehran, A Case Study of Traffic and Pollution Problems in Tajrish District. Annual Meeting of the world student community for sustainable development (WSC-SD), Goteborg, Sweden.

Kondo, H., Genchi, Y., Kikegawa, Y., Ohashi, Y., Yoshikado, H., Komiyama, H., 2005. Development of a Multi-Layer Urban Canopy Model for the Analysis of Energy Consumption in a Big City: Structure of the Urban Canopy Model and its Basic Performance. Boundary Layer Meteorology 116, 395-421.

Louka, P., Belker, S.E., Harrison, R.G., 1998. Modified street canyon flow. Journal of Wind Engineering & Industrial Aerodynamics 74–76, 485-493.

Mayer, H., 1999. Air pollution in cities. Atmospheric Environment 33, 4029-4037.

Madanipour, A., 1999. City profile: Tehran. Cities 16, 57-65.

Makar, P.A., Gravel, S., Chirkov, V., Strawbridge, K.B., Froude, F., Arnold, J., Brook, J., 2006. Heat flux, urban properties, and regional weather. Atmospheric Environment 40, 2750-2766.

Martilli, A., 2002. Numerical Study of Urban Impact on Boundary Layer Structure: Sensitivity to Wind Speed, Urban Morphology, and Rural Soil Moisture. Journal of Applied Meteorology 41, 1247-1266.

Martilli, A., Clappier, A., Rotach, M.W., 2002. An urban surfaces exchange parameterization for mesoscale models. Boundary Layer Meteorology 104, 261-304.

Masson, V., 2000. A physically-based scheme for the urban energy budget in atmospheric models. Boundary Layer Meteorology 94, 357-397

Mills, G., 2004. The Urban Canopy Layer Heat Island, IAUC Teaching Resources.

Oke, T.R., 1982. The energetic basis of the urban heat island. Quarterly Journal of the Royal Meteorological Society 108, 1-24.

Oke TR., 1987. Boundary Layer Climates. London, UK: Routledge ,435 p.

Oke, T., 1988. Street design and urban canopy layer climate. Energy and Buildings 11. pp. 103-113.

Rafailidis, S., 1997. Influence of building area density and roof shape on the wind characteristics above a town. Boundary Layer Meteorology 85, 255–271.

Raupach, M.R., Thom, A.S., and Edwards, I., 1980. A wind-tunnel study of turbulent flow close to regularly arrayed rough surfaces. Boundary-Layer Meteorology 18, 373–397.

Raupach, M.R., Antonia, R.A., Rajagopalan, S., 1991. Roughwall turbulent boundary layers. Applied Mechanics Reviews, 44, 1-25.

Rotach, M.W., 1993a. Turbulence close to a rough urban surface Part I: Reynolds stress. Boundary Layer Meteorology 65, 1-28.

Rotach, M.W., 1993b. Turbulence close to a rough urban surface Part II: variances and gradients. Boundary Layer Meteorology 66, 75-92.

Roth, M., 1999. On the influence of the urban roughness sub-layer on turbulence and dispersion. Atmospheric Environment 33, 4001-4008.

Roth, M., 2000. Review of atmospheric turbulence over cities. Quarterly Journal of the Royal Meteorological Society 126, 941–990.

Seinfeld, J.H., Pandis, S.N., 1998. Atmospheric Chemistry and Physics: From Air Pollution to Climate Change. Wiley, New York.

Sini, J.F., Anquetin, S., and Mestayer, P.G., 1996. Pollutant dispersion and thermal effects in urban street canyons. Atmospheric Environment 30, 2659–2677.

Sportisse, B., 2008. Pollution atmosphérique, Des processus à la modélisation. Springer, 345 p.

Stull, R.B., 1988. An Introduction to Boundary Layer Meteorology. Kluwer Academic Publishers. 666 p.

Taha, H., 1999. Modifying a mesoscale model to better incorporate urban heat storage: A bulk parameterization approach. Journal of Applied Meteorology 38, 466–473.

Todhunter, P., Werner, T., 1988. Intercomparison of three urban climate models. Boundary Layer Meteorology 42, 181-205.

United Nations: 2006, World Urbanization Prospects. The 2005 Revision, Department of Economic and Social Affairs, Population Division, New York.

Venkatram, A., 1980. Estimating the Monin-Obukhov length in the stable boundary layer for dispersion calculations. Boundary Layer Meteorology 19, 481.

Vu, T.C., Asaeda, T., Ashie, Y., 1999. Developpement of a numerical model for the evaluation of the urban thermal environment. Journal of Wind Engineering 81, 181-196.

CHAPTER TWO

Development and Evaluation of a High Resolution Emission Inventory for Air Pollutants and Heat Generation

2.1 Introduction

Urban agglomerations are major sources of regional and global atmospheric pollution as well as heat. This phenomenon is especially severe in cities of developing countries, where population, traffic, industrialization and energy use increase as people continue to migrate to the cities (Mage et al., 1996). Consequently, it is essential to develop energy and air quality management policies and to establish strategies for atmospheric pollution prevention and energy management for such cities. Main limitations are, however, the difficulties associated with promulgating effective environmental public policies and then implementing air pollution mitigation measures in a timely manner (Mayer, 1999). Those difficulties are compounded by a strong lack of pertinent technical information and knowledge.

In this chapter, we present methodologies used to develop an emission inventory of air pollutants and inventory of heat generation in Tehran.

2.2 Emission inventory of air pollutants in Tehran

Air pollutants are emitted into the atmosphere from stationary, area and mobile sources. Stationary sources include utility, industrial, institutional and commercial facilities. Examples are electric power plants, oil – gas refineries, phosphate processing plants, pulp and paper mills, and municipal waste combustors. Area sources include many individually small activities such as gasoline service stations, small paint shops, consumer solvent use, open burning associated with agriculture, etc. Mobile sources,

especially from on-road vehicular traffic, constitute a major source of air pollution in towns and cities.

In the current study, pollutant emissions are estimated for the year 2005 for CO, PM_{10}, $PM_{2.5}$, NO_x, SO_x, and NMVOC which are emitted from point, area and mobile sources in the Greater Tehran Area (GTA).

According to a recent estimate, there are more than 2 million vehicles and some 300 thousand industrial factories and offices in Tehran. Although there are few inventories of pollution sources available in Tehran, those available suggest that concentration of CO, NO, NO_2, SO_2, O_3 and suspended particulate matter (SPM) in the GTA are well beyond the World Health Organization (WHO) standard. Particularly, the CO concentration often exceeded the 80 ppm limit.

While a variety of sources contribute to air pollutants, it is estimated that mobile source emissions account for almost 85% of the air pollution in the GTA and are particularly important, since these emissions occur in the vicinity of the city population. Accordingly, new standards for mobile sources have been enacted to address this problem.

2.2.1 Mobile Source Emissions Inventory survey

Mobile sources mainly consist of on-road motor vehicles and other mobile sources include boats and ships, trains, aircraft and off-road equipments (garden, farm and construction).

Key literature analysis of studies (Cooper, 1989; Beaton et al., 1992; Bose, 1996; Cernuschi et al., 1995; Derwent et al., 1995; Joumard et al., 1995; Lawson et al., 1990; Mitsoulis et al., 1994; Onursal and Gautam, 1997; Riveros et al., 1995; Stein and Toselli, 1996; Sturm et al., 1997) relating to traffic pollution in urban centers indicate that studies concerning detailed impact of vehicle emissions on the ambient air quality are few outside north America and Europe. This is due to the complexity of organizing and integrating information on:

-emission of pollutants to the atmosphere from a dynamic EDB (Emission DataBase),

- meteorological conditions,

-processes affecting pollutant concentrations spatially at differnt location and time.

2.2.1.1 On-Road Motor Vehicles

On-road motor vehicles consist of passenger cars, trucks, buses, motorcycles, etc. Emissions from on-road motor vehicles are a major portion of the emission inventory and are estimated by using available vehicles and traffic data bases and related emission factors. Vehicle emissions are directly related to the variations in the traffic flow pattern, which vary in location and time. The characterization of the temporal variability of emissions is difficult because it requires an accurate dynamic EDB.

2.2.1.1.1 Emission standards

An emission performance standard is an upper limit that should not be exceeded by emissions from a regulated source. To that end, different types of emission control technologies have been implemented on vehicles. Evaluations of vehicular emissions are conducted using a special driving cycle to simulate road driving on a dynamometer chassis, and by measuring their air pollutants emissions. Dynamometer is tuned in a way that braking power is compatible with striking the barriers as it is on actual roads and using the real vehicle weight.

Table 2.1 indicates different standards for various types of vehicles before 2005 and for implementation during 2005 to 2014 (Euro IV will enter into force in the EU in 2009).

Table 2.1: Emission standard of vehicles in IRAN**.**

Time	2000-2002	2003-2004	2005-2006	2007-2009	2010-2011	2012-2014
LDV / HDV	ECE R-1503	(ECE R-1504) (ECE R-83)	Euro I		Euro II	Euro IV
Motorcycle			40.01	Euro I	Euro II	Euro III

2.2.1.1.2 Vehicles and traffic data base

In recent years, travel and traffic simulation models have been developed and calibrated in most mega-cities. For Tehran a comprehensive study for a transportation plan have been carried out by Tehran Traffic & Transportation Comprehensive Studies Co. (TCTTS).

Transportation planning computer software was used to develop the model, EMME/2 (Equilibre multimodal / multimodal equilibrium Version 2). The study area was divided into 583 transportation analysis zones and the network system was coded into EMME/2 as links (street segments) and nods (intersections). The existing network includes 4295 nods and 12768 links. Figure 2.1 depicts the Tehran municipality districts, the road network treated in this study and the traffic zones.
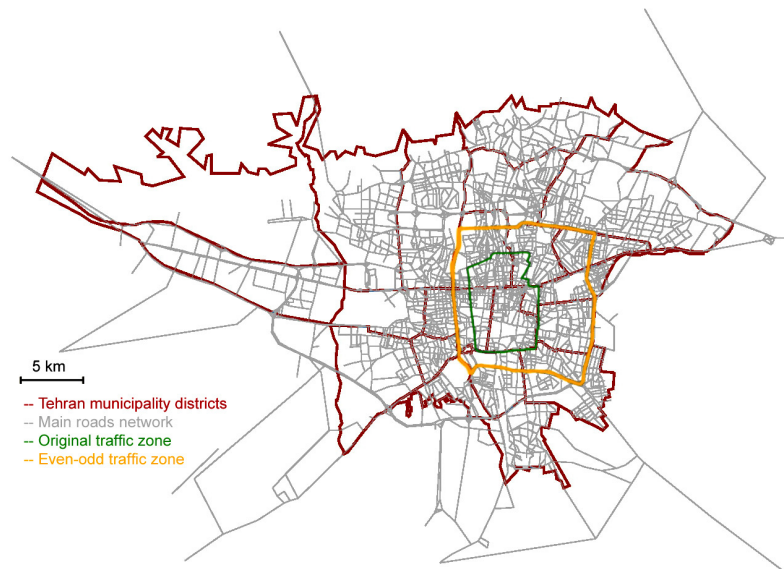
Figure 2.1: The Tehran municipality districts, main road network and traffic zones.

2.2.1.1.2.1 Categories and subcategories of vehicles

Regarding the vehicle categorizations presented in TERP project (1997), the data released by Tehran Traffic and Transportation Comprehensive Studies and vehicles registration data, the categorization presented in Table 2.2 was used to calculate emission factors.

2.2.1.1.2.2 Traffic data

In order to use the data received from TCTTS Co. and we adjusted the EMME2 outputs with actual fuel consumption. These actual consumption values were obtained from Ministry of Oil regarding the fuel consumptions. The reason for the difference between the consumptions rates of EMME2 and actual fuel consumption is due to the fact that the EMME2 network considers only the main roads of Tehran and ignores the secondary streets.

In order to calculate the emissions of all the vehicles, the vehicle kilometers traveled **(VKT)** for each subcategory must be calculated. Figure 2.2 indicates the VKT for each category.
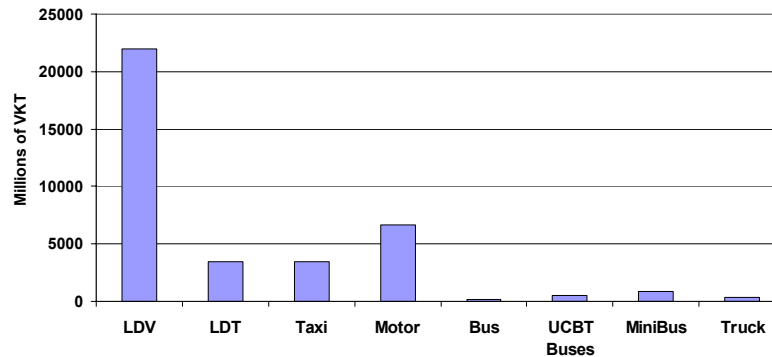
Figure 2.2: VKT values across vehicle categories.

Table 2.2: Categories & subcategories of Tehran vehicles.

Category of Vehicles	Subcategory of Vehicle	Distribution
Light Duty Vehicle (LDV)	1- All of produced Paykan before of 1996	16.29
	2- Imported Vehicle of older year	5.09
	3- Other Iranian Produced Vehicle were produced before of 1995	8.15
	4- LPG Converted Vehicle	1.22
	5- Vehicle with Emission Standard of ECE 1503	31.57
	6- Vehicle with Emission Standard of ECE 1504	16.29
	7- Vehicle with Emission Standard of ECE R-8301	10.18
	8- Vehicle with Emission Standard of ECE R-8303	11.21
Light Duty Truck (LDT)	1- All of LDT Produced before of 1995	52.43
	2- light duty truck with emission standard of ECE 1503	20.39
	3- light duty truck with emission standard of ECE 1504	7.77
	4- light duty truck with emission standard of ECE R8301	13.59
	5- light duty truck with emission standard of ECE R8303	5.83
Taxi	1- Vehicle with the emission standard of ECE1504	6.00
	2- LPG converted vehicle Taxi	85.00
	3- CNG converted vehicle	9.00
Minibus	1- Mercedes Benz Minibuses & Minibuses with similar Technology	31.00
	2- Fiat Minibuses & Minibuses with similar Technology Minibus	47.00
	3- IVECO Minibuses & Minibuses with similar Technology	22.00
Non UCBT Bus	1- Buses with Natural Aspirated Technology Non UBCT Bus	34.00
	2- Buses with Turbo charged Technology	66.00
UBCT Bus	1- Buses with Natural Aspirated Technology	80.00
	2- Buses with Turbo charged Technology	11.00
	3- LPG Converted Buses UBCT Bus	0
	4- CNG Converted Buses	9.00
Motor Cycle	1- 4 Strock Motor cycle	50.00
	2- 2 Strock Motor cycle	33.00
	3- Mopeds	17.00
Truck	1- Trucks with Natural Aspirated Technology	74.00
	2- Trucks with Turbo charged Technology	26.00

2.2.1.1.3 Emission factors

In this study, in addition to the emission factors calculated in TERP report and the emission factors of COPERT III, the methodologies of Ntziachristos and Samaras, (2000) and Samaras et al. (1998) were used.

Based on this relative fraction of vehicles, aggregation emission factors and the fuel consumption rates were calculated.

2.2.1.1.4 On-Road emissions

The contribution of LDV vehicles was estimated to be close to 47% of total on-road emissions. LDT and motorcycles come next in terms of on-road emissions (see Figure 2.3). Figure 2.4 compares the estimations of on-road emissions in Tehran as presented in GEF project (1996), JICA (2002) and the current study for 2005.
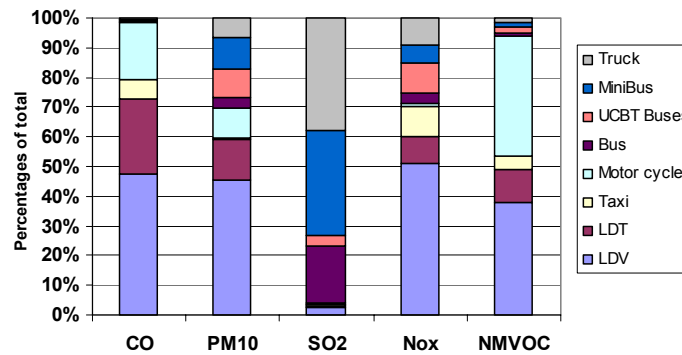
Figure 2.3: Comparison of each pollutant emission contribution to total emissions across all categories.
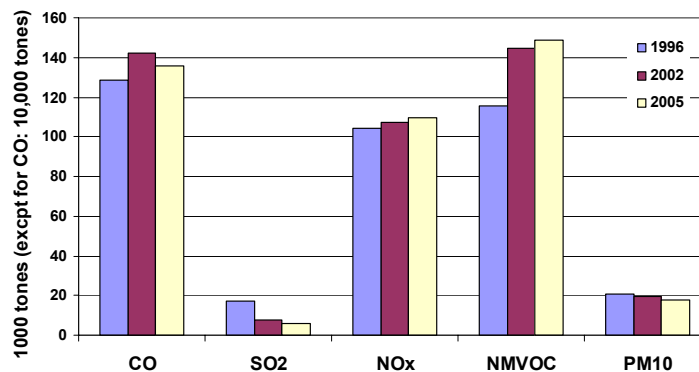
Figure 2.4: Comparison of results for on-road emissions of main pollutants with GEF project (1996) and JICA (2002).

2.2.1.2 Railway emissions inventory

Using the fuel consumption data and accounting for both "HAUL" model (running model) and "YARD" model (maneuvering model), the average fuel economy was calculated for each rail road length. Finally, emission rates by trains in the GTA were calculated using the fuel consumption rates and the emission factors.

There are 3 main rail road lines in the GTA:

1. Tehran -Rey
2. Tehran - Aprin
3. Tehran -Lashkari

According to the data released from the JICA group regarding earthquake pathology (2000), the lengths of "HAUL" and "YARD" rail road lines are respectively 133 and 87 km. (These lengths include all the rail road lines).

The emission factors used here were obtained from the US Environmental Protection Agency (EPA) report (1992).

Since emission factors for some of the running locomotives were not available in the EPA report, emission factors from similar locomotives (band, model and power) were used here. Then, the emission factors of trains (both in running and maneuvering model) were calculated based on their locomotives model composition.

The emission rate of SO_2 depends on the sulfur content in the fuel. Since the locomotives motors are equipped with the turbo charge system, the emission factors for SO_2 for heavy duty vehicles were used for locomotives. The HAUL and YARD models from of the different types of trains are provided in Appendix A.

According to the Statistics and Technology Department of Rail Road of IRI, the fuel consumption rate by trains both in running and maneuvering status was exceeding 11930 and 1620 k liters respectively in 2005. Emissions from the trains are presented in Figure 2.5 for 2005.
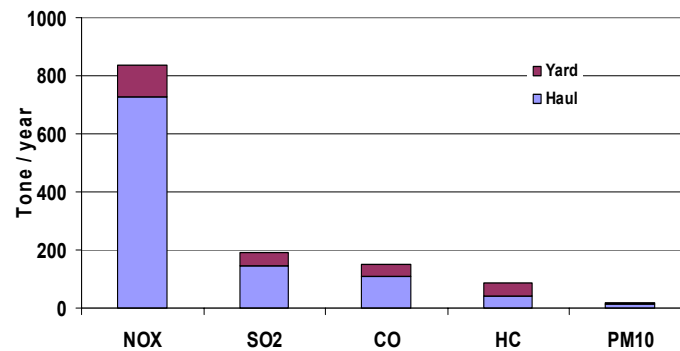
Figure 2.5: Pollutant emissions for rail road mobile sources.

2.2.1.3 Aircraft emission inventory

The contribution of airplanes which depart from or arrive at the Mehrabad international airport was estimated for 2005. Emissions are assigned to the landing strip and the flight route extended to both sides of the strip up to 1000 m height (landing – take off, (LTO) cycles). Airplanes are assumed to approach from the southwest and to take off and ascend toward the northwest (See Figure 2.6).
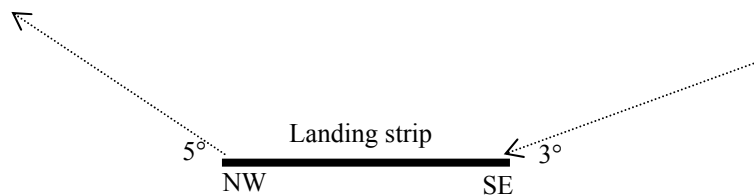
Figure 2.6: Considered cross section during taking off and ascending.

Total LTO emissions are obtained from those three lines and area sources extended around the landing strip.

The frequency of flights for each aircraft type is set based on the number of weekly flights for each company. Table 2.3 shows the weekly number of flights for each aircraft type. These aircraft types are recategorized into eleven types with engine specifications.

Table 2.3: Weekly frequency of flights from Mehrabad airport.

Type	A-300	A-306	A-310	A-312	A-320					
Number	80	15	10	4	2					
Type	B-707	B-727	B-72S	B-734	B-737	B-747	B-74F	B-74L	B-763	B-767
Number	10	20	49	2	35	16	3	2	2	3
Type	TU-134	TU-154	F-100	MD-11						
Number	5	51	118	1						

An emission factor is assigned to each engine type and each LTO step. The duration of each step is: 4.0 sec (approach), 26.0 sec (idling), 0.8 sec (take off) and 1.6 sec (ascending). Then times are slightly different in the case of the F-100 type. The emission amount by step and air pollutant is summarized in Table 2.4. In actual calculation, emissions during the idling step are equally divided among three area sources. For diurnal profile, the same flight frequency is assumed except at nighttime. The emission release height for idling and take off is set at 10 m.

Table 2.4: Total emission from airplanes.

Step / element	CO	SOx	NOx
Approach	0.63	0.45	4.79
Idling	182.15	0.97	3.94
Take off	0.34	0.29	10.18
climb	1.18	0.50	13.31

2.2.2 Stationary emissions inventory survey

The stationary point and area source emissions were originally estimated from a mail survey source registration. Activity data include the quantity and type of fuel used and also in some case fuel sales records, state registration records, fuel/material usage and default employment and per capita data. The emission factors are based on source classification codes related to the source process type. If control equipment is used at any source, its effectiveness is factored into the equation. Field staff also supplemented data based on plant inspections and manually calculated plant emissions.

Brief descriptions of the categories for projecting pollutants are shown in Table 2.5. By study of activity factors such as sector-wise energy demand, emission factors of fuels, emission rates of pollutants were estimated for each sector in Tehran. Table 2.6 shows sectorwise stationary emission quantities of pollutants in Tehran during 2005.

Table 2.5: Brief descriptions of the categories for stationary sources**.**

Sector	Category	Emission Type
Manufacturing Industry	Food, Textile, Wood, Paper, Chemicals, Nonmetal, Iron/Steel, Machinery, Other	Point (>100 employee) Area (<100 employee)
Commercial Household	Restaurant, Hotel, Office, House, etc.	Area
Energy Conversion	Refinery, Power plant	Point

Table 2.6: Sectorwise emission quantities by stationary sources
in Tehran during 2005 (combustion + evaporation) tone/year.

Sector	Emission quantity				
	SOx	NOx	CO	HC	SPM
Industry	15923	5741	1309	5748	3568
General service and household	17720	30051	7893	38347	8591
Energy conversation	9289	12014	2053	9401	2838
Total	42932	47806	11255	53496	14997

2.2.3 Results and discussion

Concerning the source contribution of air pollutants, stationary sources represent 87% of total SO_x emission while mobile sources represent respectively 70%, 99%, 72% and 56% of NO_x, CO, NMVOC and PM_{10} emissions respectively (See Figure 2.7).
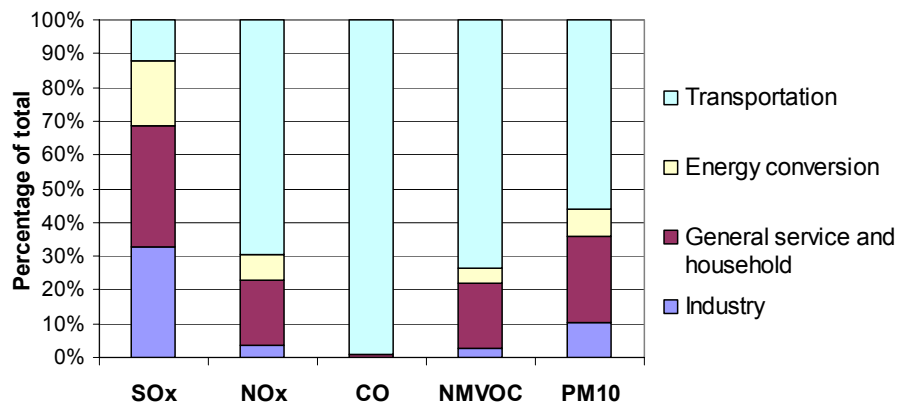
Figure 2.7: Comparison of air pollutant emission contributions to total across main sectors.

SO_x emissions from the general service and household represent 36% of the total, followed by the industrial sector (32%), energy conversion (19%), while the transportation sector represents only 13% in contrast to other kinds of pollutant emissions, because this sector uses low sulfur gasoline and diesel oil. The thermal power plants and refinery in Tehran contributions is only 19% because most of the fuels have already been substituted by natural gas expect in winter when supply of natural gas is sometimes short. NO_x emission shows different treatment to SO_x and the contribution of the transportation sector reaches 70% of total emissions. General service and household and energy conversation contribute 19% and 8% respectively, followed by industrial (4%). The general service and household sector contribution is 18%, though this sector has numerous consuming units. CO emissions are negligible in the case of stationary emission

sources, since the transportation sector has a dominant contribution of 99%. Most NMVOC emissions come from the transportation sector with 72%, general service and household (19%) and energy conversion (5%); the combined share of these three sectors totals 97%. NMVOC emission sources of the commercial sector are represented by petrol stations, printing shops, dry cleaning shops and petroleum depots and not by shops of electric metal plating and painting, since information of these sources is not available despite their possible substantial volume. It is estimated that leakage of natural gas from rubber hose connections is substantial due to a lack of proper maintenance, especially in the commercial-household sector although their volume is not estimated at this stage. PM_{10} emissions from the transportation sector represent 56% of the total, followed by general service and household (25%) and the industrial sector (10%) and energy conversion (8%).

Figure 2.8 illustrates hourly average of CO and PM_{10} emission inventories during 2005, these pollutants are the two critical pollutants in Tehran city.
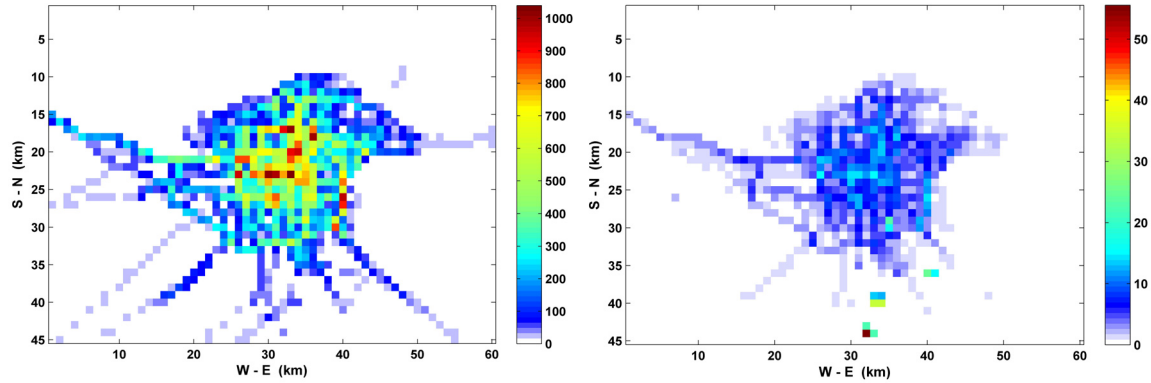
Figure 2.8: Hourly average of CO (left) and PM 10 (right) emission inventories for Tehran city during 2005 ($kg.h^{-1}.km^{-2}$).

2.3 Emission inventory of anthropogenic heating in Tehran

2.3.1 Overview

The heat generation due to human activities is an important cause of the urban heat island (Oke, 1998). The heat island of some mega-cities have been documented by investigating extensive direct and remote sensing measurements as well as simulation studies, such as urban parameterizations in mesoscale meteorological and fluid dynamics models (Kim, 1992; Aniello et al., 1995; Ichinose et al., 1999; Saaroni et al., 2000; Martilli, 2002; Kondo and Kikegawa, 2003; Kato and Yamaguchi, 2005; Hung et al., 2006).

One of the main goals of this study is to estimate diurnal profile and distribution of anthropogenic heat flux (Q_f) in Tehran city, including a detailed formulation of this flux in a high resolution mesoscale meteorological (MM) model of the urban environment.

In the past decade, parameterization schemes such as Canopy Models (CM), Building Energy Models (BEM), the Drag-force Approach (DA) and urban soil models have been implemented in MM models to better incorporate urban geometric structure and thermodynamic characteristics. Therefore, new generations of MM models (see Figure 2.9) have multi-scale systems (MM–CM–BEM) that can be used for the quantitative assessment of the urban island effect. Similarly, this kind of parameterizations can be incorporated into Computational Fluid Dynamics (CFD) models (Milliez et al., 2006).

Figure 2.9: Composition of the multi-scale MM models (MM–CM–BEM).

Formulations for Q_f or its components have been introduced into standard and modified versions of MM models (MM–CM or MM–CM–BEM) to study anthropogenic heating effects on local meteorology (Sailor et al, 2006; Martilli et al, 2002; Kikegawa et al, 2003).

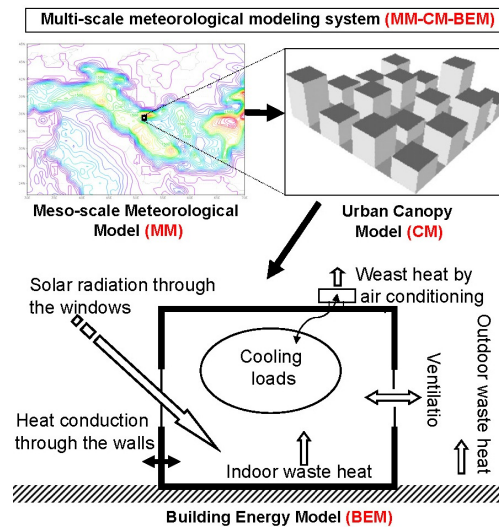Recent studies show daily average value of Q_f in the range of 25 to 50 Wm^{-2} and with maxima up to about 80 Wm^{-2} in city-scale analyses (Klysik, 1996; Steinecke, 1999; Crutzen, 2004; Sailor and Lu, 2004; Offerrle, 2005; Piringer and Joffer, 2005; Makar et al., 2006; Pigeon et al., 2006; Pigeon et al., 2007; Hamilton et al., 2009), while results with high spatial resolution in the downtown areas of mega-cities (e.g. Tokyo, San Francisco and Shenyang) show 5–10 times the magnitude of the city-scale average values (Saitoh and Shimada, 1996; Ichinose et al., 1999; Sang et al., 2000; Sailor and Lu, 2004). All recent studies confirm significant effects of anthropogenic heating on the formation of UHI and account for this flux in the urban energy balance. Taking into account Q_f in MM models of mega-cities usually increases the simulated near-surface temperature by 0.5-5°C (Saitoh and Shimada, 1996; Ichinose et al., 1999; Kondo and Kikegawa, 2003; Kikegawa et al, 2003; Sailor and Fan, 2004, Makar et al., 2006; Sailor et al., 2006).

The spatial distribution of Q_f is not easily available from monitoring data and is difficult to obtain from measurements and energy consumption inventory (Pigeon et al., 2006). Consequently, it has generally been difficult to estimate the spatial distribution of Q_f and correctly estimate both heat storage and Q_f in modeling studies (Pigeon et al., 2006; Offerle et al., 2005). The general calculating methods for spatial distribution of Q_f can be based on some available relevant urban characteristics, such as meteorological measurements (Pigeon et al., 2006), population density pattern (Sailor and Lu, 2004; Markar et al., 2006), brightness (based on satellite images) (Makar et al., 2006), landuse classification (Piringer and Joffre, 2005), emission inventory for specific pollutants and measured or simulated fields of specific pollutant concentration (Baklanov, 2005). This work presents the design and application of a suitable method to develop spatial and temporal distributions of Q_f in mega-cites.

The analysis of meteorological data from the Tehran observation network in urban, suburban and rural areas shows UHI intensity being stronger in winter, especially at night

time, than in summer. The UHI intensity can reach 10 °C and Q_f shows similar variation. One episode that can show the effect of Q_f on UHI intensity is the vacation period at the beginning of each year. In the final days of the Iranian year (end of winter), Tehran always suffers from high concentration of traffic and population, but in the first days of the next year (21 March), about half of Tehran population leave the area, thereby leading to an extreme reduction in Q_f value. In this episode, the UHI intensity shows a reduction of about 2-5 °C for the same meteorological conditions. Figure 2.10 illustrates a negative trend for the difference between the urban and rural observed temperatures during this episode and shows the effect of Q_f reduction in the last days.

The main goal of this work is to calculate the urban anthropogenic heat flux by using a method that is based on an energy consumption inventory that reflects components, sub-components, scale, diurnal and seasonal variability and spatial distribution of the anthropogenic heat flux in Tehran region. We calculated the monthly anthropogenic heat flux for the city scale using various data sources including marketing databases, categories of energy consumption, thermodynamic parameters, fuel consumption in traffic sector (gasoline, diesel, Liquefied Petroleum Gas (LPG) and Compressed Natural Gas (CNG)), fuel consumption in buildings (including all subcategories: Natural Gas (NG), diesel, kerosene and fuel oil) and electricity consumption. For example, Figure 2.11. represents monthly anthropogenic heat flux averaged over the urban area including the main components in Tehran during 2004-2005 that were calculated using such data.

After an initial study and data processing, in which we applied the top–down Sailor method based on population density and per capita consumption (Sailor and Lu, 2004) and concluded that this method is not well suited for Tehran. Figure 2.12 represents the city-scale diurnal Q_f profile and its components in winter for Tehran during 2004-2005 obtained with this method. The most important limitations that we identified are listed below:

a) using a constant temporal profile for traffic and energy consumption: observed temporal profiles vary with the diurnal population.

b) using a simple relationship between traffic densities and population density: traffic densities in Tehran depend on many other parameters.

c) using the diurnal temperature profile formulation or the daily maximum and minimum temperature formulation in order to generate average daily NG load curve: the estimated hourly load curves (based on observations) for city-gas consumption do not have high correlation with the outdoor temperature in the Tehran region.

d) using the same land use for the entire city.

e) using a unique per capita consumption rate: the model and value for per capita energy consumption varies among districts and also between the resident and guest populations; for example, the northern part of Tehran is colder than the southern part and has different socio-cultural behaviors and different technology for indoor heating.

This method leads to overestimations in midday (high diurnal population) and early morning consumption that are due to the methods used to generate the daily NG load curve. The data available for gas consumption in Tehran show a different diurnal profile with a maximum during the afternoon until midnight in wintertime. Therefore, we present hereafter an improved method that takes into account observed consumption profiles, landuse classification, population density and inventory methodology for traffic heating.
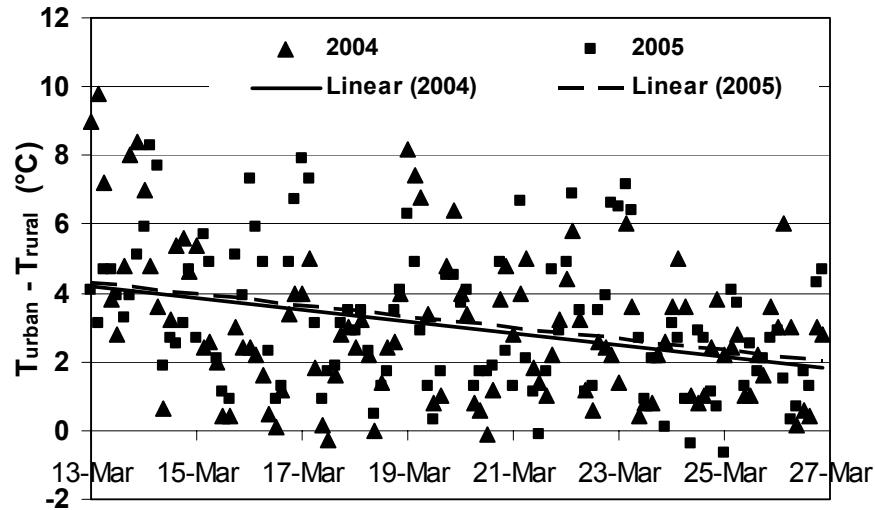
Figure 2.10: Scatter plot of observed $\Delta T = T_{urban} - T_{rural}$ from 13 to 27 March 2004 and 2005 every 3 hours.
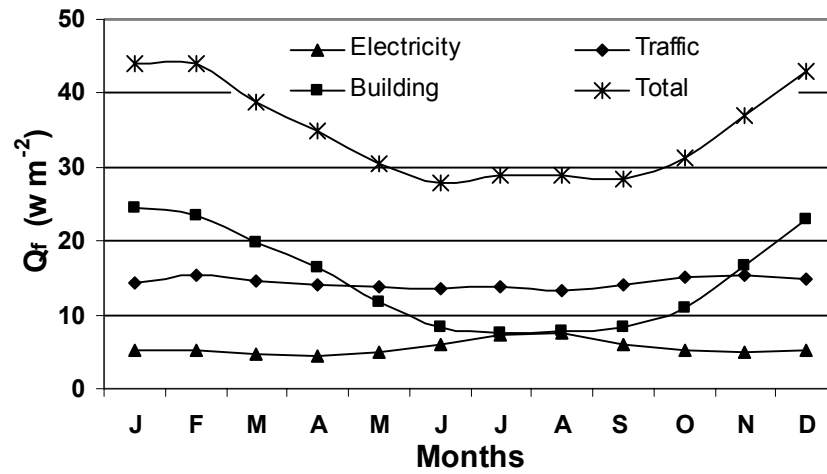
Figure 2.11: Monthly anthropogenic heat flux averaged over urban area in Tehran during 2004-2005.
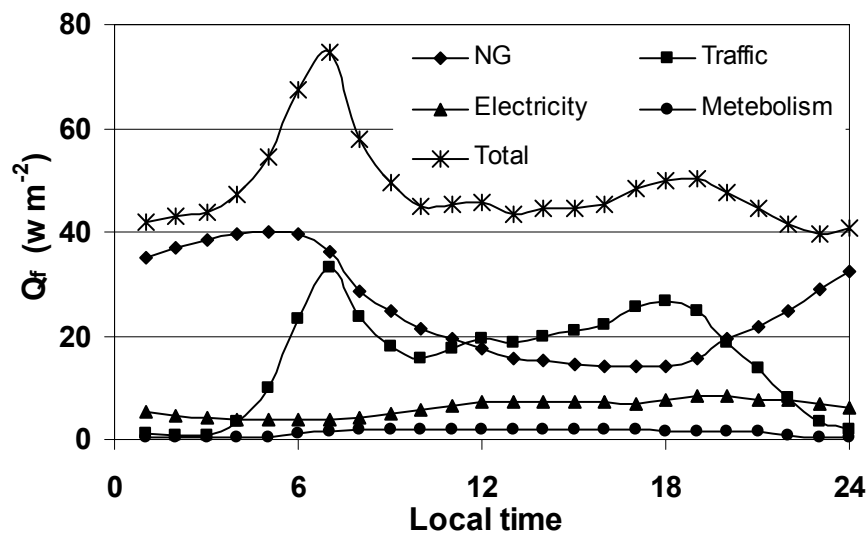
Figure 2.12: Diurnal Q_f profile in winter obtained with the Sailor method for Tehran during 2004-2005.

2.3.2 Calculation methodology

The population consumes energy in two main sectors: traffic and building sectors. Emissions due to human metabolism should also be considered although they are likely to be smaller. Vehicular traffic heat emissions are distributed spatially according to the street network and heat emissions from buildings can be divided into several subcategories such as residential, commercial, industrial, etc. and each subcategory can be further divided

into indoor and outdoor components. The reasons for this classification include different behavior of consumption and different methods for estimating heat flux in each subcategory. We summarized the building sector according to 10 subcategories by merging some similar landuse classes from 24 landuse classes available in our primary GIS database. Figure 2.13 shows the primary landuse and final subcategories contribution in the Tehran urban area. The anthropogenic heat flux will be the sum of all the heat fluxes corresponding to these sectors and their subcategories.

$$H = \sum_{i=1}^{ns} H_i \qquad\qquad (2\text{-}1)$$

where the subscript (i) indicates the subcategory number as follows: 1) transportation (street network), 2) residential and 3) commercial-office (buildings free of population at night), 4) industrial, 5) area with low level of anthropogenic heat (e.g., gardens and agricultural areas), etc. The components of H can be divided into heat released from the point of consumption for each fuel and electricity and calculated in 4D (x, y, z and t). It is necessary to have a comprehensive description of diurnal profiles, monthly and seasonal cycle of consumptions and their annual growth index for each subcategory.

(a) *(b)*
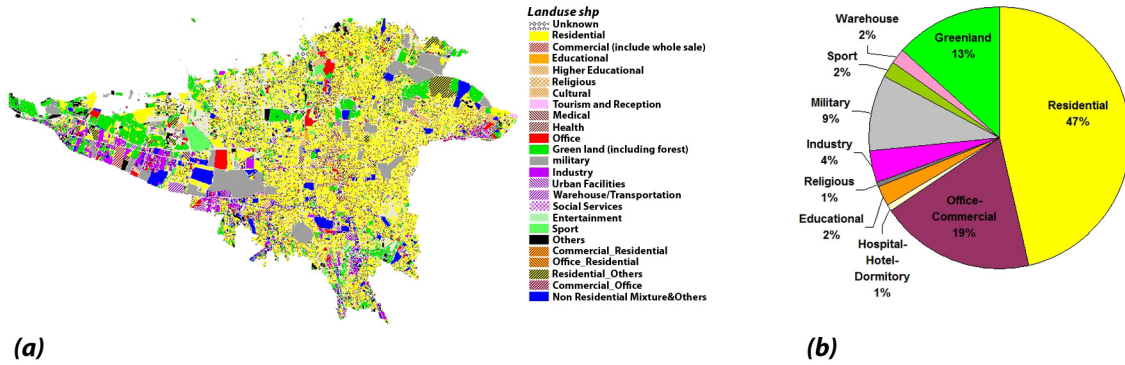
Figure 2.13: a) primary landuse and b) final subcategories contribution in Tehran urban area.

The heat flux quantity and its fractional (non-dimensional) spatial and temporal profiles are functions of many parameters, including climatic, socio-cultural, economic, vehicle categories, buildings architecture parameters, etc. In order to obtain accurate estimations of the anthropogenic spatial patterns for mega-cities similar to Tehran, it is desirable to develop a high resolution GIS database for key parameters and subsequent calculations. In

this study, various types of consumption data are converted to a GIS format in each district for traffic, NG and electricity. The computational domain has a 500 m resolution and covers an area of 60×45 km^2. This domain covers the Tehran mega city with all suburban industrial sites, factories, power plants and refinery.

Each component is developed separately based on specific formulation in order to have more validated spatial distributions. After the calculation of the spatial distribution of each component, one can estimate the net anthropogenic heating by superimposing all components. Because all components do not have the same height of release, it is disable to define a vertical profile and depth in order to generate vertical Q_f distribution. For example, in the case of power plants and refineries, Q_f can be released at heights of several hundred meters, because of the elevated plume release due to stack height as well as momentum and buoyancy of the thermal plume.

When incorporating Q_f components into a multi-scale modeling system (MM–CM–BEM), one must also divide the bulk Q_f components of each subcategories of each sector (except traffic) into indoor and outdoor fluxes.

2.3.2.1. Heating from vehicular traffic

Because of the high population density, large number of vehicles (more than 2 millions), significant traffic congestion, various fuel economy across vehicle categories and inhomogeneous traffic patterns, it was essential in this study to focus on the estimation of heat emitted from traffic. In order to control traffic and air pollution in downtown, Tehran municipality has enacted two traffic zones in recent years. One zone extends around 22 km^2 of the central downtown areas, keeping most passenger cars out during the working period (7 a.m. to 6 p.m.) and the second zone is an even-odd traffic zone, where people can drive according to the car license plate number (this second zone was originally enforced only during high air pollution episodes; it is enforced continuously since 2005). Because of their traffic zones and differences in urban design, the traffic pattern does not match the population density in Tehran mega city, therefore, as mentioned above, a top-down model based on population density is not well suited for this case.

In order to estimate the heat released from vehicles, we have used information from the database on traffic links and nods of the Tehran road network (output from EMME/2 model and available observations). The general steps for the calculation of this component are the following: preparing detail traffic parameters on network for all periods (e.g. workdays and weekends of each month from traffic model and observations), preparing GIS database, estimating and validating alternate factors for developing diurnal and monthly traffic profiles, estimating the energy release per vehicle per kilometer of travel for all vehicle categories and calculating the heat released on the traffic network (by link and by zone) in the domain to obtain the anthropogenic heating pattern due to urban traffic. It is desirable to obtain accurate key parameters for each vehicle category, its distribution of consumed fuels, mean fuel economies (FE: km l^{-1}) and some fuel chemical-physical properties such as, fuel density (ρ_f : kg l^{-1}) and mean net heat of combustion (NHC: MJ kg^{-1}) for the period of the studied episode. Examples of this information are given in Table 2.7. The average weekday hourly fractional traffic profiles (F_t) for all vehicle categories are extracted from the database. The corresponding fractional traffic profiles are given in Figure 2.14. A sharp peak appears in the morning (~ 0700-0800) and a damped peak occurs in the afternoon (~1200-1900).

The approach used here presents some similarity to that used by Grimmond (1992) and Sailor-Lu (2004), however, it is formulated in order to take advantage of the output from the traffic model and available data from the Tehran Comprehensive Transportation and Traffic Studies Company (TCTTSC). With the values listed in Table 1, traffic velocity (V: m/s) and vehicle number by category (1 to 7), one can calculate the bulk anthropogenic heat release in any link by time interval (ΔT : s) as follows:

$$H_{Link} = \sum_{i=1}^{7} \sum_{j=1}^{f_i} \frac{V_{ij} \times \Delta T \times NHC_{ij} \times \rho_{f_{ij}}}{FE_{ij}(V)} \qquad (2\text{-}2)$$

where f_i is the number of vehicles in each category (i), so that one can use fuel economy data FE(V) with this approach. In this study, all links are considered flat and the effect of slope on FE(V) is neglected. In order to estimate the mean Q_f for a given time interval, one estimates the influence area for each link as follows:

$$HF_A = \frac{H_{Link}}{\Delta T \times A_{Link}} \qquad (2\text{-}3)$$

After reviewing the distribution of values by month, it was observed that it was feasible to develop monthly alternative factors (and also for weekends) to approximate the variability of traffic. It is suggested that values of 0.9 and 0.5 for the first (Thursday in Iran) and second day of weekend, respectively, be used as alternative factors in comparison with workdays. We consider November as the reference for the calculation of monthly alternative factors. Table 2.8 represents suggested alternative factors for each month.

Table 2.7: Fuel consumption and characteristics for Tehran vehicle categories (2004).

Vehicles categories %		Fuel and Consumption distribution %		Fuel density (kg l^{-1})	Mean net heat of combustion (MJ kg^{-1})	Mean fuel economy (km l^{-1})
LDV	45	Gasoline	100	0.702	47	7.692
Taxi	25	LPG	85.5	0.496	46	8.197
		CNG	5.6	0.128	42	7.812
		Gasoline	8.9	0.702	47	6.892
LDT	8	Gasoline	100			6.020
Bus	2	CNG	17.9	0.128	42	1.174
		Diesel (NAT)	68.4	0.85	45	1.333
		Diesel (TCT)	13.7			1.538
Truck	2	Diesel	100			5.669
Minibus	3	Diesel	100			3.246
Motor cycle	15	Gasoline	100	0.702	47	20.790

LDV: Light duty vehicle, LDT: Light duty truck, NAT: Natural aspirated technology, TCT: Turbo charge technology

Recently, the Iran government implemented an encouragement strategy for vehicle manufacturing factories, organizations and people to produce and use vehicles adapted with compressed natural gas (CNG), to renew their cars and to improve the public transportation systems in order to reduce pollutant emissions and control energy consumptions. Consequently, we will observe a significant decrease in fuel consumption by vehicle in the near future.

This Q_f component due to traffic is released outdoor (H_t) and inside street canyons. It is incorporated into multi-scale systems as one of the outdoor anthropogenic heat flux components.
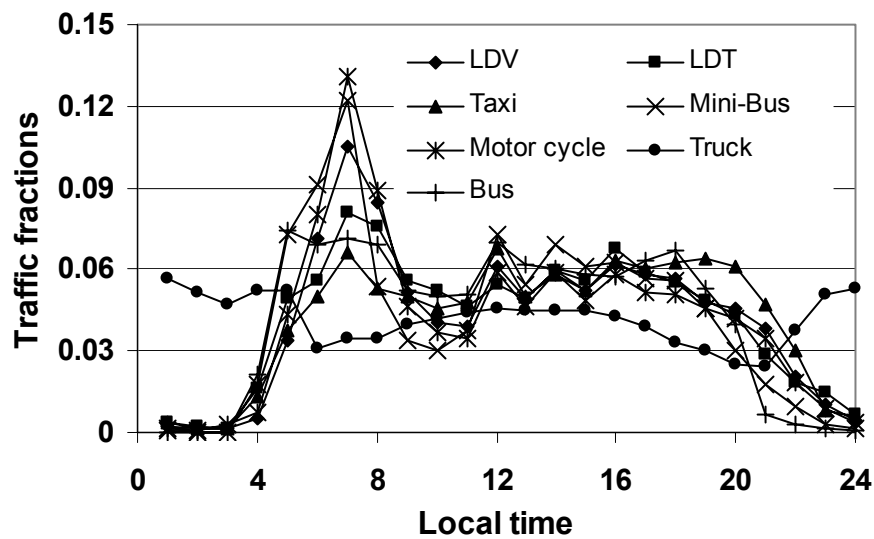
Figure 2.14: Weekday hourly fractional traffic profiles for various vehicle categories (2004).

Table 2.8: The suggested alternative factor for each month

Month	Factor	Month	Factor
April	0.810	October	1.068
May	0.978	November	1.055
Jun	0.965	December	1.057
July	0.974	January	1.006
August	0.951	February	1.080
September	0.972	March	1.084

2.3.2.2. Heating from electricity consumption

A high percentage of electric power is used for lighting, air conditioning and a host of domestic and office appliances in the residential and commercial sectors; the remaining consumption occurs in the industrial, street lighting, agricultural and transportation subcategories. We developed an accurate dynamic distribution of electricity consumption for all these sectors. Figure 2.15 illustrates the average distribution of electricity consumption in the main sectors.
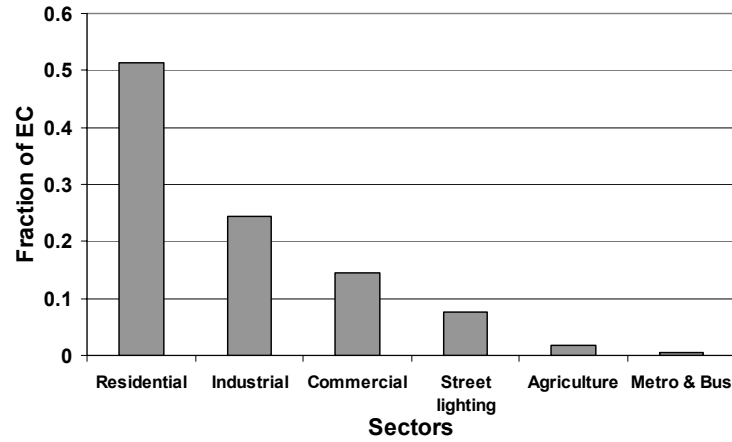
Figure 2.15: The distribution of electricity consumption for each main sector.

In order to develop an accurate diurnal and monthly variability of electricity consumption in Tehran, we used an hourly digital database derived from scanning of available electrical division posts. These hourly consumption data are archived by Tehran Province Regional Electricity Company (TREC)'s Consumption Management Administration. TREC divides Tehran into 6 districts (NE, NW, SW, SE, W and central). For more accurate calculations, all parameters pertaining to this component were treated individually in each district. For example, Figure 2.16 shows the hourly electricity fraction for the average diurnal cycle in each of 12 months for Tehran (in the area free of factories).

To generate consumption profiles for all subcategories, we used the following time-varying function that modules diurnally by means of a Fourier series fitting function.

$$F(t)|_e = a_0 + \sum_{i=1}^{n}\left[a_i \cos\left(\frac{2n\pi t}{24}\right) + b_i \sin\left(\frac{2n\pi t}{24}\right)\right] \tag{2-4}$$

where a_i, b_i and n are estimated from data fitting. Figure 2.17 shows that the number of harmonics *n* equals 3 is sufficient to give a valid fitting. The diurnal electricity profiles for weekends are different from those for workdays. These are also differences between the first and second days in weekends.
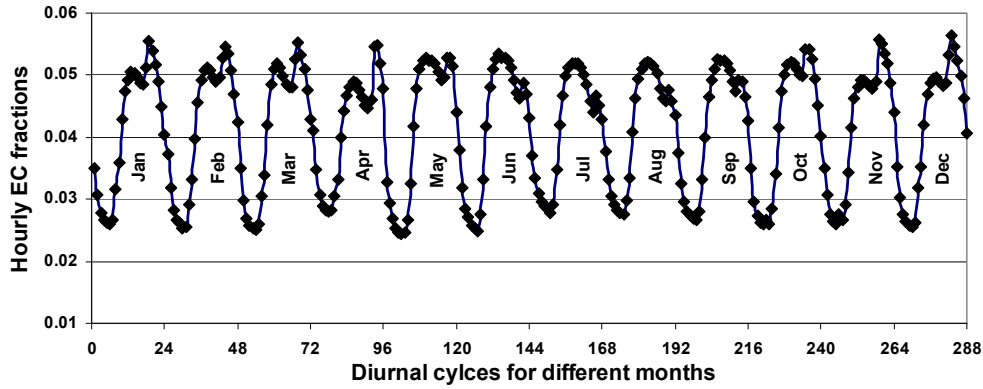
Figure 2.16: Hourly electricity fraction for average diurnal cycle in each of 12 months for Tehran city.
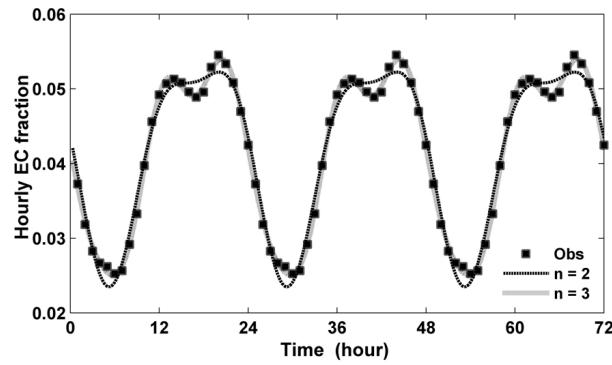
Figure 2.17: Fourier fitting on diurnal electricity fraction on February 7 until 9th in 2005 (winter) in residential sector.

By the electricity consumption function, daily electricity consumption $(DC)_e$ and heating production rate (HPR) for each sector, one can calculate the total heat release in any sector and in one hour as follows:

$$H_{es} = [(DC)(HPR)F(t)]_{es} \tag{2-5}$$

We used HPR equals 0.9, because about 10% of electricity is lost during transmission (Khan and Simpson, 2001). The next step is to calculate the spatial distribution of this heat flux. To that end, we use population density following Sailor and Lu (2004) for the residential subcategory. For the other subcategories, we used category-specific information about consumption and its diurnal profiles. Figure 2.18 shows the resident population density pattern in our domain.
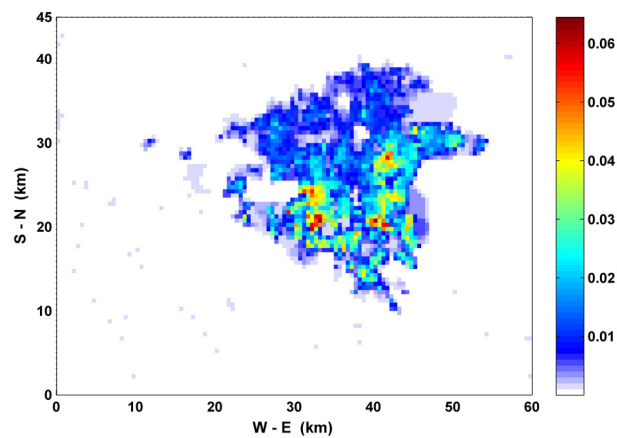
Figure 2.18: Resident population density (person per square
meter) pattern in Tehran domain.

In winter, the main part of this Q_f component is released indoor (H_e). It is incorporated
into multi-scale modeling systems as an indoor flux. Some function of this component
(that coming from outdoor lighting) is released outside of buildings.

In summer, one of the important parts of H_e comes from air conditioning and is released
outdoor. In BEM, this part is simulated and one has to force BEM only with the indoor
anthropogenic heat from other applications. However, one must filter the air conditioning
electricity consumption share from the total electricity consumption. One can estimate the
air conditioning electricity consumption from detailed measurements or by comparing
diurnal consumption between two episodes that have different diurnal temperature: one
with diurnal temperature around comfort level and other one with higher temperature.

2.3.2.3. Heating from fuels consumption

Natural gas (NG) is the dominant heating fuel in Tehran building sectors (more than
96%). NG is used for the purpose of space heating, water heating and cooking in urban
buildings. It is the essential fuel in factories, especially in refinery and power plant
industries. Other fuels include fuel oil, diesel, kerosene and LPG.

Tehran Gas Company (TGC) divides Tehran into 12 districts and the marketing database
of NG on Tehran region has 16 subcategories. Figure 2.19 illustrates the average
distribution of NG consumption in the main sectors.

We tested both the diurnal temperature profile formulation and the daily maximum and minimum temperature formulation (Sailor et al., 1998; Sailor and Lu, 2004) in order to generate average daily NG load curve in Tehran. We found some differences between the estimated profiles from observations (with some approximations) and the generated profiles from these formulations. Recent intensive experimental studies show that the hourly load curves for city-gas consumption do not follow exactly the outdoor temperature (Ueno, 2006) and do not show a main peak of consumption in early morning. For example, in Tehran, the main peak is observed near midnight in winter. The models that have been based on outdoor temperature are suitable for generating daily and monthly profiles but not hourly profiles, because consumption terms (except space heating) have important effects on diurnal profiles. Figure 2.20 compares NG consumption profiles using the two Sailor formulations and the profile estimated from observations in winter.

We used a time-varying NG consumption profile that modules diurnally using Fourier fitting of observations (similar method as that used for electricity component), HPR equal 0.8 (on the other hand thermal combustion efficiency in this case) and nominal heating value for NG of 8250 kcal per cubic meter from TGC analysis and measurements. We considered that 60% of the gross energy in the fuel is lost as waste heat at power plants. In the case of refineries, it is important to know the strategy of fuel consumption, because some refineries produce their own fuel. We used the same method for developing the spatial distribution of this component as for the electricity component.

The main fraction of this Q_f component is released indoor (H_g). It is incorporated into multi-scale modeling systems as an indoor flux. Some fraction comes out from building chimneys (H_c). The outdoor fractions depend on season and for example in winter, we considered 25% of total value in residential area.
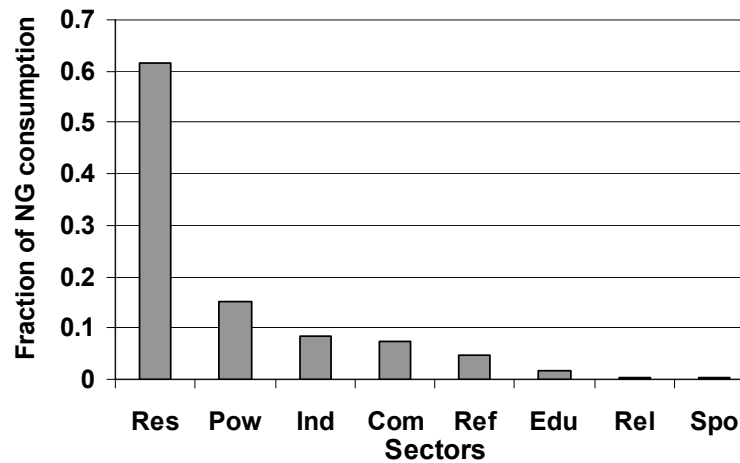
Figure 2.19: The distribution of NG consumption in each sector (Res: Residential, Pow: Power plants, Ind: Industrial, Com: Comersial, Ref: Refinery, Edu: Educational, Rel: Religious and Spo: Sport).
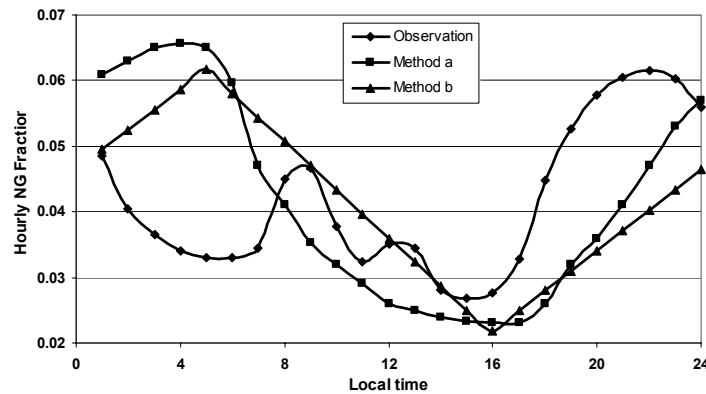
Figure 2.20: Comparison of hourly fractional NG consumption profiles using the two Sailor formulations and observations for Tehran in winter.

2.3.2.4. Heating from human metabolism

Humans represent the dominant source of metabolic heat in urban settings. The metabolic rates are not constant over the course of a day. For example, metabolic rates for sleeping, sitting (at rest), slow walking and more intense activities are suggested to be about 75, 115, 230 and 300-350 W, respectively (Fanger,1972; Guyton,1986). The method used here is similar to that used by Sailor and Lu (2004) and uses a profile for metabolic rate.

For comparison, the city-wide metabolism heat flux is 0.7 (nighttime) to 2.3 (daytime) Wm^{-2} in Tehran and it contributes only 4-5% of the total city- wide Q_f.

This component has indoor and outdoor components (H_m) and estimates of the population density indoor and outdoor are needed as a function of time during the day.

2.3.3 Results and discussion

By using a new detailed methodology, we calculated representative summer and winter diurnal city-wide Q_f profiles for Tehran. Figure 2.21 illustrates the Q_f profiles and their components. Wintertime Q_f is larger than summertime Q_f with values of 20-25 Wm^2. The contributions of fuel consumption, traffic, electricity and human metabolism are 54, 32, 13 and 4 %, respectively, in winter, reflecting the importance of heating emissions from buildings in this period. In summer, traffic is more important than all other components and the respective contributions change to 25, 44, 26 and 5 %.
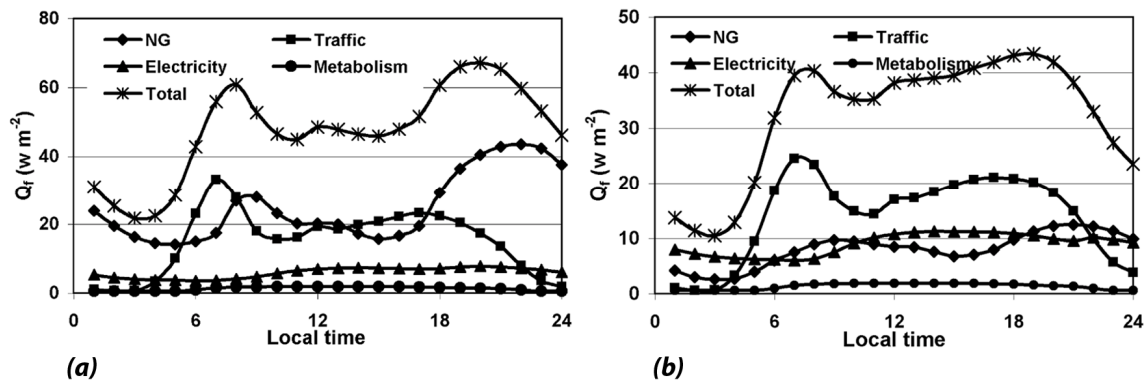
Figure 2.21: Representative city-scale Q_f profile and its components for winter (left) and summer (right) in Tehran urban area (2004-2005).

Both profiles exhibit a dual peak shape, with a morning peak and a slightly larger evening peak. These patterns can cause a significant effect on the energy balance during meteorological transition periods.

In the case of indoor and outdoor anthropogenic heat fluxes, we find that both of them show a dual peak shape but that the morning peak is stronger for the indoor flux and the before midnight peak is stronger for the outdoor flux. In winter, the indoor Q_f flux shows

larger values especially before midnight. In summer, the outdoor Q_f flux shows a similar profile, because this flux does not include the air conditioning flux (see Figure 2.22).

According to the results of this study, we find that in the urban core region, all components of Q_f can show maximum values and Q_f can be 4-7 times the magnitude of the city-wide values. Those values are greater than those in industrial areas except for the main Tehran power plants and oil refinery that are located in the south part of Tehran. Also estimated Q_f in crowded intersections, facilities with high consumption (such as some factories, hotels, dormitories, department stores, etc.) and high rise and high population density areas can produce Q_f with values for 200-300 Wm^2 when using fine spatial resolutions.

Figure 2.23 presents the results of the heat flux budget developed in this study and shows the spatial distribution of the daily mean Q_f in Tehran region.
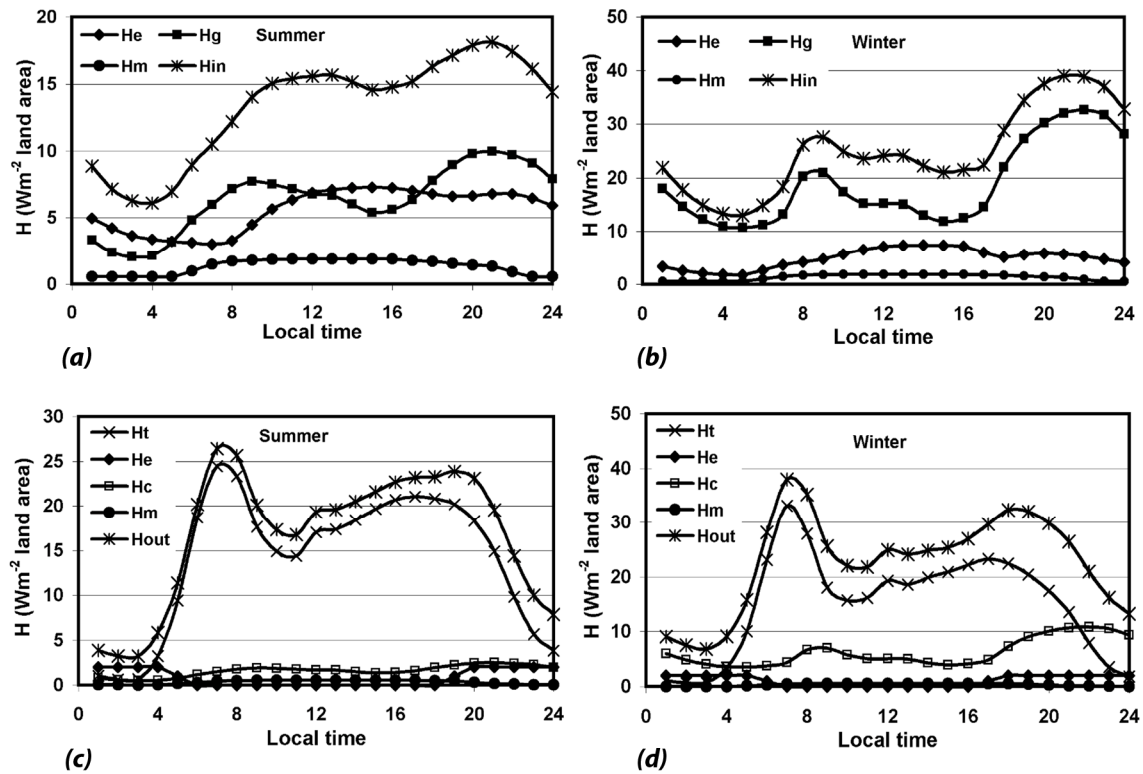
Figure 2.22: Representative indoor (top) and outdoor (down) Q_f components profile (to find out the signification, please refer to the text) for winter (right) and summer (left) in north central Tehran urban area (2004-2005).
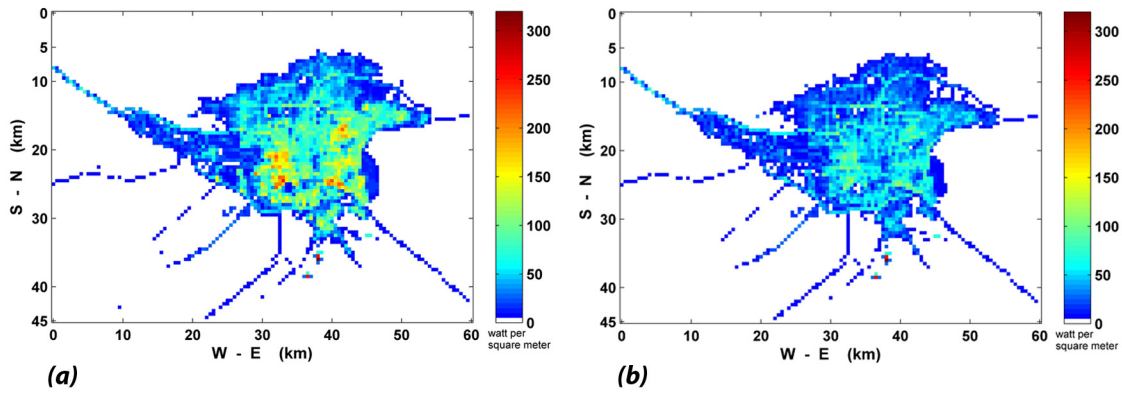
Figure 2.23: Daily average Q_f patterns released near surface (first 40 meters) relate to workdays in winter (a), and summer (b) in 2004-2005 period.

We recommend that future heat budget studies for mega-cities use a similar approach as the one used here, based on local observations and marketing data (rather than per capita parameters for a province or a country), diurnal consumption profiles that all specific to each subcategories and accurate traffic spatial and temporal distributions. The results of this study can be of benefit for mesoscale meteorological modeling in urban areas and studies of the interaction between urban canopy heat island and topographic flows in the Tehran region. In the next chapter, this heat flux inventory is used in a multi-scale meteorological model of the Tehran region.

References

Aniello, C., Morgan, K., Busbey, A., Newland, L., 1995. Mapping micro-urban heat islands using landsat TM and a GIS. Computers & Geosciences 21, 965–969.

Baklanov, A., Mestayer, P., Clappier, A., Zilitinkevich, S., Joffre, S. Mahura, A., Nielsen, N.W., 2005. On the parameterisation of the urban atmospheric sublayer in meteorological models. Atmospheric Chemistry and Physics Discussions 5, 12119–12176.

Beaton, S.P., Bishop, G.A., Stedman, D.H., 1992. Emission characteristics of Mexico City vehicles. Journal of the Air & Waste Management Association 42, 1424–1429.

Bose, R.K., 1996. Energy demand and environmental implications in urban transport - case of Delhi. Atmospheric Environment 30, 403–412.

Brown, M.J., 2000. Urban parameterizations for mesoscale meteorological models. Mesoscale Atmospheric Dispersion, Z. Boybeyi, Ed., Wessex Press, 193-255.

Cernuschi, S., Giugliano, M., Cemin, A., Giovannini, I., 1995. Modal analysis of vehicle emission factors. Sci. Total Environ., 175–183.

Cooper, D.C., 1989. Persistence factors for mobile source (roadway) - carbon monoxide modeling. Journal of the Air & Waste Management Association 39, 714–720.

Crutzen, P.J., 2004. New Directions: The growing urban heat and pollution"island" effect-impacts on chemistry and climate. Atmospheric Environment 27, 3539–3540.

Derwent, R.G., Middleton, D.R., Field, R.A., Goldstone, M.E., Lester, J.N., Perry, R., 1995. Analysis and interpretation of air quality data from an urban roadside location in Central London over the period from July 1991 to July 1992. Atmospheric Environment 29, 923–946.

EPA, 1992. U.S. Environmental Protection Agency, Procedures for Emission Inventory Preparation, Volume IV: Mobile Sources. EPA-450/4-81-026d.

Fanger, P.O., 1972. Thermal Comfort: Analysis and Applications in Environmental Engineering. McGraw-Hill, New York, 244pp.

Grimmond, C.S.B., 1992. The suburban energy balance: methodological considerations and results for a midlatitudes west Coast City under winter and spring conditions. International Journal of Climatology 12, 481–497.

Guyton, A.C., 1986. Textbook of Medical Physiology. W.B. Saunders Company, Philadelphia, USA, 1057pp.

Hamilton, I.G., Davies, M., Steadman, P., Stone, A., Ridley, I., Evans, S., 2009. The significance of the anthropogenic heat emissions of London's buildings: A comparison against captured shortwave solar radiation. Building and Environment 44, 807–817.

Hung, T., Uchihama, D., Ochi, S., Yasuoka, Y., 2006. Assessment with satellite data of the urban heat island effects in Asian mega cities. International Journal of Applied Earth observation and Geoinformation 8, 34–48.

Ntziachristos, L., Samaras, Z., 2000. COPERT III Computer program to calculate emissions from road transport. Methodology and emission factors (Version 2.1). Technical Report No 49. European Environment Agency, Copenhagen.

Lawson, D.R., Groblicki, P.J., Stedman, D.H., Bishop, G.A., Guenther, P.L., 1990. Emissions from in-use motor vehicles in Los Angeles: a pilot study of remote sensing and inspection and maintenance program. Journal of the Air & Waste Management Association 40, 1096–1105.

Ichinose, T., Shimodozono, K., Hanaki, K., 1999. Impact of anthropogenic heat on urban climate in Tokyo. Atmospheric Environment 33, 3897–3909.

JICA, CEST, 2000. The study on Seismic Microzoning of the Greater Tehran Area in the Islamic Republic of Iran. Draft Final Report.

TEIS project (JICA project) report, 2002. Tehran's Emission Inventory Survey. JICA, DOE and AQCC.

Joumard, R., Jost, P., Hickman, J., Hassel, D., 1995. Hot passenger car emissions modeling as a function of instantaneous speed and acceleration. Science of the Total Environment169, 167-174.

Kato, S., Yamaguchi, Y., 2005. Analysis of urban heat-island effect using ASTER and ETM+ Data: Separation of anthropogenic heat discharge and natural heat radiation from sensible heat flux. Remote Sensing of Environment 99, 44–54.

Khan, S.M., Simpson, R.W., 2001. Effect of heat island on the meteorology of a complex urban airshed. Boundary-Layer Meteorology 100, 487–506.

Kikegawa, Y., Genchi, Y., Yoshikado, H., Kondo, H., 2003. Development of a numerical simulation system toward comprehensive assessments of urban warning countermeasures including their impacts upon the urban buildings' energy-demands. Applied Energy 76, 449–466.

Kim, H.H., 1992. Urban heat island. International Journal of Remote Sensing 13, 2319–2336.

Kondo, H., Kikegawa, Y., 2003. Temperature variation in the urban canopy with anthropogenic energy use. Pure and Applied Geophysics 160,317–324.

Kłysik K. 1996. Spatial and seasonal distribution of anthropogenic heat emissions in Łodz, Poland. Atmospheric Environment 30, 3397–3404.

Mage, D., Ozolins, G., Peterson, P., Webster, A., Orthofer, R., Vandeweerd, V., Gwynne, M., 1996. Urban air pollution in Megacities of the world. Atmospheric Environment 30, 681-686.

Makar, P.A., Gravel, S., Chirkov, V., Strawbridge, K.B., Froude, F., Arnold, J., Brook, J., 2006. Heat flux, urban properties, and regional weather. Atmospheric Environment 40, 2750–2766.

Martilli, A., Clappier, A., Rotach, M.W., 2002. An urban surface exchange parameterization for mesoscale models. Boundary-Layer Meteorology 104, 261–304.

Mayer, H., 1999. Air pollution in cities, Atmospheric Environment 33, 4029-4037.

Milliez, M., Musson-Genon, L., and Carissimo, B., 2006. Radiative transfers in CFD modeling of the urban canopy. Proceedings of the 28th NATO International Technical Meeting on Air Pollution Modeling and its Applications, Leipzig, Germany.

Mitsoulis, E., Alexopoulos, A., Assimacopoulos, D., 1994. Model for traffic emissions estimation. Atmospheric Environment Part B 27, 435–446.

Offerle, B., Grimmond, C.S.B., Fortuniak, k., 2005. Heat storage and anthropogenic heat flux in relation to the energy balance of a central European city centre. International Journal of Climatology 25, 1405–1419.

Onursal, B., Gautam, S.P., 1997.Vehicular Air Pollution: Experiences from Seven Latin American Urban Centers. World Bank Technical Paper No. 373, The International Bank of Reconstruction and Development, Washington, DC, USA.

Oke, T.R., 1998. The urban energy balance. Progress in Physical Geography 12, 471–508.

Pigeon, G., Durand, P., Masson, V., 2006. Evaluating parameterization of anthropogenic heat release in urban land surface scheme from measurements and energy consumption inventory over Toulouse during CAPITOUL. American Meteor Society 6th Symposium on the Urban Environment, Atlanta, United States.

Pigeon, G., Legain, D., Durand, P. and Masson, V., 2007. Anthropogenic heat releases in an old European agglomeration (Toulouse, France). International Journal of Climatology 27, 1969-1981.

Piringer, M., Joffer, S., 2005. The urban surface energy budget and mixing height in European cities: Data, models and challenges for urban meteorology and air quality. Final Report of WG2 COST Action 715, 194pp.

Riveros, H.G., Tejada, J., Ortiz, L., Sanchez, A.J., Riveros, H.R., 1995. Hydrocarbons and carbon monoxide in the atmosphere of Mexico City. Journal of the Air & Waste Management Association 45, 973–980.

Saaroni, H., Ben-Dor, E., Bitan, A., Potchter, O., 2000. Spatial distribution and microscale characteristics of the urban heat island in Tel-Aviv, Israel. Landscape and Urban Planning 48, 1–18.

Samaras Z., Coffey R., Kyriakis N., Koufodimos G., Weber F.J., Hassel D., Joumard R., 1998. Methodologies for estimating air pollutant emissions from transport MEET - Emission factors for future road vehicles. Bron, France: INRETS, Rapport, 108 p.

Sang, J., Liu, H. and H., Liu, 2000. Observational and numerical studies of wintertime urban boundary layer. Journal of Wind Engineering and Industrial Aerodynamics 87, 243–258.

Sailor, D.J., Rosen, J.N., Munoz, J.R., 1998. Natural Gas Consumption and Climate: a Comprehensive Set of Predictive State-Level Models for the United States. Energy-the International Journal 23, 91–103.

Sailor, D.J., Fan, H., 2004. The importance of including anthropogenic heating in mesoscale modeling of the urban heat island. 84th Annual meeting of the American Meteor Society, Symposium on planning, now casting, and Forecasting in the urban Zone, Seattle.

Sailor, D.J., Lu, L., 2004. A top–down methodology for developing diurnal and seasonal anthropogenic heating profiles for urban areas. Atmospheric Environment 38, 2737–2748.

Sailor, D.J., Heiple, S., Hart, M., 2006. Modeling the effects of anthropogenic heating on the urban heat island – The role of spatial scale. Sixth International Conference on Urban Climate, Goteborg, Sweden.

Saitoh, T.S., Shimada, T., 1996. Modeling and simulation of the Tokyo urban. Atmospheric Environment 30, 3431–3442.

Stein, A.F., Toselli, B.M., 1996. Street level air pollution in Cordoba City, Argentina. Atmospheric Environment 30, 3491–3495.

Steinecke, K., 1999. Urban climatological studies in the Reykjavik subarctic environment, Iceland. Atmospheric Environment 33, 4157–4162.

Sturm, P.J., Almbauer, R. , Sudy, C. , Pucher, K. , 1997. Application of computational methods for the determination of traffic emissions. Journal of the Air & Waste Management Association 47, 1204–1210.

TERP project (GEF project) final report , 1997.Tehran's Transportation Emission Reduction. AQCC, SWECO, SMHI and MTC.

Ueno, T., Inada , R., Saeki, O., Tsuji, K., 2006. Effectiveness of an energy-consumption information system for residential buildings. Applied Energy 83, 868–883.

CHAPTER THREE

Local Meteorology and Urbanization Effects

3.1 Introduction

The planetary boundary layer (PBL) structure and its evolution play a major role in the physical and chemical processes related to air pollution formation and dispersion in the atmosphere. Local thermally driven mesoscale circulations and flows such as sea breezes, topographic flows and urban heat island (UHI) circulation can have significant effects on local weather, the diurnal evolution of the boundary layer structure and pollutant transport, particularly under synoptic anticyclonic conditions.

The effects and interactions of two local thermally driven processes, topographic flows and UHI under different meso and synoptical conditions play an important role in the Tehran region's weather.

The term of topographic flows will refer to any or all of upslope, downslope and valley flows as a group. In valley cities and during calm periods, meteorological conditions may lead to critical air quality problems due to low horizontal ventilation especially during transition between slope flows in early morning and in the late afternoon (Whiteman, 1990, 2000) and also due to the interaction of slope winds with the urban heat island, especially during winter and night times, when vertical diffusion is small (Atkinson, 1981). Following the convention of Segal and Arritt (1992), nonclassical mesoscale circulations (NCMCs) can be generated by differential sensible and latent heat fluxes to the atmosphere produced by spatial gradients in thermal and radiative properties such as albedo and thermal conductivity, differences in snow cover or vegetation (Segal et al., 1989 ; Segal et al., 1991 ; Rife et al., 2002). Also, aerodynamic contrasts can lead to

enhanced or suppressed mechanical mixing and, therefore, affect vertical and horizontal momentum transport (Grimmond and Oke, 1999). In real situations, the driving forces behind these circulations can interact in complicated ways, making accurate simulations difficult. Poulos (1996) provides an excellent review of the literature on katabatic flows. Analytical models of slope flows have explained these winds using various dynamics and thermodynamic forcing terms. Mahrt (1982) defined several types of downslope flows in terms of the relevant forcing mechanisms, based on a scale analysis of the momentum equations. Since the theoretical treatments of Prandtl (1952) and Defant (1949), there have been few papers regarding the understanding of daytime upslope winds. They occur under generally benign conditions and are considered relevant mainly because of their role in heat transport within the valley atmosphere, allthough valley venting of pollutants can occur as a result of converging upslope flows on ridge tops (e.g., de Wekker, 2002; Reuten et al., 2005).

Severals factors can cause deviations from classical slope/valley flow patterns: along-valley changes in topography, differential heating of slopes with different aspects and slope angles, ridgetop geometry, and variations in surface energy properties (Whiteman, 1990). Several studies of local-scale thermally driven flows have been conducted in arid places; they describe the diurnal cycles of slope and valley wind systems with a climatology that encompasses the combined effects of the mountain/plain, valley, slope, land/lake, and urban wind systems, especially under the condition of weak synoptic forcing (Stewart et al., 2002 ; Rife et al., 2002 ; Banta , 2004 ; Zumpfe, 2004).

Urbanization is often associated with surface temperature anomalies such as the UHI and the oasis effect. Changes in local and regional atmospheric processes associated with urbanization are complex and difficult to generalize (Oke, 1982), but we now have the computational and observational tools to explore how particular urbanization scenarios affect meteorology and climate. There are several causes of a UHI, including canyon effects (blocking of radiation and wind), longwave re-emission from the warmer air above the city (local greenhouse effect and induced vertical warm advection) , changes in the thermal properties of materials (thermal storage), anthropogenic heating (heat generation by human activity) and lack of evapotranspiration (lack of vegetation and

standing water) (Oke, 1988). The urban area cools off more slowly than the surrounding countryside and UHIs are often strongest at night (e.g., Bornstein, 1968; Oke, 1982; Draxler, 1986; Morris et al., 2001).

Atkinson (2003) ran sensitivity studies using a numerical model of an idealized urban area configured to reperesented London, England. Among the various possible contributors to UHI (albedo, anthropogenic heat, emissivity, roughness length, sky view factor, surface resistance to evaporation, and thermal inertia), surface resistance to evaporation was the most important factor controlling heat island strength during the day, while anthropogenic heating dominated at night. The increased roughness length associated with urbanization was the only factor that decreased the strength of the heat island, by increasing turbulent mixing in the surface layer. The heat island of some mega-cities (cities with population in excess of 10 million people) has been investigated by extensive direct and remote sensing measurements and also by simulation studies, especially using urban parameterizations in mesoscale meteorological and fluid dynamics models (e.g., Aniello et al., 1995; Ichinose et al., 1999; Saaroni et al., 2000; Martilli, 2002; Kondo and Kikeyawa, 2003; Kato and Yamaguch, 2005; Hung et al., 2006).

The magnitude of the urbanization impact on climate is sensitive to both the local climate regime and to various urban parameters. It remains a major research challenge to determine how, in various situations, urbanization interacts with other local forcing factors. Because generalizing the effects of urbanization on local weather is impossible, the problem must be broken down into more specific pieces.

Climate, terrain, and land-surface contrasts make Tehran Mega-City (TMC) a unique laboratory for studying PBL development in complex terrain.

In the present chapter, the PBL structure in TMC is studied during a high pollution episode.

Unfortunately, TMC area is very poor in urban meteorological background information from either field campaign observations or modeling studies. In this study, we selected November and December 2005 as two-month study period and we focus on the episode of 2 until 8 December where high concentrations of pollutants were observed. Results are presented for December 5th.

3.1.1 Topography of the region

The principal highland regions of the Tehran province are the Alborz mountain in the north and the Kavir desert in the south east. Tehran lies in a basin, situated south of the Alborz mountain range that crosses the north part of Iran (Figure 3.1). It is located at 35.7 °N and 51.4 °E. The TMC is 45 km long and 30 km wide with a valley bottom elevation of ~1050 to 1800 m above mean sea level (MSL). It means that the average slope is 0.026 in the north-south direction. It is bounded on about three sides by steep mountains and on the south by the Kavir desert (see Figure 3.1 for location map). The surrounding topography rises to as high as 3000-3700 m MSL in ~7 km toward north and about 1800-2200 m MSL in ~10 km toward east and south-east. Several deep and narrow valleys enter the TMC from the Alborz mountains to the south and wide narrow valleys to the south-west. More than 10 million people live within and adjacent to the TMC in this valley, which includes the urban, residential, and agricultural land covers. These topography and land-surface contrasts produce a variety of flows, although their characteristics vary with season and synoptic situations.

3.1.2 Main features of the climate and meteorology in the region

The TMC has a steppe or semi-arid climate with mean annual precipitation (MAP) of 230 mm. The Alborz mountain blocks moist air from the Caspian sea and the rainfall is produced by Mediterranean synoptic systems, which move eastward along with westerly winds during the cold season. The prevailing synoptic wind is generally from the west in TMC, but combination of high terrain, urbanization and weak synoptic forcing can lead to weak and variable winds with complex circulation patterns in this area.

North-east of Tehran (Aghdasiyeh station), SW and NE winds are about the most prevailing in the day and night time respectively (with a frequency of 50 – 60 %). It means that during weak synoptic forcing period, this area is affected by mountain and valley winds. Areas west and south of Tehran show some lower frequency in the cycling of diurnal wind direction (Figure 3.2). The mean wind speed during night time is somewhat weaker than that during day time. The mean standard wind speed in the west

(3.1 m s^{-1}) is larger than that observed in the east (1.5 ms^{-1}), because regional wind flows can enter this area during periods of moderate and strong synoptic forcing.
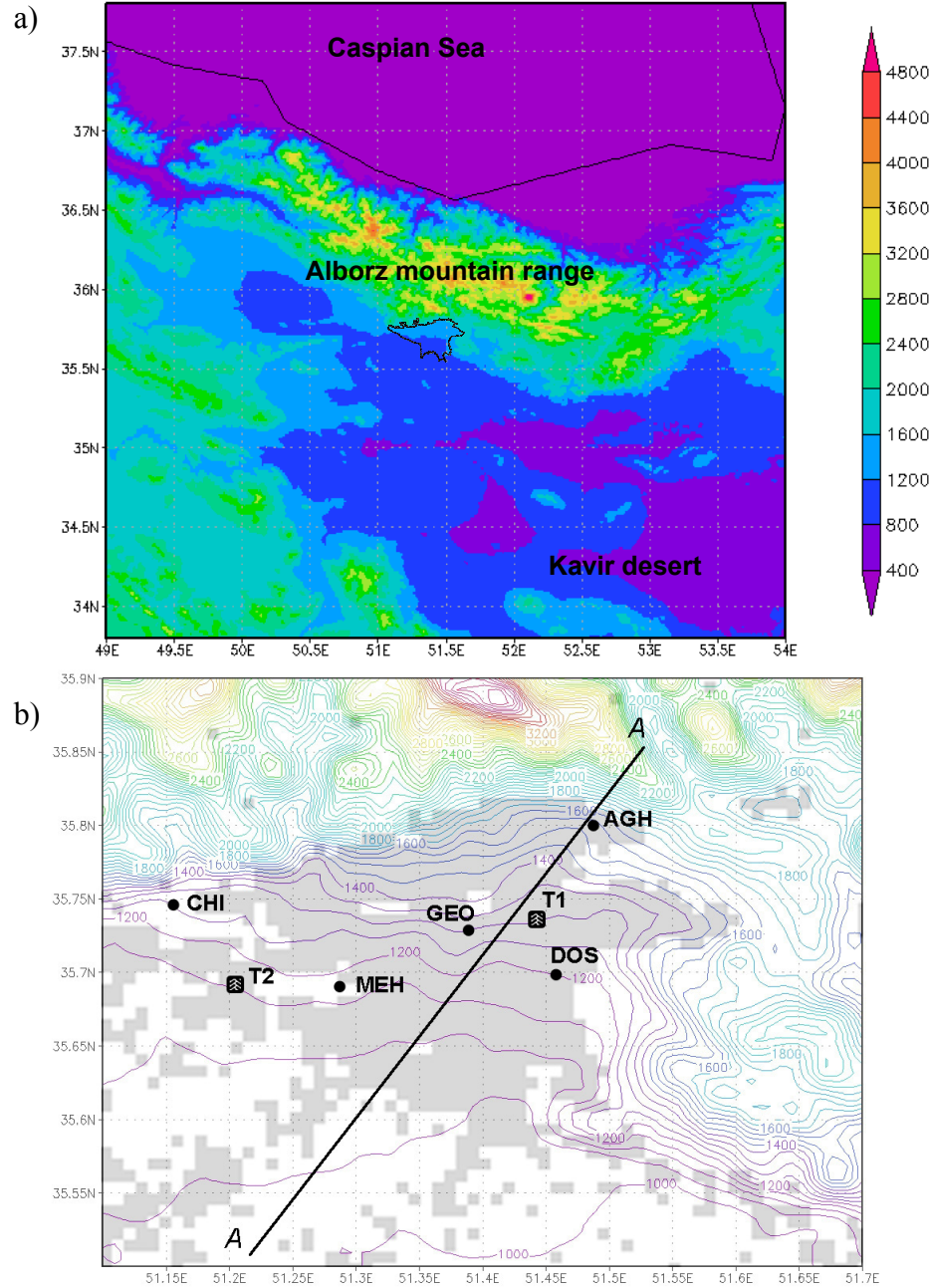
Figure 3.1: (a) Surface topography with 200 km around Tehran (400 km x 400 km, resolution of two km). The central black square indicates Tehran metropolitan: (b) Surface topography closed to Tehran (55 km x 45 km, resolution of one km), AGH: Aghdasiyeh station, DOS: Doshantapeh station, GEO: Geophysics station (including Sodar observation), MEH: Mehrabad station (including Radiosonde observation), CHI: Chitgar station, T1: Resalat tower and T2: Tehransar tower.

The vertical profiles of temperature and wind observations obtained with captive sonde and low level sonde during the JICA campaign (a: October 8, through October 15, 1996 and b: February 22 through March 1, 1997) show some discontinuity originating from local circulations. As mentioned before, the thick southwesterlies toward the northern mountains during daytime and the shallow northeasterlies from the mountains correspond to the up slope and down slope winds, respectively. during the day, the prevailing wind direction is SSW~SW, SW, SSW~SW and SW~WSW at the surface level, 50 m, 100 m, 150 – 400 m, and 450 – 700 m, respectively; at night, NNE~NE prevails at the surface, N – NE at 50 m and WSW in upper 300 m, but there is no prevailing wind direction between 100 and 250 m (JICA, 1997).

The inversion observed at night and early morning forms by a combination of surface radiative cooling and cold advection of down slope winds especially in north east of Tehran (Aghdasiyeh station). The inversion thickness can sometimes exceed to more than 100 m and its difference temperature between the top and bottom can reach 5 °C (JICA, 1997).

The sodar observations at the Institute of Geophysics (see location in Figure 3.1) clearly illustrate an upslope flow during the day and downslope flow at night, both having magnitudes of ~1-3 m s^{-1} during weak synoptic forcing conditions (e.g. Figure 3.3). The main observations show strong time variations and wind observations show semi-periodic oscillations during both night and day with periods typically longer than 40 minutes that could be due to internal waves induced by drainage flows at night, instability of the upslope flow during the day (Bidokhti and Noroozi, 2004).

The thickness of anabatic flow was between 220–300 m and the thickness of katabatic flow appears to be decreasing with the increasing speed of headwinds aloft; typical thicknesses varied from 150 to 250 m. The morning and evening transitions were characterized by low speed and highly variable winds.
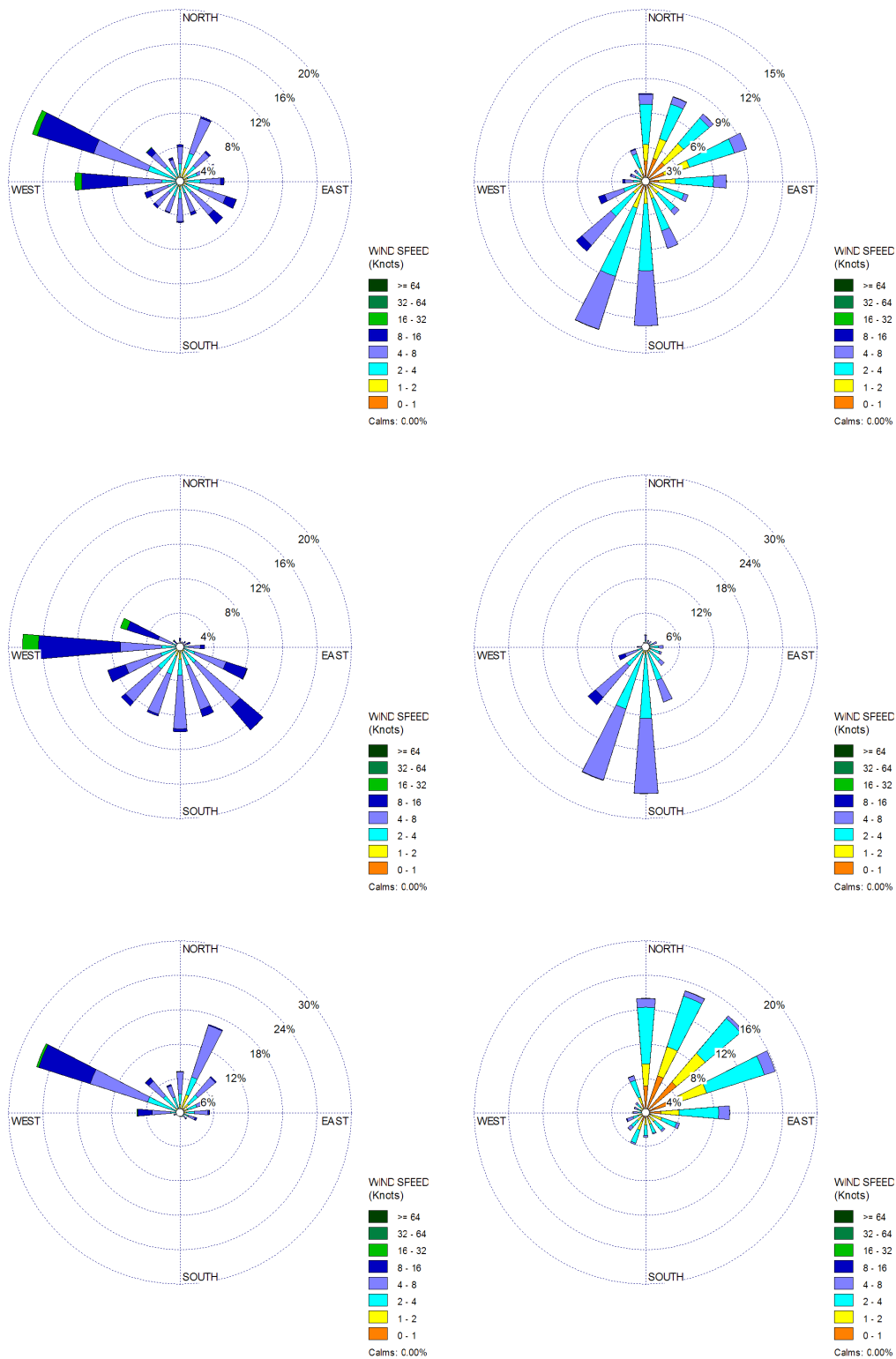
Figure 3.2: 10 meter windrose of Tehransar: "T2" (left ones) and Resalat: "T1"towers (rights ones), during the entire day (first row), between 8am until 4pm (second row) and 8pm until 4am (third row) in 2005.

Layers of different temperature and wind speed/direction characterize the vertical structure of the flow. The formation of such layers in TMC may occur due to different air masses of different densities originating at slopes of different orientations surrounding the air basin. This formation is similar that was observed on an eastern slop of the Salt lake basin during the Vertical Transport and Mixing Experiment (VTMX) and we have the same interpretation as Monti et al. (2002) for this case.

The TMC UHI intensity usually shows a maximum value in winter that can reach 6-7 °C at night; very high values of 9-10°C have been observed on calm winter nights. Such high UHI intensities are due to the anthropogenic heat effect that is the most important factor affecting UHI intensity at night.
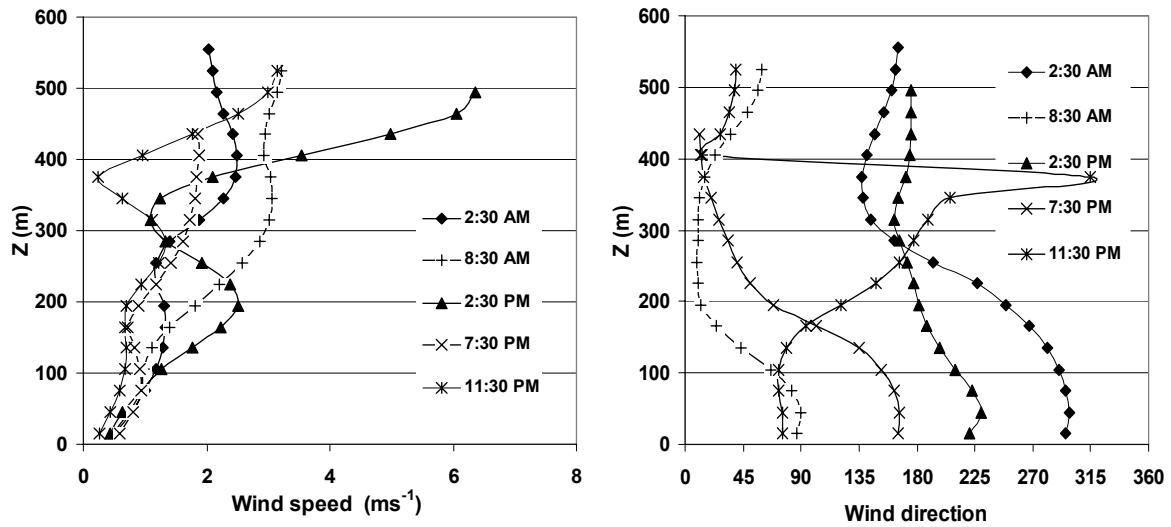
Figure 3.3: Observed vertical profiles of wind speed (left) and wind direction (right) by sodar at an urban location during December 5th, 2005.

3.2 Model and methods

In order to achieve realistic simulations of air quality at urban and neighborhood scales (i.e., on the order of 1-km horizontal grid spacing), detailed meteorological fields are required; particularly inside the roughness sub-layer (RSL). As discussed in chapter 1, the drag-force approach (DA) is preferable to the roughness approach at such scales (note that the latter is used by most mesoscale meteorological models). This chapter provides a

summary of applied urban parameterizations used in the model and the estimation of essential parameters used to initialize the modified model applied to the Tehran basin.

The model used in this study is the standard version of the fifth-generation Pennsylvania State University–National Center for Atmospheric Research Mesoscale Model (MM5; Grell et al. 1994) and a modified parameterization of MM5 that is called DA-SM2-U (Dupont et al., 2004). DA-SM2-U includes some improvements are able to simulate all meteorological fields within and above the rural and urban canopies.

The DA-SM2-U parameterization uses the DA approach to represent the dynamics and turbulent effects, (i) of the buildings following the work of Lacser and Otte (2002) and Martilli et al. (2002), and (ii) of the vegetation. The DA is developed inside the E - l Gayno-Seaman planetary boundary layer (GSPBL) model (Shafran et al., 2000). The DA is coupled with a modified version of the soil model SM2-U (Dupont et al., 2002 ; Dupont and Mestayer, 2006 ; Dupont et al., 2006), which is capable of determining the heat fluxes and surface temperatures in each in-canopy computational cell following the vertical distribution of the vegetation and buildings. In addition, it takes into account different detailed processes such as shadowing effects, radiative trapping inside street canyons, heat storage, vegetation transpiration, evaporation from the bare soil and from the water intercepted by the canopy elements, etc. A comparison of the drag-force approach (DA) coupled with urban soil model SM2-U with the roughness approach is illustrated in Figure 3.4 (see also section 1.3 of chapter 1).

A summery of DA-SM2-U modifications are present in this section that include considered morphological characteristics, the modifications to use the DA approach and the urban soil model "SM2-U(3D)", adapted for this approach. The modifications of the hydrological representation of roofs and vegetation are not described here because the model is not applied for a rainy event (see Dupont et al., 2006). The modifications of the vertical turbulent transport in DA approach modifications and also the surface temperature and heat flux equations related to the SM2-U(3D) soil model are not described here (see Dupont et al., 2004).

Table 3.1 presents the surface types considered in DA-SM2-U.

DA-SM2-U modifications have been implemented inside two main parts of MM5:

▪ MM5 GSPBL scheme by modification of the conservation equations and turbulence length.

▪ Soil model SM2-U by modification of the surface canopy heat fluxes equations and ground equations.
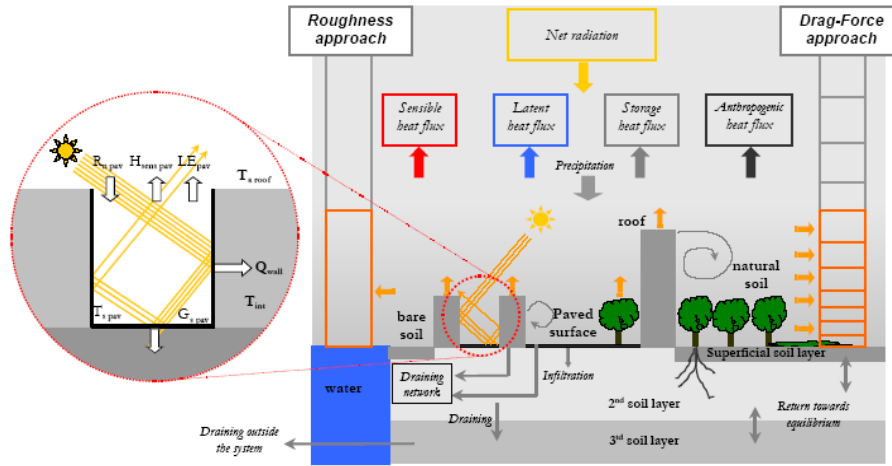
Figure 3.4: Scheme of the canopy parameterization of DA-SM2-U with layers inside the canopy, compared with the RA-SM2-U configuration (Dupont et al., 2004).

Table 3.1: Considered surface types in DA-SM2-U

Surface types for DA-SM2-U			
Nat	Bare soil located between the sparse vegetation elements	Pav	Paved surface located between the sparse vegetation elements
Bare	Bare soil without vegetation	Cova	Paved surface located under the vegetation
Vegan	Vegetation over the bare soil	Bui	Building roofs
Vega	Vegetation over paved surface	Wat	Water surface

The indexes and parameters used in DA-SM2-U for the urban canopy representation are listed below with their descriptions.

j: index for surface type
k: level above the ground
$Surf_j$ (k): top area density of the surface type '*j*' at the level k (m^2 m^{-2})
f_j: horizontal surface density of the surface type '*j* ' (m^{2}m^{-2})

$$Surf_{tot}(k) = \sum_j f_j Surf_j(k)$$:total top area density at the level k (3.1)

A_{fj} (k) and A_{pj} (k): frontal area density (m^{2}m^{-3}) and plan area density (m^2 m^{-3}), respectively

$$S_{air}(k) = (1 - f_{bui}) + \sum_{p=0}^{k-1} f_{bui} Surf_{bui}(p) \qquad \text{: horizontal air density at the level } k \qquad (3.2)$$

$$V_{air}(k) = \int_{z(k)-0.5\Delta z(k)}^{z(k)+0.5\Delta z(k)} S_{air}(z')dz' \qquad \text{: volume air density (m}^3\text{ m}^{-2}\text{) at the level } k \qquad (3.3)$$

where z is the altitude above the ground and Δz is the vertical thickness of the cell.

3.2.1 MM5 GSPBL scheme modifications

3.2.1.1 Momentum equation

$$\frac{\partial \rho <u_i>}{\partial t} = R_{ui} + F_{ui}^{bui} + \sum_j D_{ui}^j \qquad (3.4)$$

where ρ is the air density, $<\ >$ denotes the Reynolds averaged variables, u_i is the horizontal wind speed component, R_{ui} represents the general forcing terms in the equation of $<u_i>$ and the other two terms added to the momentum equation are:

- F_{ui}^{bui} corresponds to momentum sources due to the presence of horizontal surfaces of buildings.

$$F_{ui}^{bui} = -\left(\frac{\rho(k)}{V_{air}(k)}\right) \frac{f_{bui} Surf_{bui}(k)[u_{*bui}(k)]^2 <u_i(k)>}{(<u_x(k)>^2 + <u_y(k)>^2)^{0.5}} \qquad (3.5)$$

where u_{*bui} is the friction velocity induced by roofs.

- D_{ui}^j corresponds to momentum sources due to the pressure and viscous drag force induced by the presence of the vegetation and of the building vertical surfaces.

$$D_{ui}^j(k) = -\rho(k) C_{dj} A_{fj}(k) \langle u_i(k) \rangle \sqrt{\langle u_x(k) \rangle^2 + \langle u_y(k) \rangle^2} \qquad (3.6)$$

where C_d is the effective drag coefficient.

3.2.1.2 Thermal equation

$$\frac{\partial \rho \langle \theta_L \rangle}{\partial t} = R_\theta + D_\theta + A_\theta \qquad (3.7)$$

This equation is the liquid-water potential air temperature equation, θ_L is the liquid-water potential temperature, R_θ represents the general forcing terms in the equation of $<\theta_L>$ and the other two terms is added into this equation are:

D_θ corresponds to the sensible heat sources from buildings and the vegetation:

$$D_\theta(k) = \left(\frac{1}{V_{air}(k)}\right)\frac{H_{sens-mean}(k)}{c_p} \tag{3.8}$$

where $H_{sens-mean}(k)$ is the sensible heat flux emitted at the level k by buildings and vegetation per unit of ground (see Eq. 3.21 for details) and c_p is the specific heat of air. A_θ corresponds to the heat source from the anthropogenic heat flux Q_{urb} (see section 2.3.2 for details).

$$A_\theta(k) = \left(\frac{1}{V_{air}(k)}\right)\frac{Q_{urb}(k)}{c_p} \tag{3.9}$$

3.2.1.3 Humidity equation

$$\frac{\partial\rho\langle q_w\rangle}{\partial t} = R_q + D_q \tag{3.10}$$

This equation is the total air water content equation, q_w is the total water content equal to the sum of the specific humidity and the liquid water content, R_q represents the general forcing terms of this equation and D_q is added .

D_q corresponds to the humidity sources from buildings and vegetation (the evapotranspiration from the vegetation and the evaporation of the water intercepted by buildings).

$$D_q(k) = \frac{E_{mean}(k)}{V_{air}(k)} \tag{3.11}$$

where E_{mean} is the humidity flux per unit of ground from surfaces located at the level k inside the canopy (see Equ. 3.21 for details).

3.2.1.4 Turbulent kinetic energy equation

$$\frac{\partial E}{\partial t} = \underbrace{-\frac{\partial\langle u_i\rangle E}{\partial x_i}}_{[1]} + \underbrace{\left\{K_m\left[\left(\frac{\partial\langle u_x\rangle}{\partial z}\right)^2 + \left(\frac{\partial\langle u_y\rangle}{\partial z}\right)^2\right]S_{air} + F_E^{bui}\right\}}_{[2]} \tag{3.12}$$

$$+ \underbrace{\left\{\frac{g}{\theta_v}\langle w\theta_v\rangle + H_E\right\}}_{[3]} \underbrace{-\frac{1}{\rho}\frac{\partial(\rho\langle wE\rangle)}{\partial z}}_{[4]} \underbrace{-\varepsilon}_{[5]} + \underbrace{\sum_j W_E^j}_{[6]} - \underbrace{\sum_j D_E^j}_{[7]}$$

where E is the TKE, θ_v is the virtual potential temperature, g is the gravity acceleration, and K_m is the eddy diffusivity for momentum and the terms on the right-hand side of the equation represent:

[1]: advective transport term by the mean flow

[2]: dynamic shear production term that is divided into two parts, the first part corresponds to the dynamic shear production by the mean flow and the second part corresponds to the shear production by the building horizontal surfaces, which is parameterized from the friction velocity and the eddy diffusivity K_m for momentum:

$$F_E^{bui}(k) = \frac{f_{bui}Surf_{bui}[u_{*bui}(k)]^4}{K_m(k)}$$ (3.13)

[3]: buoyancy production term that is divided into two parts, the first part corresponds to buoyancy production by vertical heat flux (except D_θ and A_θ) and the second part corresponds to buoyancy production by D_θ and A_θ .

$$H_E(k) = \frac{g}{\theta_v(k)}V_{air}(k)[D_\theta(k) + A_\theta(k)]$$ (3.14)

[4]: turbulent transport term

[5]: turbulent dissipation term

[6]: TKE accelerated cascade term

$$W_E^j(k) = 4C_{ij}A_{fi}(k)(\langle u_x\rangle^2 + \langle v_y\rangle^2)^{1.5}$$ (3.15)

[7]: wake production term

$$D_E^j(k) = 4C_{ij}A_{fj}(k)(\langle u_x\rangle^2 + \langle u_y\rangle^2)^{0.5}E(k)$$ (3.16)

3.2.1.5 Turbulent length scale (TLS)

$$\frac{1}{l(k)} = \frac{1}{l_{BL}(k)} + \frac{1}{l_{can}(k)}$$ (3.17)

where l_{BL} ,TLS parameterisation of Bougeault and Lacarrère (1989), is derived from the upward and downward displacements (l_{up} and l_{down}) :

$$\frac{1}{l_{BL}} = \frac{1}{2}\left(\frac{1}{l_{up}} + \frac{1}{l_{down}}\right)$$ (3.18)

where l_{up} and l_{down} are determined from the following equations:

$$\int_{z}^{z+l_{up}} \frac{g}{\theta_{vs}}\left[\theta_v(z') - \theta_v(z)\right]dz' = E(z) \text{ and } \int_{z-l_{down}}^{z} \frac{g}{\theta_{vs}}\left[\theta_v(z) - \theta_v(z')\right]dz' = E(z)$$ (3.19)

where $l_{down} < z$, and θ_{vs} is the virtual potential temperature near the surface.

l_{can} is the TLS induce by higher canopy elements determined from the following equations:

$$\frac{1}{l_{can}(k)} = \sum_{p=k}^{k_{top}} \frac{\sum_{j} f_j Surf_j(p)}{[1 - Surf_{tot}(0)]} \frac{1}{z(p)}$$ (3.20)

for $Surf_{tot}(0) \neq 1$, and

$1/l_{can}(k) = 0$

for $Surf_{tot}(0) = 1$.

3.2.2 Description of the SM2-U(3D) Model

The new version of SM2-U, called SM2-U(3D), assesses at each level inside the canopy the heat fluxes (sensible and latent) from the canopy elements and the water intercepted by the canopy elements (Dupont, 2001 ; Dupont et al., 2002 ; Dupont et al., 2004 ; Dupont and Mestayer, 2006 ; Dupont et al., 2006). The ground part in SM2-U(3D) (i.e., the soil layer water content and the ground surface heat flux equations) is identical to SM2-U.The modifications of the hydrological representation of roofs and vegetation are not described here because the model is not applied for a rainy event. But with the DA, the roofs and vegetation water reservoirs are vertically distributed following the surface vertical distribution. Thus, the equations of evolution of the water intercepted by these reservoirs are solved at each level inside the canopy.

3.2.2.1 Mean heat flux inside the canopy

$$\Phi_{mean}(k) = \sum_{j} f_j Surf_j(k)\Phi_j(k) + f_{pav}\Phi_{pav}^*(k)$$ (3.21)

Φ : represents either the net radiation flux *(Rn)*, the sensible heat flux *(Hsens)*, the latent heat flux *(LE)*, or the storage heat flux *(Gs)*.

The superscript $*$ indicates that the variable has been modified from the initial parameterisation to consider the heat repartition inside the street canyons, which is described in Subsection 3.2.2.3-4. The parameterisations of the surface temperatures and of the sensible and latent heat fluxes are similar to those used in SM2-U but extend to all levels inside the canopy (Dupont et al., 2004).

3.2.2.2 Net radiation flux

$$R_{nj}(k) = \left[(1-\alpha_j) R_G(k_{top}) - \varepsilon_j \sigma \left(T_{sj}(k)^4 - \varepsilon_a T(k+1)^4 \right) \right] \times \exp\left[\frac{-k_{ex} \sum\limits_{p=k+1}^{k_{top}} \left[\sum\limits_i f_i A_{pi}(p) \right] \Delta z(p)}{|\cos Z_e|} \right] \qquad (3.22)$$

R_G is the direct and diffused solar radiation, σ the Stefan-Boltzmann constant, α_j and ε_j the surface albedo and emissivity, ε_a and T the air emissivity and temperature, $k_{ex} = 1.5$ the radiation extinction coefficient, and Z_e the zenith angle.

3.2.2.3 Latent heat flux from paved surfaces

$$LE^*_{pav}(k) = 0 \qquad (3.23)$$

the water interception by walls being neglected.

The latent heat flux is considered as emitted at the floor level, thus,

$$LE^*_{pav}(0) = \sum_{p=0}^{k_{top}} Surf^*_{pav}(p) LE_{pav}(p) \qquad (3.24)$$

where Surf$^*_{pav}$ is the top area density of the street canyon.

3.2.2.4 Sensible and net radiative fluxes

$$\phi^*_{pav}(k) = \frac{2\Delta z(k)\Psi_{w\to s}(p,k)}{\sum\limits_{t=1}^{p-1}\left[2\Delta z(t)\Psi_{w\to s}(p,t)\right] + W(p)\Psi_{r\to s}(p,0)}\phi_{pav}(p) \qquad (3.25)$$

where $\phi \in \{H_{sens}, R_n\}$, $\psi_{r\to s}(p, 0)$ is the sky view factor from the street canyon floor having its top at the level *p*, $\psi_{r\to s}(p, k)$ the sky view factor at the level *k* from one wall of

the street canyon having its top at the level *p*, and *W(p)* is the width of the street canyon having its top at the level *p*.

$$\phi_{pav}^{*}(0) = \frac{W(p)\Psi_{r\to s}(p,0)}{\sum_{t=1}^{p-1}\left[2\Delta z(t)\Psi_{w\to s}(p,t)\right] + W(p)\Psi_{r\to s}(p,0)}\phi_{pav}(p) \tag{3.26}$$

$$\phi_{pav}^{*}(k) = \sum_{p=k+1}^{k_{top}}\left[\frac{2Surf_{pav}^{*}(p)\Delta z(k)\Psi_{w\to s}(p,k)}{\sum_{t=1}^{p-1}\left[2\Delta z(t)\Psi_{w\to s}(p,t)\right] + W(p)\Psi_{r\to s}(p,0)}\phi_{pav}(p)\right] \tag{3.27}$$

$$\phi_{pav}^{*}(k) = \sum_{p=1}^{k_{top}}\left[\frac{2Surf_{pav}^{*}(p)W(p)\Psi_{r\to s}(p,k)}{\sum_{t=1}^{p-1}\left[2\Delta z(t)\Psi_{w\to s}(p,t)\right] + W(p)\Psi_{r\to s}(p,0)}\phi_{pav}(p)\right] + Surf_{pav}^{*}(0)\phi_{pav}(0) \tag{3.28}$$

$$W(p) = \frac{Surf_{pav}^{*}(p)(S_{bui})^{0.5}}{2Surf_{bui}(p)} \tag{3.29}$$

$$\psi_{r\to s}(p,k=0) = \left[\left(\frac{z(p)}{W(p)}\right)^{2} + 1\right]^{0.5} - \frac{z(p)}{W(p)} \tag{3.30}$$

$$\psi_{r\to s}(p,k) = \left\{\frac{z(p)-z(k)}{W(p)} + 1 - \left[\left(\frac{z(p)-z(k)}{W(p)}\right)^{2} + 1\right]^{0.5}\right\} - \left(\frac{z(p)-z(k)}{W(p)}\right)^{-1} \tag{3.31}$$

3.3 Model configuration

The coupling of DA with SM2-U (3D), is tested in the Tehran basin, during 2-8 December 2005 (three episodes as long as three days with one day overlap). The five nested computational domains use 81-, 27-, 9-, 3-, and 1-km horizontal grid spacing (see Figure 3.5). The standard version of MM5 was run in a one-way nested configuration for three outer domains by applying multiscale four-dimensional data assimilation (FDDA) as in Stauffer and Seaman (1994). FDDA is not used in the 3 and 1-km domains so as to

enable us to evaluate independently the influence of the UCP and also in order to avoid a significant loss in the contribution of diurnal variations in wind that can be important in quality of simulated local wind circulations at these fine resolutions.
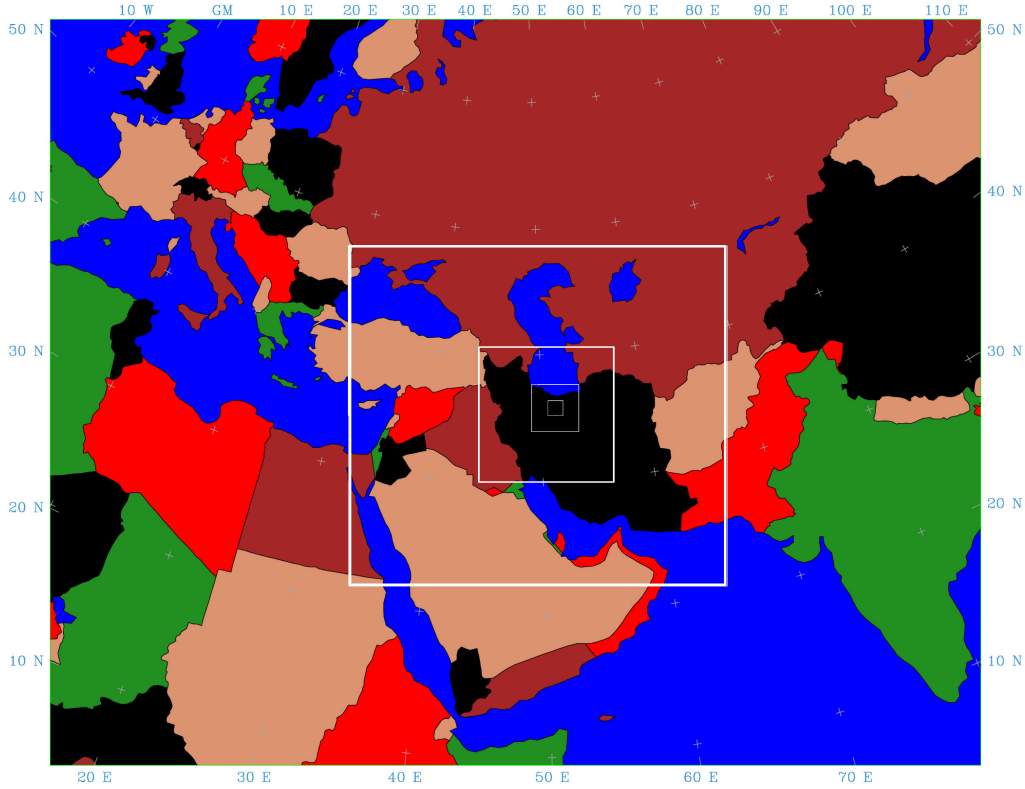
Figure 3.5: Configuration of computational domains.

For all three outer domains, the vertical resolution consists of 30 (terrain-following ''sigma'') layers (about 12 layers in the PBL with a lowest-layer depth of 20 m) and physics options appropriate for each resolution.

DA-SM2-U is used only on the 3 and 1-km inner domains. To compare DA-SM2-U with RA MM5 versions, other simulations using RA are performed: a 'standard' version of MM5 (hereafter, RA-SLAB) and other one, DA-SM2-U parameterization with switching off anthropogenic heat flux. These three MM5 configurations use the GSPBL model including the parameterization of the TLS of Bougeault and Lacarrère (1989) inside the PBL (described in sub-section 3.2.1.5).

For the two inner domains, the vertical resolution consists of 50 layers (12 layers were added in the lowest 100 m with lowest layer depth of 4 m), and the anthropogenic heat fluxes are considered as in DA-SM2-U to focus to the thermodynamic comparisons on the soil model parameterizations. Table 3.2 shows the model configuration for these two inner domains.

In RA-SLAB (standard version), there is a single urban category defined from the U.S. Geological Survey (USGS) 24-category database. By comparing Tehran GIS landuse data and urban landuse defined by WRF preprocessing system (WPS) and terrain module of MM5 model, we considered a bigger area for Tehran than the terrain module urban landuse. For DA-SM2-U parameterization, six urban sub-categories have been roughly constructed to cover the urban area following our simple classification, as represented in Figure 3.6. Each of these urban sub-categories is characterized by the surface density of buildings and buildings mean height (see Table 3.3). All physical properties of artificial surfaces are the same in each urban sub-category: buildings are represented with a) clay blocks wall-one way concrete block roof (60%), b) old brick wall - brick arch roof (40%), and with a horizontal section equal to 100 m^2, and paved surfaces are made with asphalt. For DA-SM2-U, the vertical distributions of buildings and vegetation have been constructed following their average height and the shaped profiles indicated in Figure 3.7. A mean vegetation height has been assigned for each of the USGS categories. It is assumed that the vertical distribution of the street canyon tops is identical to the roof vertical distribution, i.e., $Surf^*_{pav}$ = $Surf_{bui}$. The building plan and frontal area density, respectively $A_{p\text{bui}}$ and $A_{f\text{bui}}$, are deduced from the roof area density by considering that the roof area is equal to the building section area, which is assumed to be vertically constant.

The main differences of the parameterization of DA-SM2-U adapted in this work with the parameterization modified and evaluated in Dupont et al., (2004) work are the method used in order to present spatial and temporal distribution of anthropogenic heat flux (see Chapter 2) to the model. In recent work, anthropogenic heat flux is introduced into the model directly from heat emission data base in order to generate 4D anthropogenic heat flux distributions. In primary modifications anthropogenic heat flux was presented by fixed values for each urban subcategory.

**Table 3.2**: a) Model configuration for domains 1,2 and 3, b) different configurations in domain 4 and 5.

a)

Science Options	Configuration Domain 1 / Domain 2 / Domain 3	Details/Comments
Grid dimension	80✕100 / 109✕121 / 130✕130	(in Y ✕ X direction)
Horizontal grid mesh	81 / 27 / 9 km	
Vertical grid mesh	30 layers	
Model top	100 kPa	
Grid interaction	One-way interaction	
Initialization	NCEP Final Analyses (FNL) / LittleR	
Boundary conditions		
Cumulus scheme	Grell	(Grell et al., 1994)
Explicit moisture scheme	Mixed-Phase microphysics	(Reisner et al., 1998)
PBL scheme	MRF PBL	(Hong and Pan, 1996)
Shortwave radiation	Dudhia Scheme	(Dudhia, 1989)
Longwave radiation	Rapid-Radiation Transfer Model	(Mlawer et al., 1997)
Landuse and vegetation data	USGS	24 Category Scheme
Surface scheme soil model	Noah Land-Surface Model	(Chen and Dudhia, 2001)
Shallow convection	None	
Sea surface temperature	Do not update SST	
Thermal roughness	Default	
Snow cover effects	None	
4D data assimilation	3D analysis and Surface analysis nudging	(Stauffer and Seaman, 1994)
Simulation length	72 hours	
Integration time step	243 / 81 / 27 seconds	
Simulation periods	2005.12.02 - 2005.12.09	
Platform	Linux Intel P4 Cluster (16 processors)	Done at UMD

b)

Science Options	Configuration Domain 4 / Domain 5	Details/Comments
Grid dimention	136✕136 / 130✕130	(in Y ✕ X direction)
Horizontal grid mesh	3 / 1 km	
Vertical grid mesh	50 layers	
Initialization	Domain 3 / 4 output	
Boundary conditions	NESTDOWN module adjustment	
PBL scheme	Gayno-Seaman PBL RA approach	(Shafran et al., 2000)
	Gayno-Seaman PBL DA approach	(Dupont et al., 2004)
Urban categories	7 classes	
Surface scheme soil model	Force-restore	(Zhang and Anthes, 1982)
	SM2-U(3D)	(Dupont and Mestayer, 2006)
4D data assimilation	None	
Integration time step	9 / 3 seconds	

Table 3.3: Simple morphology classifications used for UCP parameterization.

Urban categories	Mean Height (m)	Roof fraction of the artificial surfaces
1	10	0.35
2	10	0.40
3	10	0.45
4	22	0.35
5	22	0.40
6	22	0.45
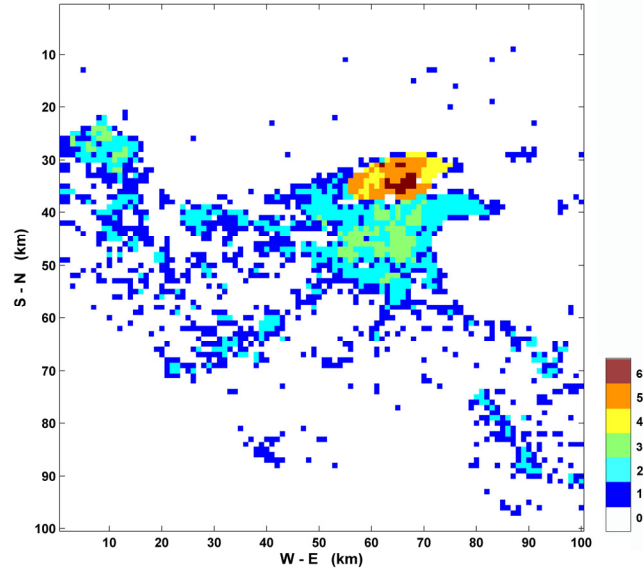
Figure 3.6: Grid cells designated as urban areas (by land use) are shaded in Tehran basin. Urban area is partitioned into urban subcategories 1–6 as shown on the map. Refer to Table 3.3 for definitions of these subcategories.
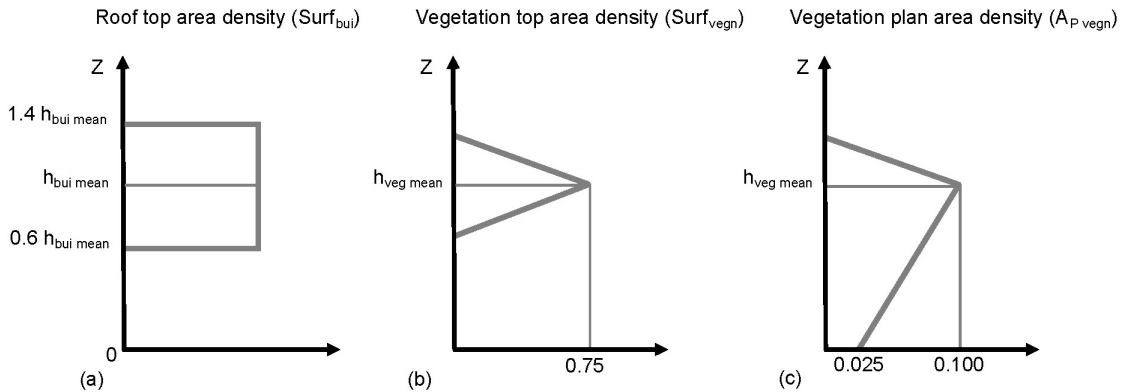
Figure 3.7: Shape profiles used for describing (a) the roof area density, (b) the vegetation area density, and (c) the vegetation plan area density. $h_{buimean}$ is the mean height of the building defined for each urban category, and $h_{vegmean}$ is the mean height of the vegetation defined for each vegetation category.

3.4 Case study simulations and results

3.4.1 Synoptic condition during episode

Clear skies and light crest-level (700 hPa) winds prevailed during the study period, allowing thermally driven winds to develop. Figure 3.8 shows the 500 hPa heights (m MSL) of model analysis (nest 2) including isotherms (°C) and wind field at 0330 LST (0000 UTC) December 5th 2005. At 500 hPa, the geopotential height gradient indicates large-scale zonal flow over Iran with a weak short-wave ridge moving eastward behind an exiting short-wave trough. At 700 hPa, relative humidities are low (<60%) and winds are light (<5 m s^{-1}) and northwesterly with little or no temperature advection.

Unfortunately, the archives of routine radiosonde meteorological upper air observations (00 and 12 UTC) in Mehrabad station have some failed sounding during 4-6 December 2005 (only 12 UTC in 5 Dec 2005 is available) and contains only meteorological data for synoptic levels.

Observed and simulated potential temperature, wind speed and wind direction profiles are shown in Figure 3.9.
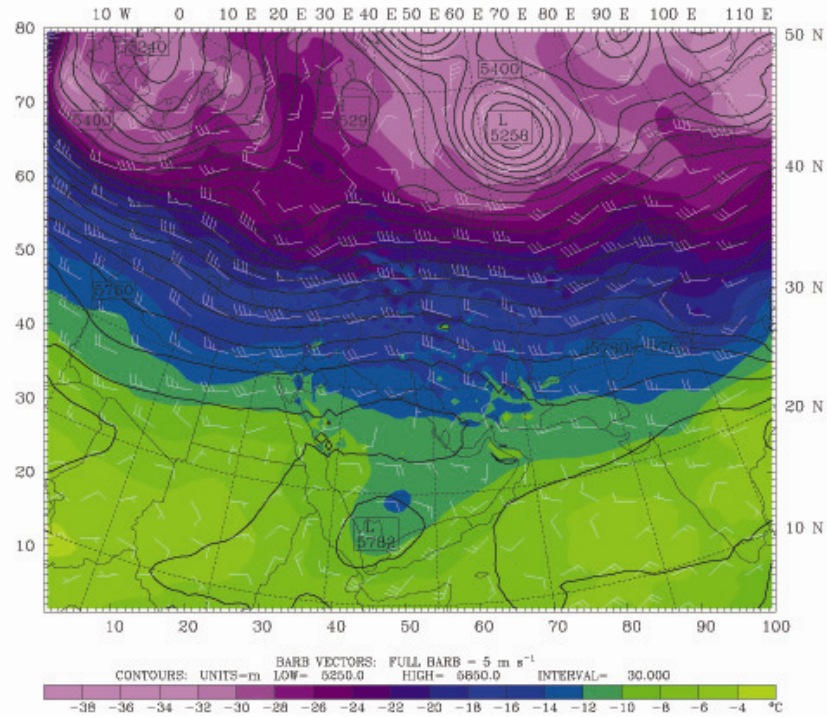

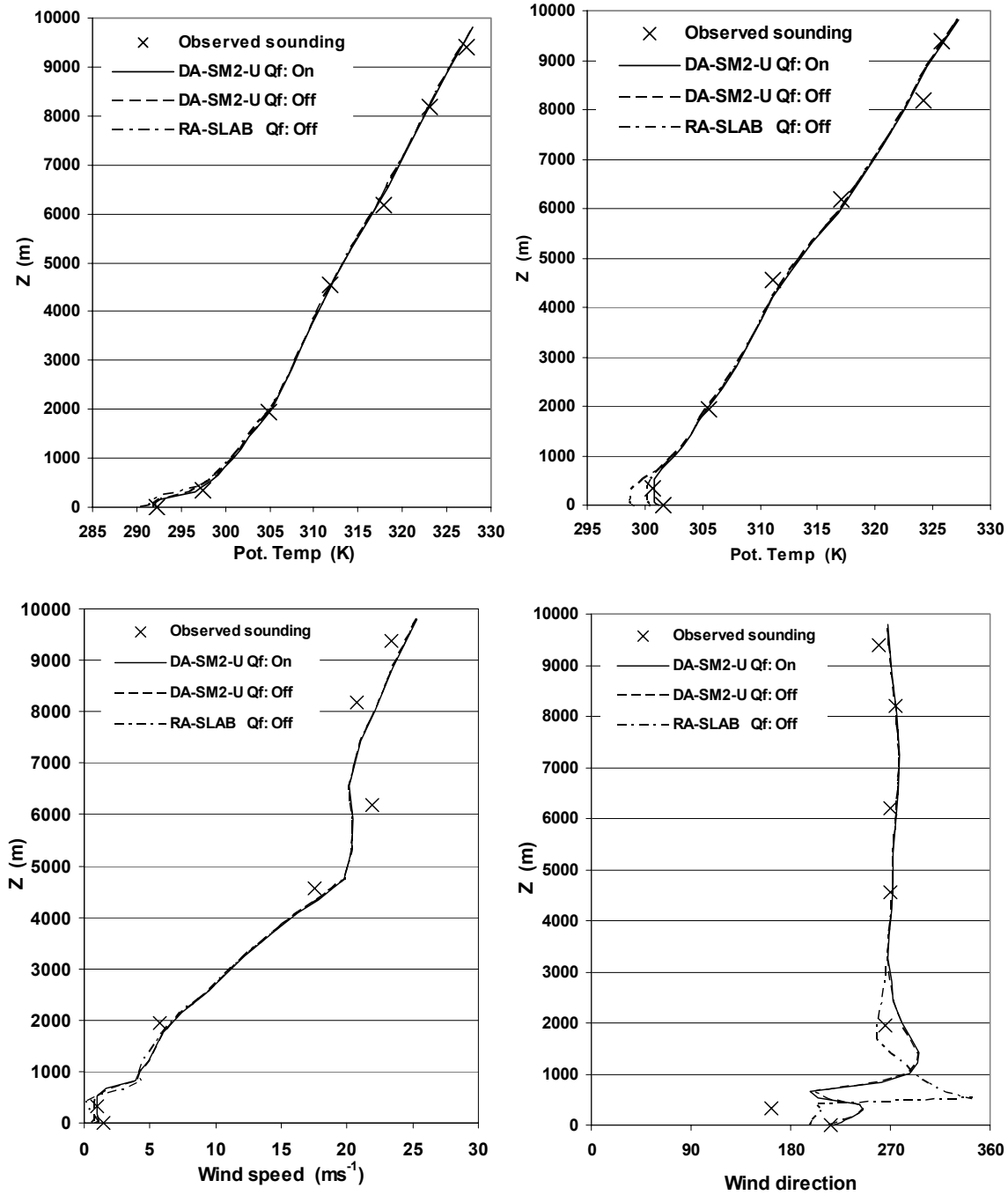**Figure 3.8**: Synoptic condition at 00 UTC December 5th 2005 [500mb chart].

Figure 3.9: vertical profiles of Potential temperature at 00 UTC (top left) and at 12 UTC (top right), wind speed at 12 UTC (down left) and wind direction (down right) at 12 UTC 5 December 2005.

3.4.2 Numerical experiments and observation data

We have selected here only simulations during the period of UTC 12:00 12/4/2005 – 12:00 12/7/2002. During this period, Tehran suffered fro; unhealthy air pollution condition. The first 5 hours were used as the model spin-up period and were not included in subsequent analyses.

3.4.2.1 Analyses of the Vertical Profiles inside the PBL

a) Potential air temperature

From the vertical profiles of the potential air temperature above the urban areas (Figure 3.10), it seems that DA-SM2-U simulates a neutral layer during the night up to 75 m above the urban canopy, and an unstable stratification within the urban canopy (building height and roof fraction are 22 m and 0.40 at this point respectively), however the "RA-SLAB Q_f: Off" simulates a stable stratification within the urban canopy. The urban neutral layer is consistent with the observed reduction of atmosphere stability near urban surfaces (Roth, 2000). As in Martilli et al. (2002), the depth of the neutral layer is in agreement with values given by Oke (1995). Inside the urban canopy, the air is constantly warmer than the air in the upper part of the RSL as observed by Rotach (1995) in a street canyon of Zurich. The PBL height (Mixing layer depth) in DA-SM2-U is simulated larger than one simulated by "RA-SLAB Q_f: Off" and showed an increasing to 550 m with "Q_f: Off" and to 650 m with "Q_f: On" during the day.

b) Wind

In the street canyon, the urban parameterization is able to represent the deceleration of the flow field resulting from the presence of obstacles (buildings and trees), while near the top of canopies it computes larger values (Figure 3.11). The reason for these differences arises from the fact that the urban parameterization takes into account the repartition of the drag force in the momentum equation along the vertical direction, from the ground up to roof height (Martilli, 2002). The RA approach calculates the momentum sink at the ground by calculating a friction velocity and, hence, produces a conventional log-type profile for wind speed, which does not hold in urban areas, as earlier field measurements

have shown (Rotach, 1993). By extending the momentum sink calculation, derived from the drag force that is produced by obstacles at each model layer, to the entire height of the building, the formation of a boundary layer resulting from shear with a rigid surface is shifted from the ground level (in RA approach) up to the top of the buildings (in DA approach).

Both simulations and sodar observations show a vertical structure of the flow with two layers during the nights. DA-SM2-U simulations do not show strong stratification in PBL flows that can be due to the building drag and thus more mixing in PBL. The RA approach overestimates wind speed in the first 100 m of PBL and its wind direction shows highly imprecise results (see Figure 3.12).

The thickness of the first layer of flow is about 250 and 350 m during the night and the day, respectively.
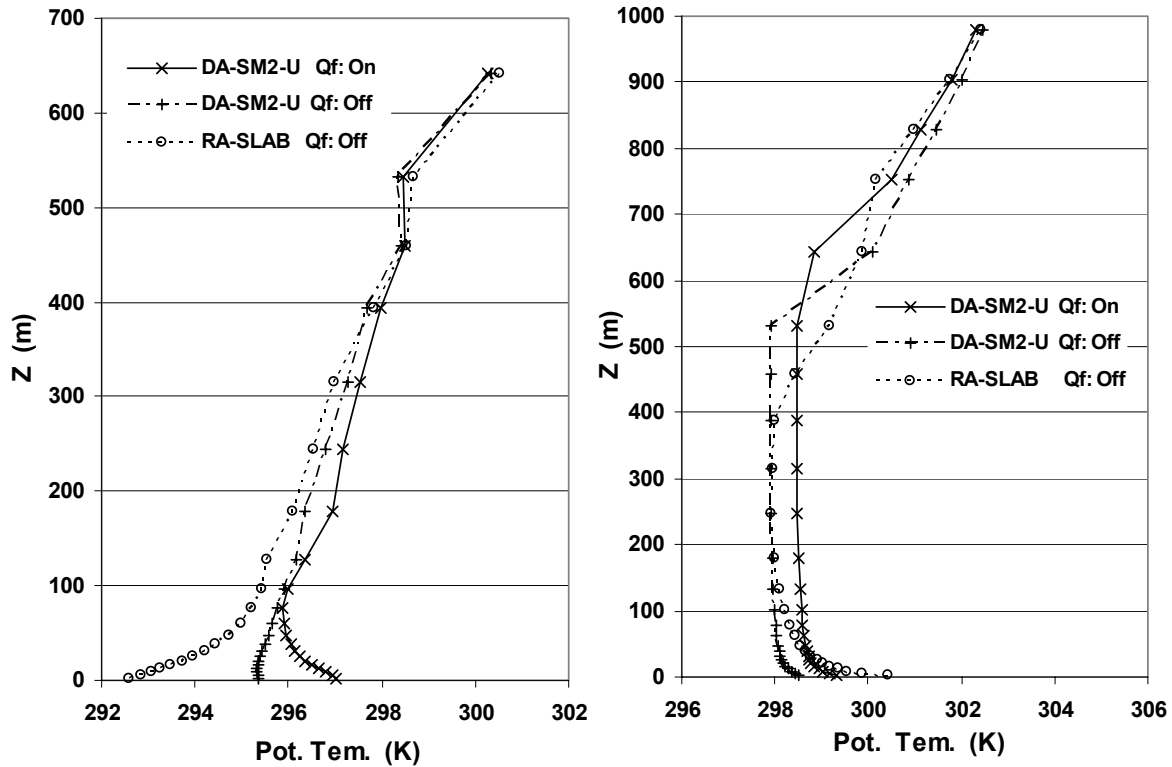
Figure 3.10: Vertical profiles of potential air temperature in urban point (Geophysics station: average in 2×2 km^2, average building height: 22 m) at 2 am (left) and 2 pm (Right) 5th December 2005, for the three simulations, "DA-SM2-U Q_f: On", "DA-SM2-U Q_f: Off" and "RA-SLAB Q_f: Off".
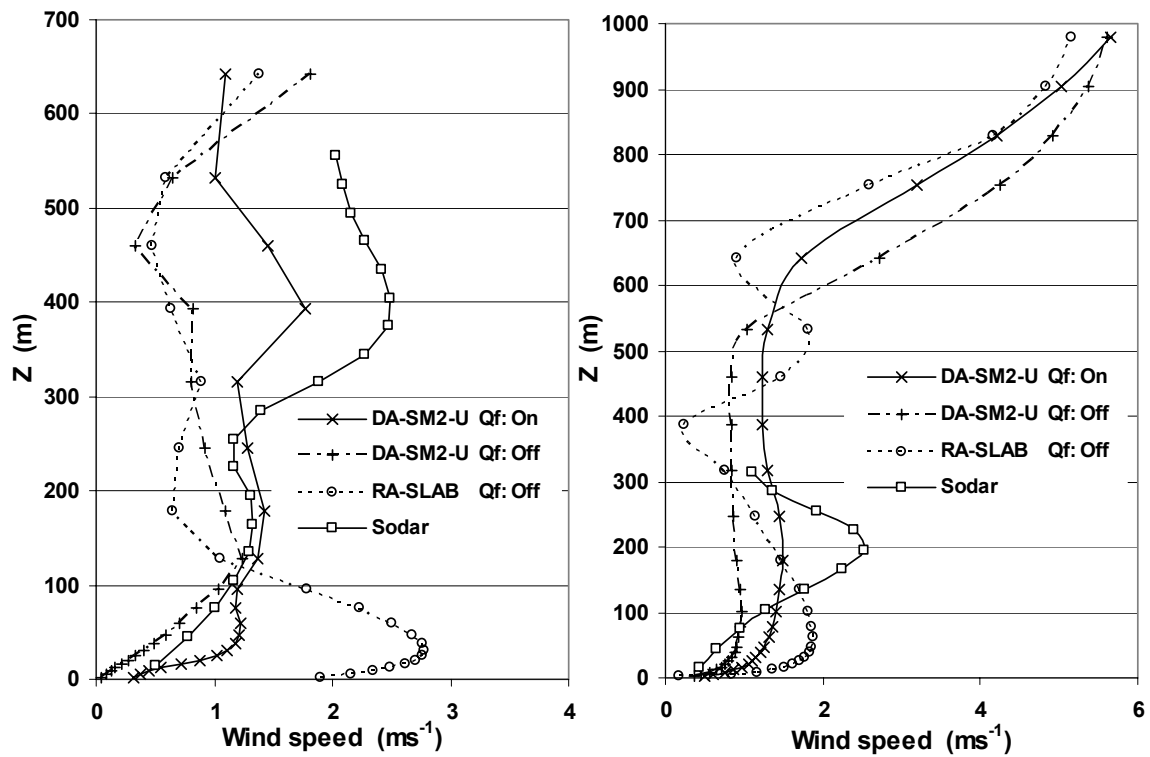
Figure 3.11: As in Figure 3.10, but for the wind speed and sodar observation.
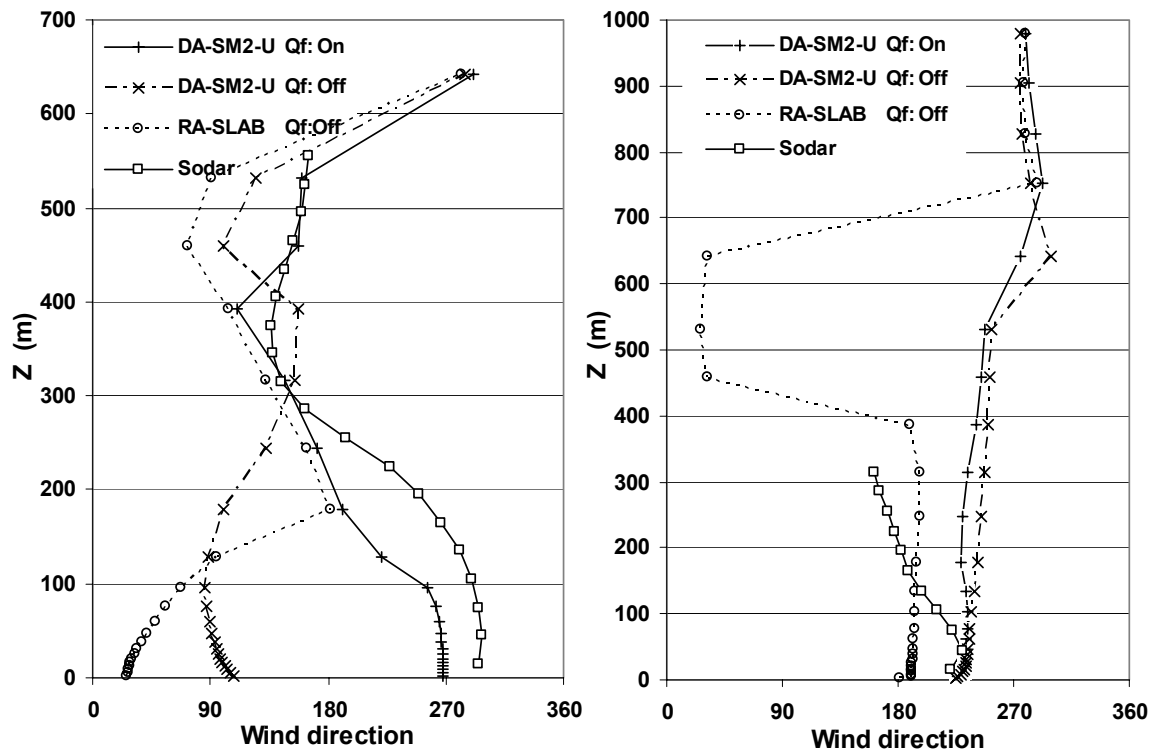
Figure 3.12: As in Figure 3.10, but for the wind direction and sodar observation.

C)TKE

the TKE profile simulated at urban location is presented in Figure 3.13. The DA-SM2-U TKE profile continues to increase above the urban canopy toward a quasi-constant value due to the stronger mixing inside the PBL during the day. In the TKE profile simulated without considering Q_f during night, one TKE maximum appears, which in induced by the shear production at the top of urban canopies for DA-SM2-U simulation and by the shear production near ground for RA-SLAB simulation, and another appears, which depends on the residual mixed layer. In simulation with "DA-SM2-U Q_f: On" configuration, this TKE maximum which is much larger appears in a higher height with more thickness due to convective mixing inside canopy. This TKE maximum has also been observed in near-neutral conditions by Kastner-Klein (2001) and Rotach (1995) for modeled and real urban canopies.

Martilli et al. (2002) have also simulated the same diurnal behaviour of the TKE profiles above an urban canopy, which is in agreement with measurements. However, the maximum values of the TKE profiles seem lower than measurements made in urban canopies by Rotach (1993), Oikawa and Meng (1995) and Louka et al. (2000).

Figure 3.13: As in Figure 3.10, but for the turbulence kinetic energy.

3.4.2.2 Surface Meteorological Fields

Figure 3.14 and 3.15 compare the 10-m wind speed, wind direction and the 2-m air temperature simulated by the three configurations with measur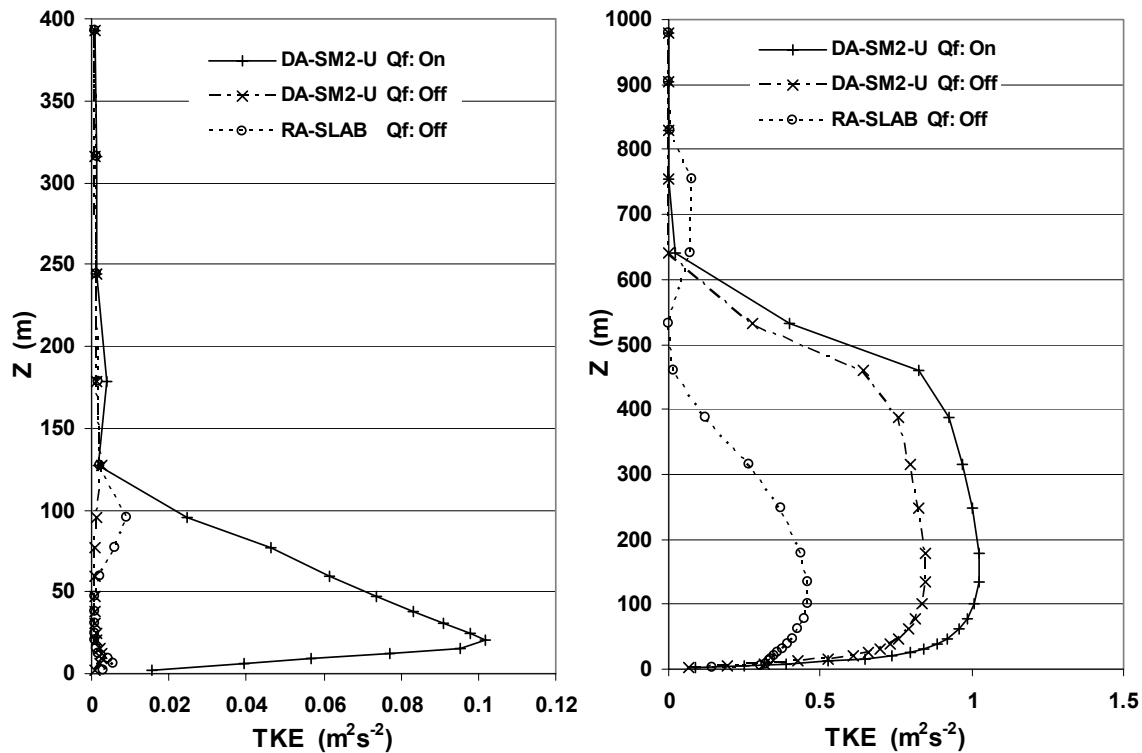ements in Resalat station (tower 1: T1) and in Tehransar station (tower 2: T2) during 5 December 2005. Resalat and Tehransar stations are located in west and east part of the Tehran city, respectively.

The 24-h evolution of T_{2m} simulated by RA-SLAB shows underestimation of T_{2m} up to 3 °C, whereas T_{2m} simulated by "DA-SM2-U Q_f: On" is very close to observations than "Q_f: Off" configuration. In the "Q_f: On" case, T_{2m} is overestimated by up to 0.4 °C during night, whereas underestimation of the "Q_f: Off" configuration is larger. Cooling in T_{2m} simulated by RA-SLAB starts around 2 pm, 1 hour earlier than that observed and simulated by "DA-SM2-U Q_f: On", whereas warming in T_{2m} simulated by RA-SLAB starts around 7 am, 1-2 hour later than that observed and simulated by "DA-SM2-U Q_f: On" at the urban stations. Variations in simulated diurnal temperature explain some of the differences in urban warming/cooling rates among them. RA-SLAB cools and worms at higher rates compared to those observed and simulated by "DA-SM2-U Q_f: On" at the urban sites in the morning and in the afternoon respectively (see Figure 3.14 and Figure 3.15). It results in a decrease of UHI intensity throughout the cooling period hours in RA-SLAB simulation. It is noticeable that the "DA-SM2-U Q_f: On" simulations reveal a decrease in the diurnal temperature range in interval of 0.31-1.27 °C in Tehran urban areas with spatial mean equal to 0.57 °C for all urban points from December 2 until December 9, 2005.

 The RA-SLAB simulation generally overpredicts the wind speeds (especially in Resalat station) whereas the DA-SM2-U with "Q_f: On" simulates wind speeds that match the observations slightly better.

The simulated and observed 24-h evolutions of wind direction represent daily and nightly regimes. The wind direction simulated by the RA-SLAB shows shorter period for anabatic flows than observations. It means that upslope winds start later and reverse sooner in this simulation than in the observations, whereas the "DA-SM2-U Q_f: On" simulates anabatic regime slightly better.
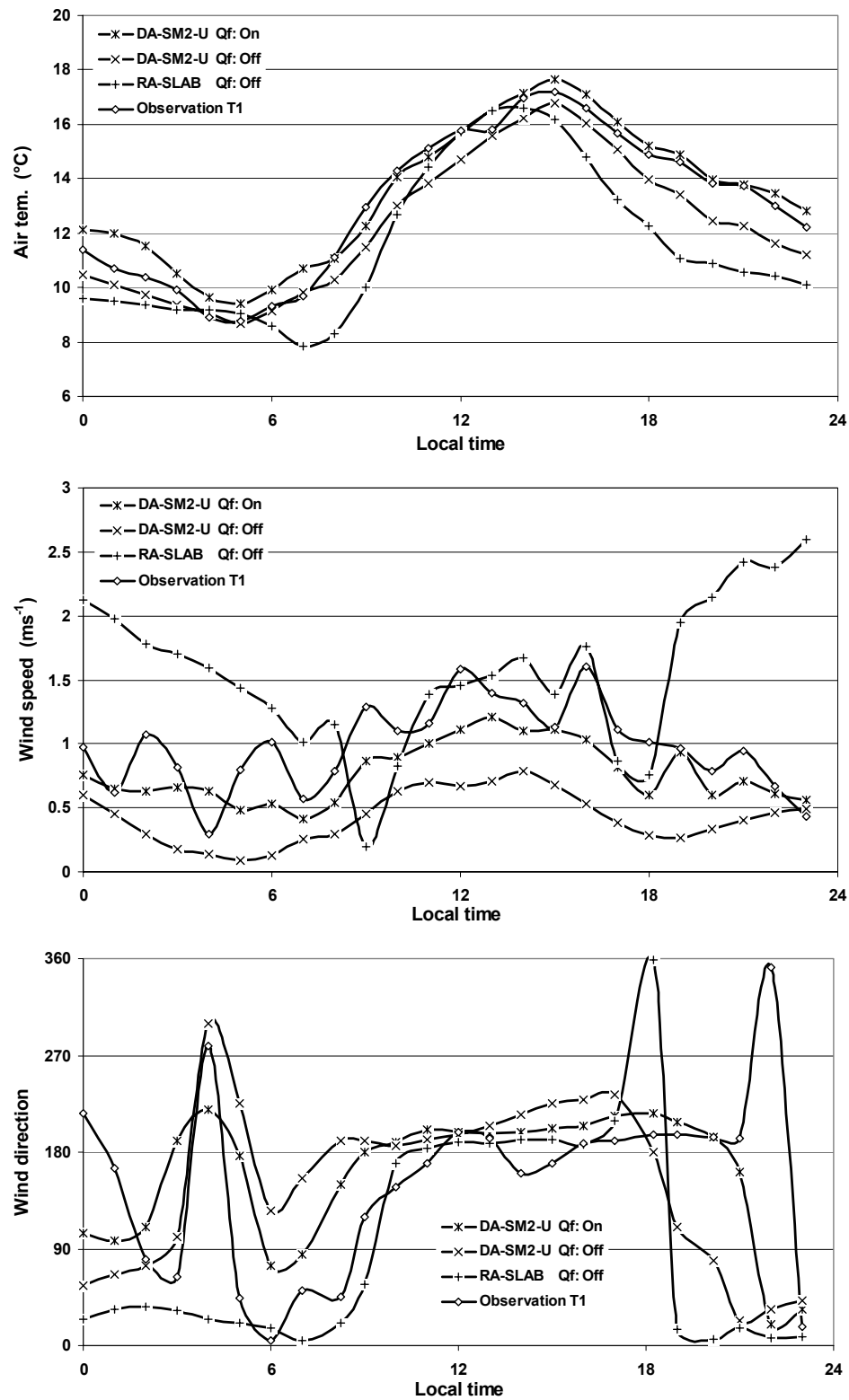
Figure 3.14: Comparison between the observed and simulated temperature at 2 m, wind speed and wind direction at 10 m in Resalat station (tower 1) during 5th December 2005.
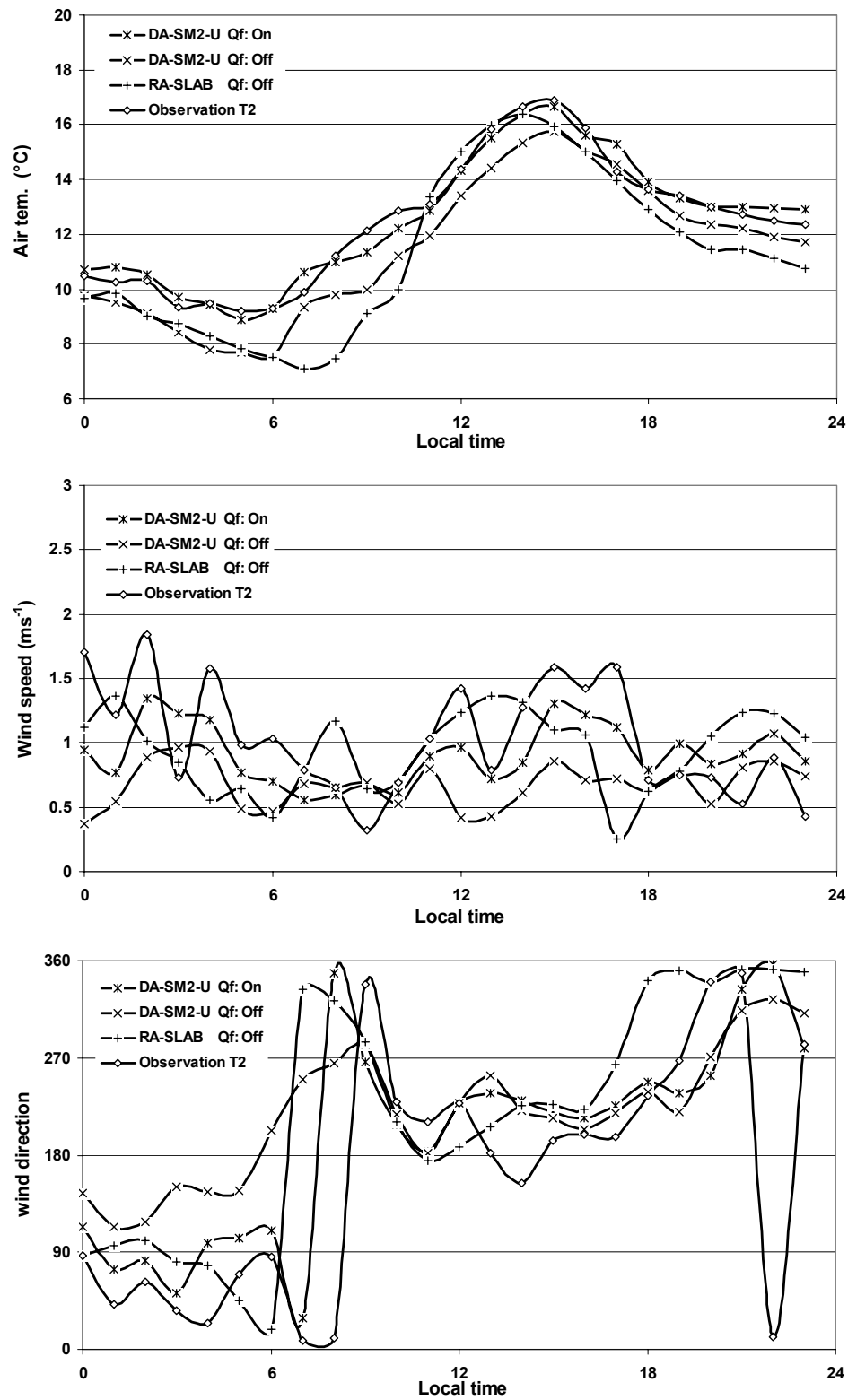
Figure 3.15: As in Figure 3.14, but for Tehransar station (tower 2).

Figure 3.16 shows time series of the root mean square error (RMSE) for temperature and root mean square (RMS) for vector wind difference (VWD) calculated for the five urban stations.

VWD allows for the total horizontal wind to be evaluated using a single statistic, and it is defined by Stauffer and Seaman (1990) as

$$VWD = \left[\left(U - U_o \right)^2 + \left(V - V_o \right)^2 \right]^{0.5}$$ (3.32)

where U and V are the horizontal wind components and the subscript O refers to the observed values.
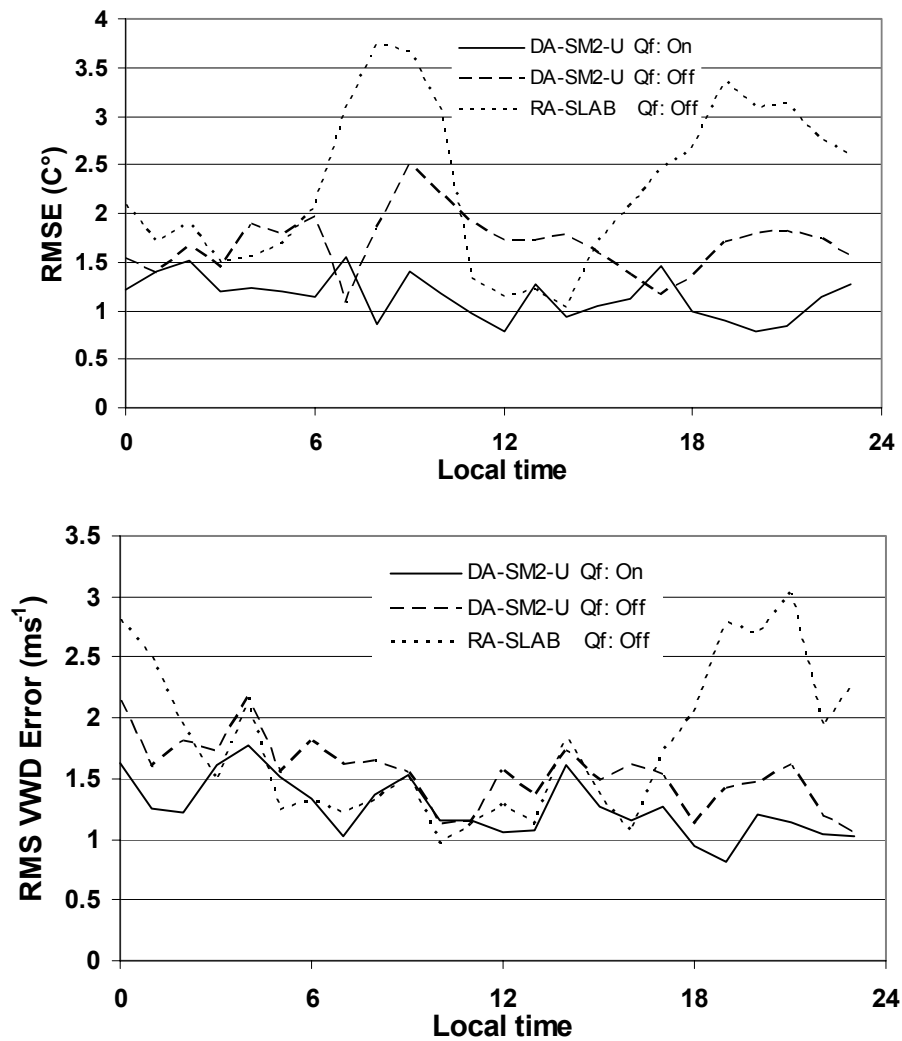
Figure 3.16: Time series of RMSE for temperature (top) and VWD rms (down) for urban sites (as shown in Figure 3.1), during 5 December 2005.

Several statistical measures are also computed using the observations of stations shown in Figure 3.1. Willmott (1982) suggests a variety of measures to quantify model performance (see table 3.4, that statistical parameters are provided). Figure 3.16 shows time series of RMSE for temperature and RMSE for vector wind difference (VWD) calculated only for the five urban sites for 5 December 2005. The temperature RMSE is usually lower for "DA-SM2-U Q_f: On" than others, only the hourly RMSE values in "DA-SM2-U Q_f: On" are higher than the "DA-SM2-U Q_f: Off" in transitions periods. Overall, RMSE in "DA-SM2-U Q_f: On" is below 1.52 C°. The result in "DA-SM2-U Q_f: On" can be attributed to the ability to simulate better the nocturnal urban heat island effects, as well as the improved maximum daytime temperatures, by specifically including urban radiation sources.

For the VWD, during nighttime hours, "DA-SM2-U Q_f: On" is nearly the best of the three cases. There is no clear trend in verification over day and "DA-SM2-U Q_f: On" is best at various hours except for two hours, similarly at night time. In fact, "DA-SM2-U Q_f: On" maintains a VWD rms of less than 1.71 ms^{-1}. When both fields are considered together, "DA-SM2-U Q_f: On" outperforms the simulations of "DA-SM2-U Q_f: Off" and "RA-SLAB Q_f: Off" overall for the urban sites.

Table 3.3 contains the aggregate 24-h statistics for all stations (see Figure 3.1) during 5-6 December 2005. For temperature, "DA-SM2-U Q_f: On" is consistently superior to "DA-SM2-U Q_f: Off" and "RA-SLAB Q_f: Off" for all statistical categories. The mean absolute error (MAE) and RMSE are reduced in "DA-SM2-U Q_f: On" by 0.5–1.2 K, and the mean error (MEAN ERR) is reduced by 1.3–1.8 K. The Mean error shows that a cold bias exists for "RA-SLAB Q_f: Off" and "RA-SLAB Q_f: Off", but shows a worm bias in "DA-SM2-U Q_f: On". The index of agreement (IOA) is higher with "DA-SM2-U Q_f: On", which suggests that it is a better model for temperature prediction. The generally high IOA for all cases results from the model's ability to capture the diurnal temperature cycle. The improvements in the urban nocturnal temperatures (as shown in Figure 3.14 and 3.15) account for some of the statistical advantage with "DA-SM2-U Q_f: On". The systematic error (SYS) and the unsystematic error (UNSYS) show that "DA-SM2-U Q_f: On" greatly improves the proportion of errors as compared with "DA-SM2-U Q_f: Off" and "DA-

SLAB-U Q_f: Off". Both "DA-SM2-U Q_f: Off" and "RA-SLAB Q_f: Off" have about 65% of the error attributable to systematic error, whereas it is about 41% in "DA-SM2-U Q_f: On".

As with the temperature, "DA-SM2-U Q_f: On" is consistently superior to "DA-SM2-U Q_f: Off" and "RA-SLAB Q_f: Off" in all statistical categories for wind. The MEAN ERR for wind speed shows that "RA-SLAB Q_f: Off" tends to overpredict and "DA-SM2-U Q_f: Off" tends to underpredict wind speed, whereas "DA-SM2-U Q_f: On" slightly underpredicts wind speed. There is an improvement of 0.3–1.5 m ms^{-1} in MAE with "DA-SM2-U Q_f: On". The IOA in "DA-SM2-U Q_f: On" is higher, and the RMSE is lower by 0.3–0.6 ms^{-1}. SYS is much lower in "DA-SM2-U Q_f: On" than "DA-SM2-U Q_f: Off" and "RA-SLAB Q_f: Off". For the mean VWD, during all observations, "DA-SM2-U Q_f: On" is the best of the three cases and the mean VWD is lower by 0.37–0.78 ms^{-1}.

These improvements in wind speed and direction in "DA-SM2-U Q_f: On", are important for simulating the transport and production of air pollutants through urban areas. When the mixing height and stability improvements are also considered for air-quality modeling at this scale, the "DA-SM2-U Q_f: On" might be better than the roughness approach "RA-SLAB Q_f: Off".

Table 3.4: Aggregate 24-h statistics for temperature and wind during 5-6 December 2005 for all urban sites.

$$MAE = \frac{1}{N}\sum_{i=1}^{N}|P_i - O_i| \; , \;\; ME = \frac{1}{N}\sum_{i=1}^{N}(P_i - O_i) \; , \;\; IOA = 1 - \left[\sum_{i=1}^{N}(P_i - O_i)^2 \Big/ \sum_{i=1}^{N}\left(\left|P_i - \overline{O}\right| + \left|O_i - \overline{O}\right|\right)^2\right]$$

$$Rmse = \left[\frac{1}{N}\sum_{i=1}^{N}(P_i - O_i)^2\right]^{0.5} \; , \;\; Rmses = \left[\frac{1}{N}\sum_{i=1}^{N}(\hat{P}_i - O_i)^2\right]^{0.5} \; , \;\; Rmseu = \left[\frac{1}{N}\sum_{i=1}^{N}(P_i - \hat{P}_i)^2\right]^{0.5}$$

$$SYS = \frac{MSES}{MSE} \;\; \text{and} \;\; UNSYS = \frac{MSEU}{MSE}$$

O_i : observed quantity
P_i: model-predicted quantity
N: number of observations
$\overline{O}$: mean of the observed variable
$\hat{P}$: least squares regression that compare observed and predicted ($\hat{P}_i = a + bO_i$)

MAE: mean absolute error
ME: mean error
IOA: index of agreement (dimensionless)
Rmse: root mean-square error
Rmses: systematic Rmse
Rmseu: unsystematic Rmse
SYS: systematic portion of the error (fraction)
UNSYS: systematic portion of the error (fraction)

	Wind statistics								
	MAE (ms⁻¹)	ME (ms⁻¹)	IOA	Rmse (ms⁻¹)	Rmses (ms⁻¹)	Rmseu (ms⁻¹)	SYS	UNSYS	VWD (ms⁻¹)
DA-SM2-U Q$_f$: On	0.97	-0.16	0.72	1.26	0.78	0.99	0.38	0.62	1.14
DA-SM2-U Q$_f$: Off	1.29	-0.61	0.61	1.54	1.01	1.16	0.43	0.57	1.51
RA-SLAB Q$_f$: Off	1.43	1.19	0.56	1.88	1.43	1.22	0.58	0.42	1.92

	Temperature statistics							
	MAE (K)	ME (K)	IOA	Rmse (K)	Rmses (K)	Rmseu (K)	SYS	UNSYS
DA-SM2-U Q$_f$: On	0.63	0.33	0.98	1.12	0.73	0.88	0.41	0.59
DA-SM2-U Q$_f$: Off	1.12	-1.01	0.95	1.64	1.33	1.02	0.63	0.37
RA-SLAB Q$_f$: Off	1.87	-1.53	0.89	2.29	1.87	1.28	0.68	0.32

3.4.2.3 Meteorological Fields within and above the Canopies

The air temperature and the wind fields near the ground are particularly dependent on the structure of the urban canopies and on their parameterization, as well as on the heat fluxes emitted by the canopy elements. Just above the canopy, these meteorological fields are influenced by the heat and momentum fluxes from the canopies. Their correct simulation is critical since it is principally at this level that the pollutants arising from the canopy are dispersed toward neighboring areas. In this section, the air temperature and wind fields simulated by three configurations are analyzed at a height of 2 m above the ground surface (within the canopy), and at a height of 40 m above the ground surface (above the canopy). In order to analyze the wind and air temperature fields in the Tehran region, we focus on a part of the computational domain that includes urban area and surrounding valleys and mountains (see Figure 3.1). This area represents a region with a very complex wind regime, where an interaction between UHI circulation and mountain/valley winds exists. Although, the frequency of the appearance of the mountain/valley winds is more than 75% of the days during the year (see Figure 3.2).

It is expected that fields simulated with "DA-SM2-U Q_f: On" show interaction among UHI and mountain-valley circulations better than other configurations.

3.4.2.3.1 Within the canopy

From air temperature fields, the urban canopy is warmer than the surroundings at the same elevation because of the heat released by the urban artificial surfaces and anthropogenic sources and also morphology-radiation effects (see chapter 2). Additionally, the small ventilation inside the urban canopies accentuates the difference of temperature between the air inside the canopies and above the open areas by decreasing the renewal of air. The air temperature decreases rapidly above the open areas whereas the air remains warm within the canopies, as observed during the night.

Figure 3.17 and Figure 3.18 represent the simulated air temperature fields at 2 m above the ground in the Resalat and Tehransar stations at 4 am and 4 pm on December 5th, 2005, respectively. The air temperature simulated by "DA-SM2-U Q_f: On" at 2 m AGL shows the greatest canopy layer UHI intensity up to 8 °C at night. This intensity was in the range

of 1° to 3°C with this configuration during the day. The "DA-SM2-U Q_f: Off" simulated canopy layer UHI intensity is up to 4 °C at night and in the range of 1° to 2°C during the day. The "RA-SLAB Q_f: Off" is not capable to simulate the canopy layer UHI intensity correctly, because of over-predictions of upslope and downslope flows and their temperature advections.

Figure 3.19 and Figure 3.20 present the simulated wind fields at 2 m above the ground in Tehransar and Resalat stations at 4 am and 4 pm on December 5th, 2005, respectively. The results demonstrate the model's ability to simulate the interaction between UHI and mountain-valley flows in this area. The wind field simulations by the RA-SLAB approach show that, in the main part of the city katabatic winds are dominated with one NW-SE wind front in southwest of city during the night. This approach represents anabatic winds during the day with a similar wind front between local wind and synoptic regime. As discussed above, wind speeds simulated with this configuration are overpredicted and show the same regime over the entire city in contradiction observations. The "DA-SM2-U Q_f: Off" simulates katabatic and anabatic winds with lower speed and this flows cannot dominate the entire city. The building drag can be one of reasons for decreasing the topographic flow intensity in Tehran area by this simulation, because the north Tehran area are introduced with higher and medium density of building canopies. The interaction between topographic flows and flows forced by UHI is more complex than obtained with the RA-SLAB results, especially during night. The wind field simulations with the "DA-SM2-U Q_f: On" approach, show that only the suburban part of city is dominated by topographic flows whereas the center and south of city are more affected by UHI forcing during night. It means that flows in low elevations are dominated by UHI thermal forcing. Furthermore, during the night period, the combination of katabatic winds with the UHI is conjoined by upslope flow from the south which causes an amplified UHI in this simulation. It means that cold advection induced by katabatic winds and upslope flow from the other side generates a strong UHI during the night. This convergence induced by combination of locals and non local regimes is evident in wind fields simulated by "DA-SM2-U Q_f: On" approach during night (see Figure 3.19).

In the "RA-SLAB Q_f: Off" simulation, the cold advection induced by topographic flows shows an important role in control of temperature felids in this basin and how conflict with the UHI forming and observations.

During the night, all simulations show one horizontal temperature gradient in southwest of city that it relates to the front between two different wind regimes (local and non-local).

3.4.2.3.2 Above the canopy

Figure 3.21 and Figure 3.22 present the air temperature fields at 40 m above the ground in Tehran region at 4 am and 4 pm on December 5th, 2005, respectively. The nocturnal air is warmer for the DA-SM2-U configuration above the city, whereas it can be warmer in some area where convergence occurs in lower levels in city.

The UHI intensities are up to 4, 2 and 0.3 °C in simulations conducted with "DA-SM2-U Q_f: On", "DA-SM2-U Q_f: Off" and RA-SLAB approaches, respectively, during night. They show lower values than within canopy UHI intensities. The UHI intensities decrease to 1, 0.5 and 0 °C, respectively, during the day. The presence of a small heat island during the day is in agreement with previous observations over many cities (Oke, 1978).

Figure 3.23 and Figure 3.24 represent the wind fields at 40 m above in the ground in the Tehran region at 4 am and 4 pm on December 5th, 2005, respectively. The wind fields simulated for this level are similar with inside canopy but show stronger winds. During the night, the phenomena of flowing southly countary breeze in south of Tehran can be important, because we have some stationary emission sources such as the Tehran refinery and main Tehran power plant in this area and it can cause the significant air pollution advection form these sources to the city. The pollutant advected in such conditions can be trapped by the flow recirculation inside the area induced by the UHI.

Figure 3.17: Temperature field simulated by "RA-SLAB Q_f: Off" (top), "DA-SM2-U Q_f: Off" (middle) and "DA-SM2-U Q_f: On "(bottom) at 2 m AGL at 4 am December 5th 2005.

Figure 3.18: As in Figure 3.14, but in 4pm.

Figure 3.19: Wind vector simulated by "RA-SLAB Q_f: Off" (top), "DA-SM2-U Q_f: Off" (middle) and "DA-SM2-U Q_f: On" (bottom) at 2 m AGL at 4 am December 5th 2005.

Figure 3.20: As in Figure 3.16, but in 4pm.

Figure 3.21: Temperature field simulated by "RA-SLAB Q_f: Off" (top), "DA-SM2-U Q_f: Off" (middle) and "DA-SM2-U Q_f: On" (bottom) at 40 m AGL at 4 am December 5th 2005.
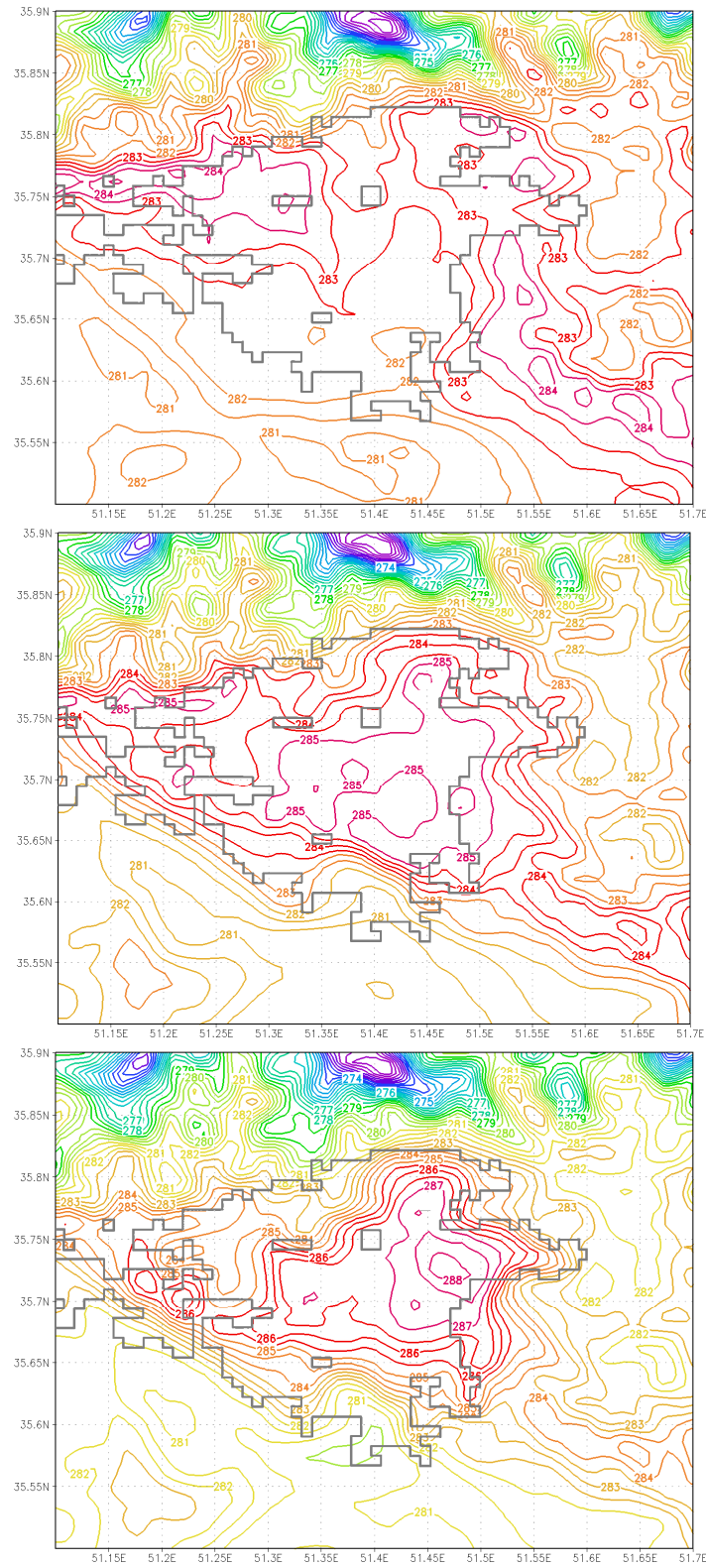
Figure 3.22: As in Figure 3.18, but in 4pm.

Figure 3.23: Wind vector simulated by "RA-SLAB Q_f: Off" (top), "DA-SM2-U Q_f: Off "(middle) and "DA-SM2-U Q_f: On" (bottom) at 40 m AGL at 4 am December 5th 2005.
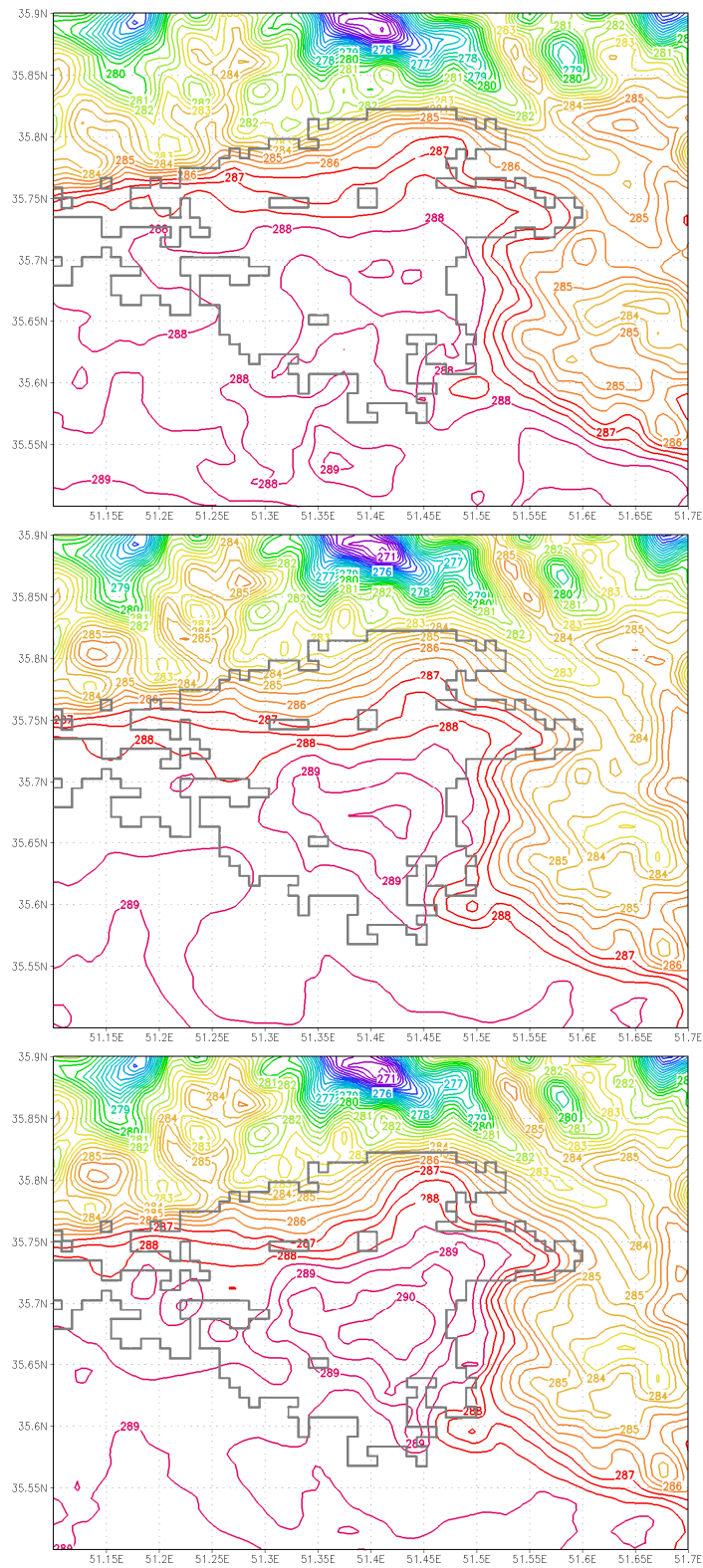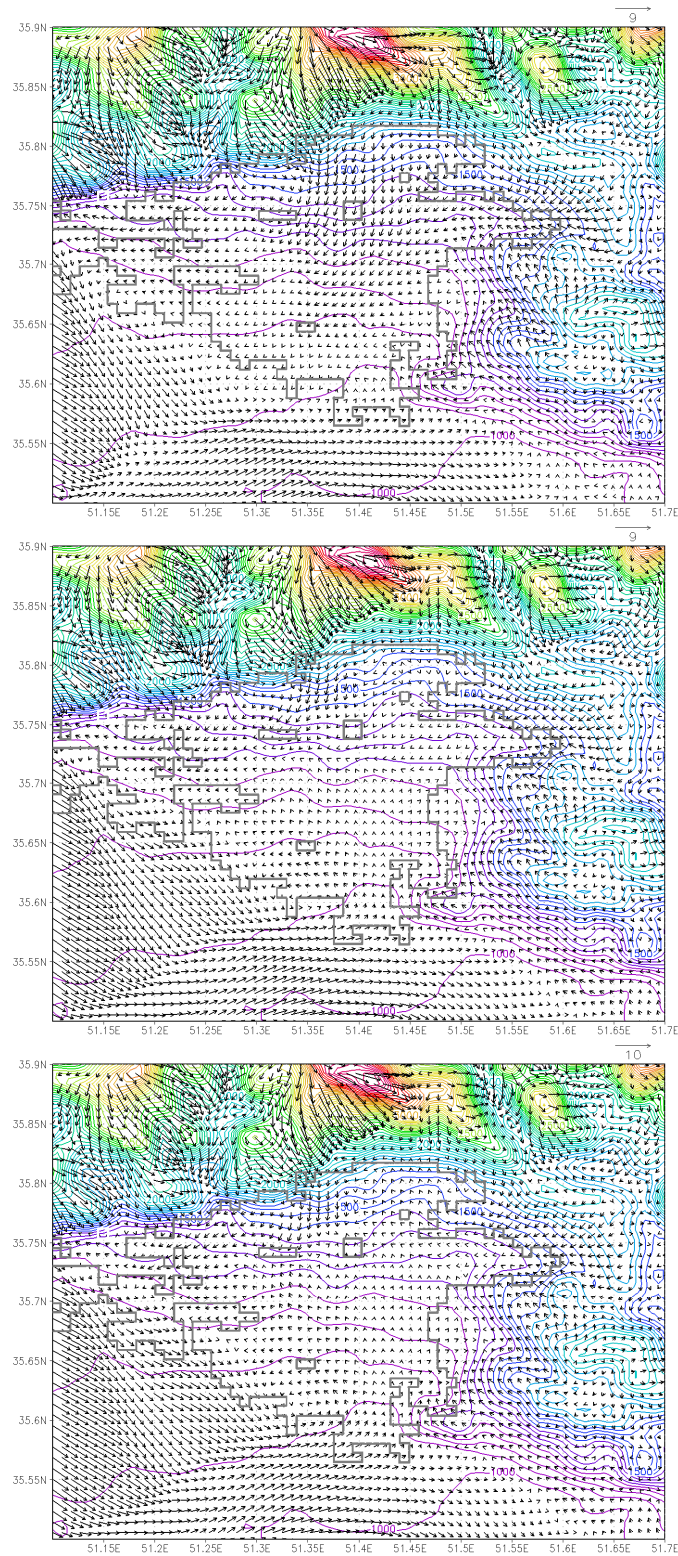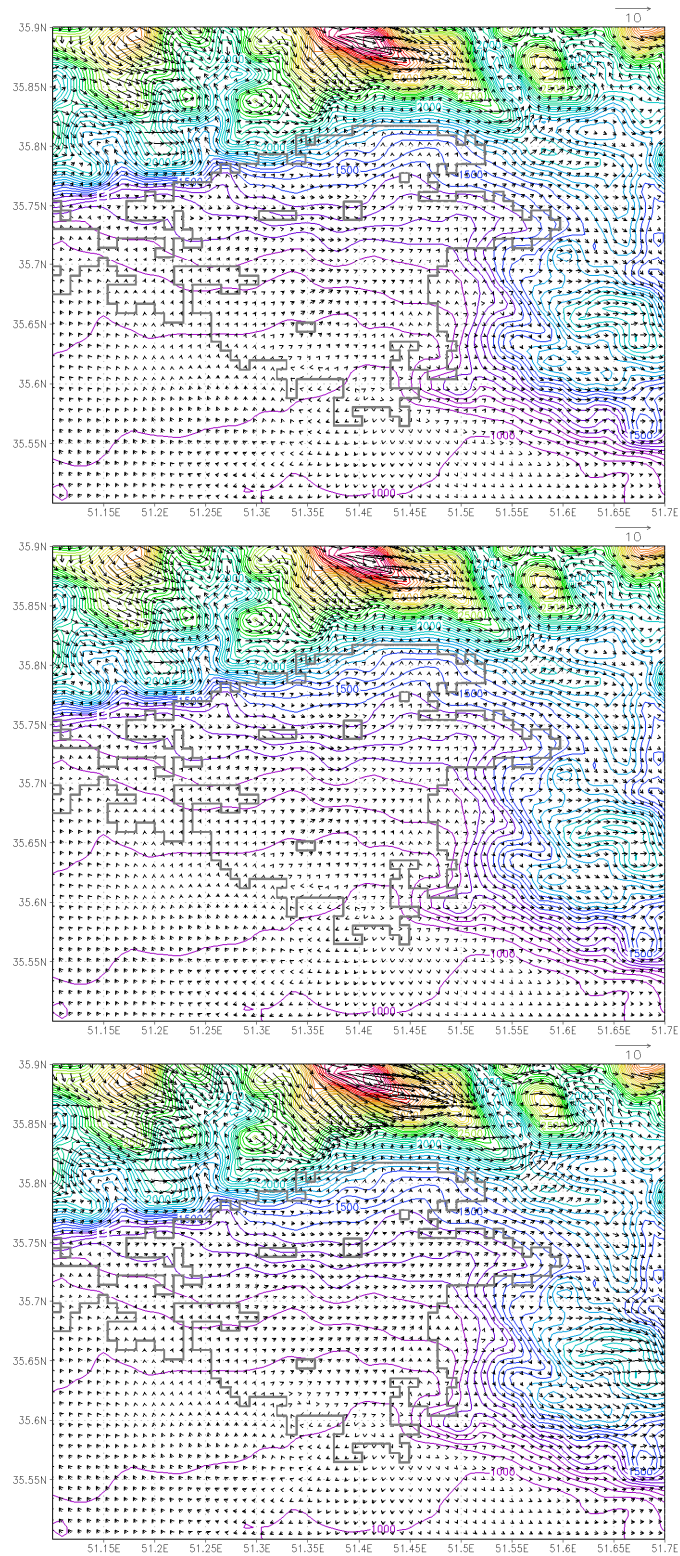
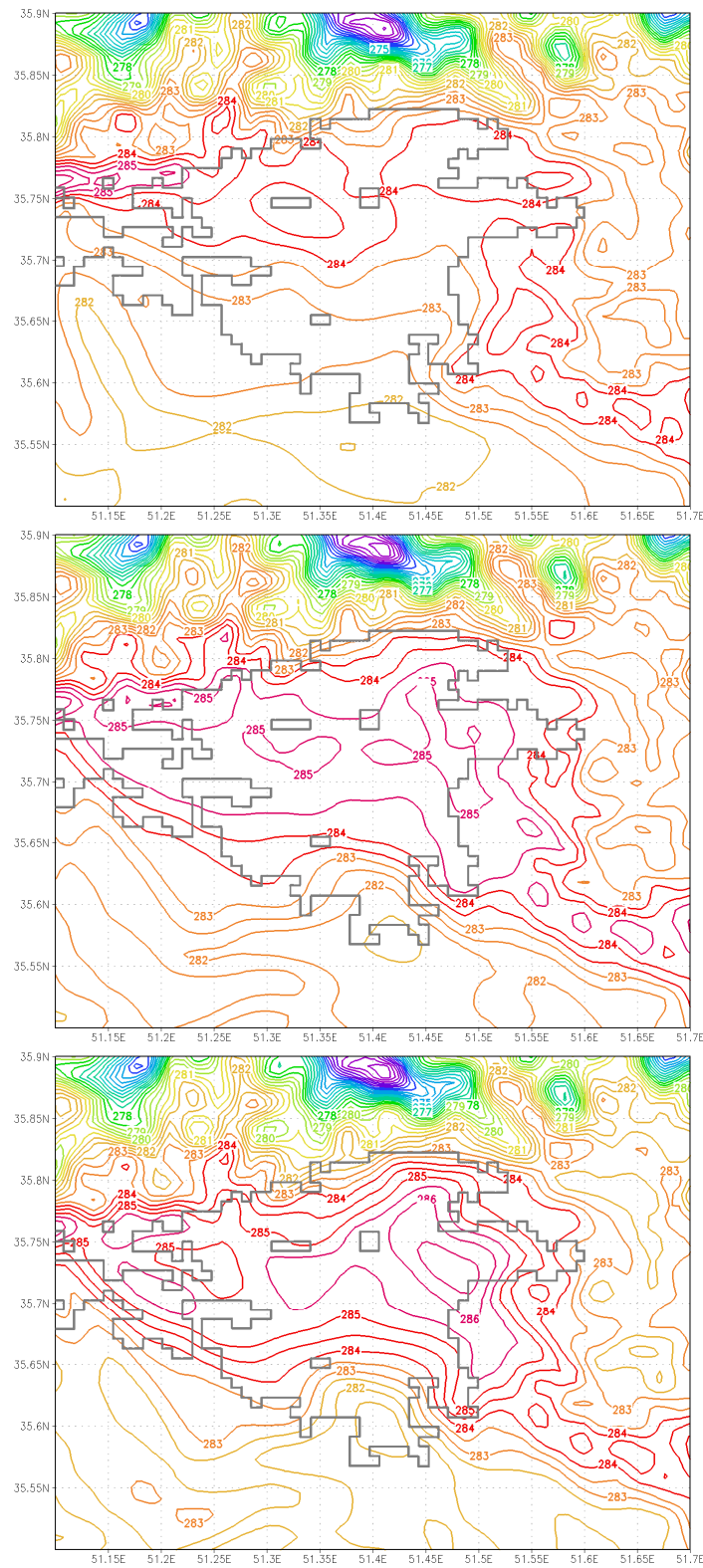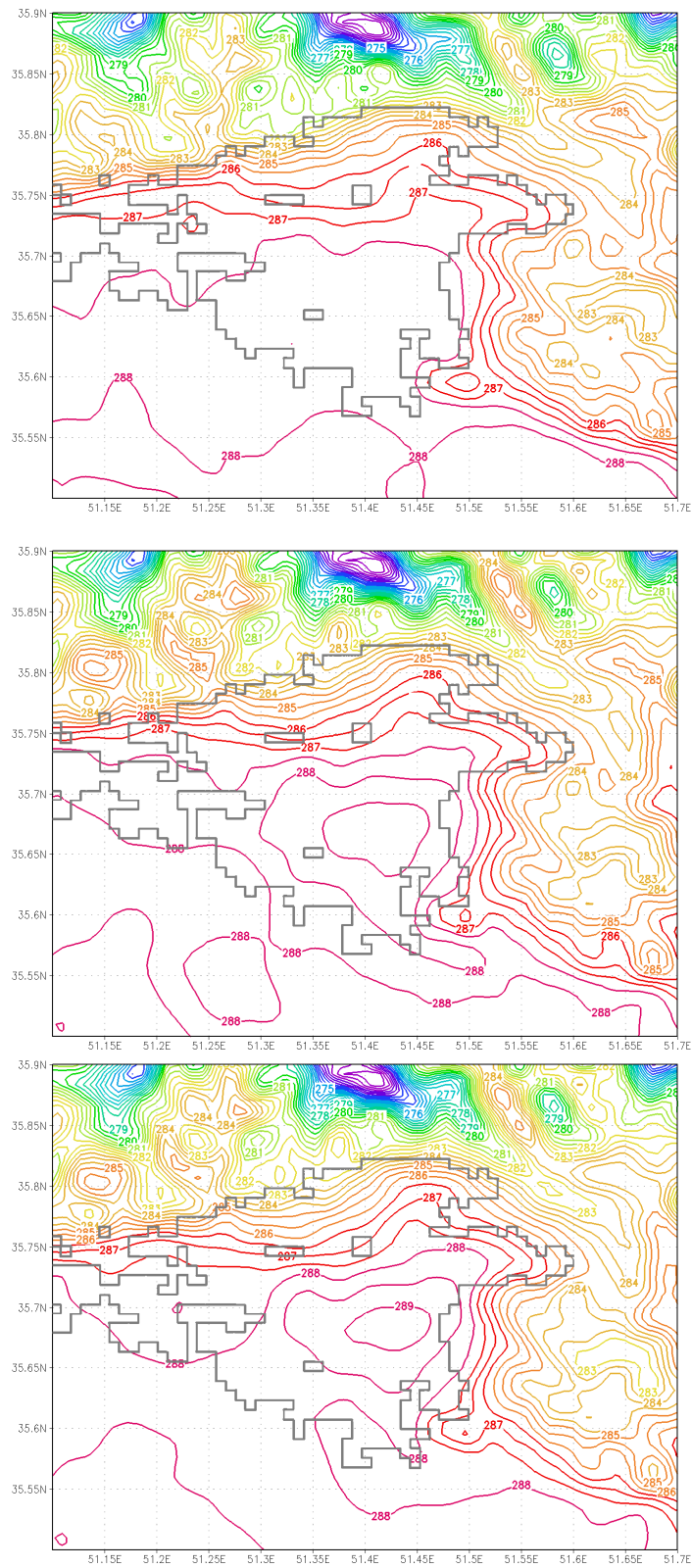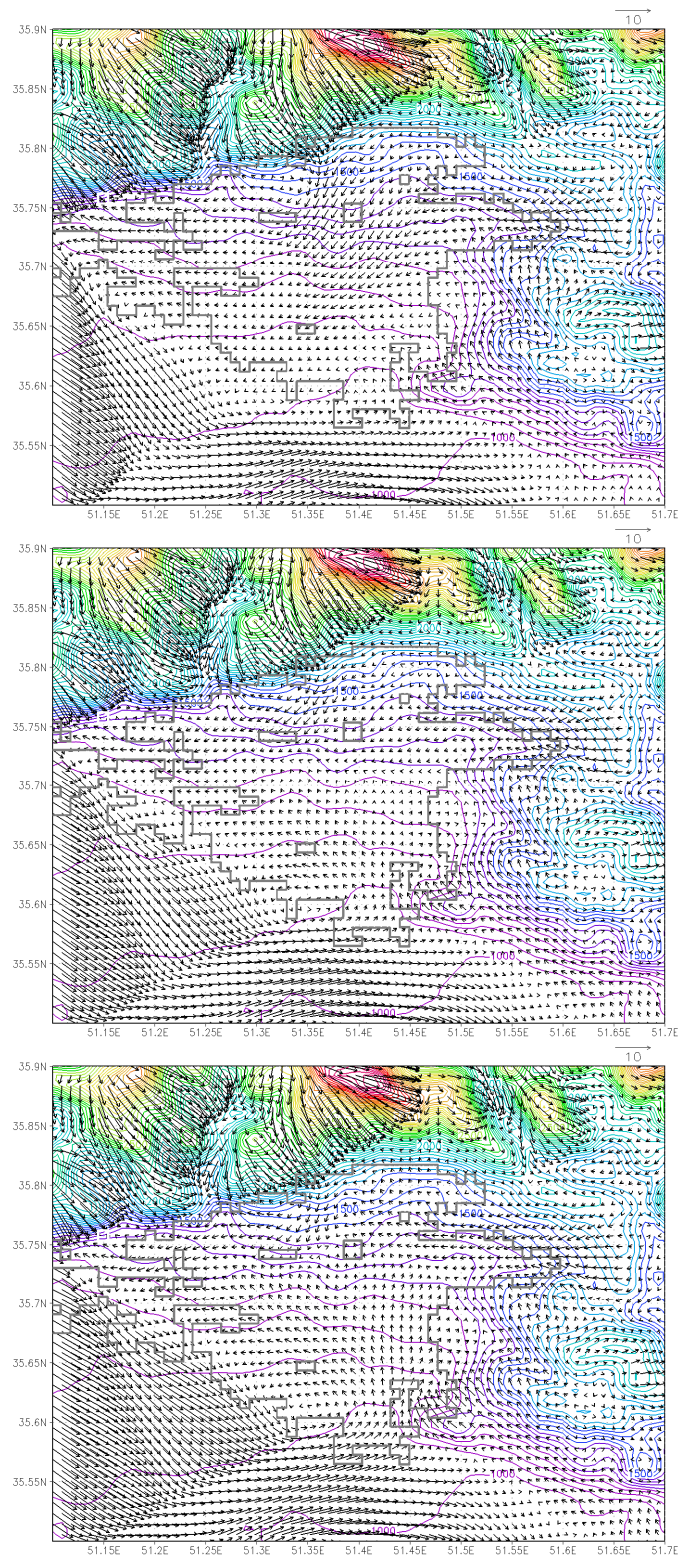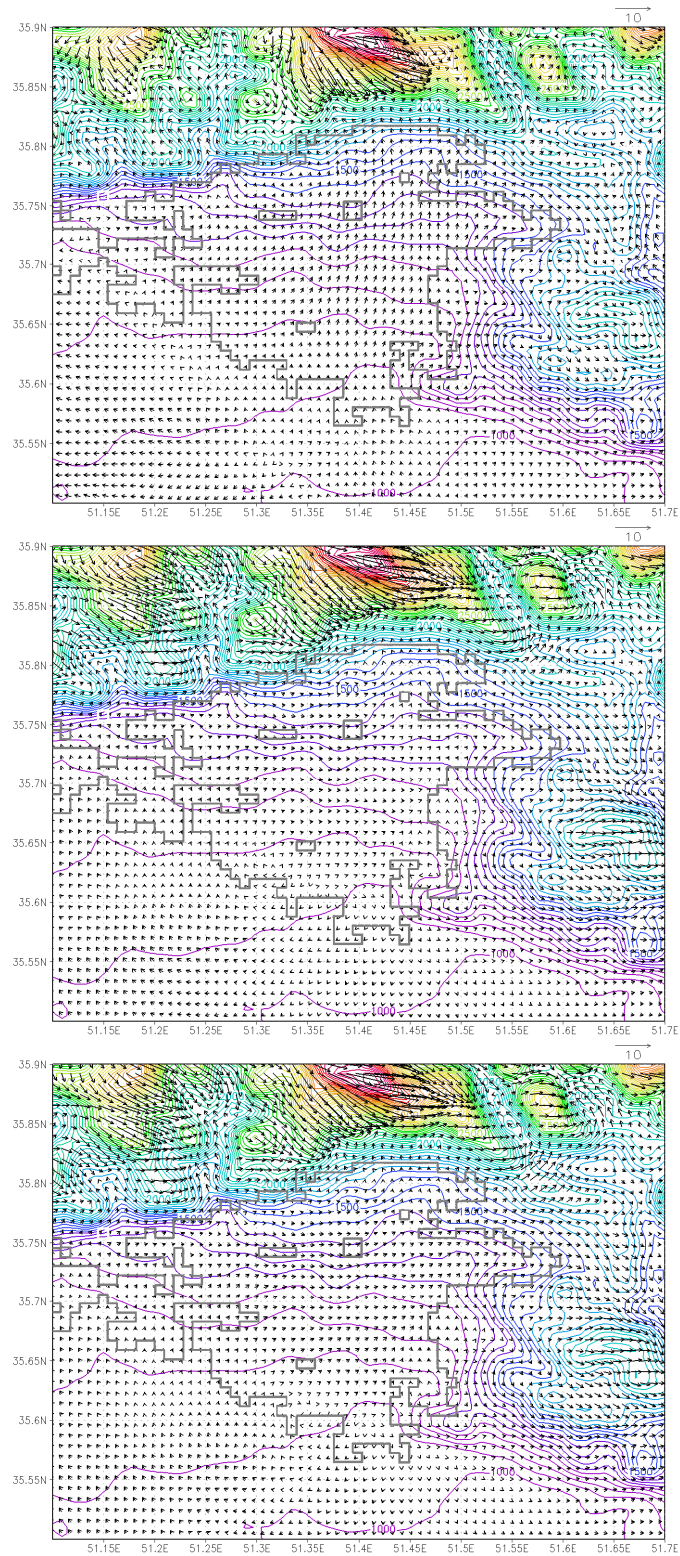**Figure 3.24:** As in Figure 3.20, but in 4pm.

3.4.2.4 Analyses of the PBL height

Spatial variation of the PBL height and structure occurs as a result of changes in landuse and topography of the underlying surface. In general, larger surface sensible heat fluxes will lead to a deeper PBL; however, boundary layer characteristics arising from one land cover type can be advected over a nearby region with differing surface characteristics (see Arya 1988; Garratt 1990; Mahrt et al. 1994). The PBL height**s** over complex topography are of particular importance for a good prediction of the dispersion of air pollutants, because the PBL height is determining the volume available for pollutants to dispersion (Seibert et al., 2000).

Figure 3.25 shows cross section of calculated PBL heights in the south – north direction in Tehran center with different configurations at 4 pm December 5th 2005. The PBL heights in the urban core simulated with "DA-SM2-U Q_f: On" configuration are generally 200–300 m higher than those with "RA-SLAB Q_f: Off". This result can be explained by the higher surface heat fluxes, air temperature that forcing convergence in "DA-SM2-U Q_f: On". In addition, this configuration explicitly enhances the TKE in the urban canopy, in particular at the rooftop level, which results in additional mixing in the URSL and a deeper PBL than that from the "RA-SLAB Q_f: Off". The PBL heights of "DA-SM2-U Q_f: On" and "Q_f: Off" show close values in south of city that can be explained by advection progresses from south to this area.

Figure 3.26 shows the evolution of the PBL height at the city center (the same point as for the profiles shown above). The PBL height is consistently greater with the "DA-SM2-U Q_f: On" configuration with maxima near 698 m between 2pm and 4pm. In this case, the PBL height collapses later and shows a secondary peak at 7 pm with 410 m. In "RA-SLAB Q_f: Off" case, the PBL reaches a maxima near 521 at 1 pm and rapidly collapses after 4 pm to 160 m.
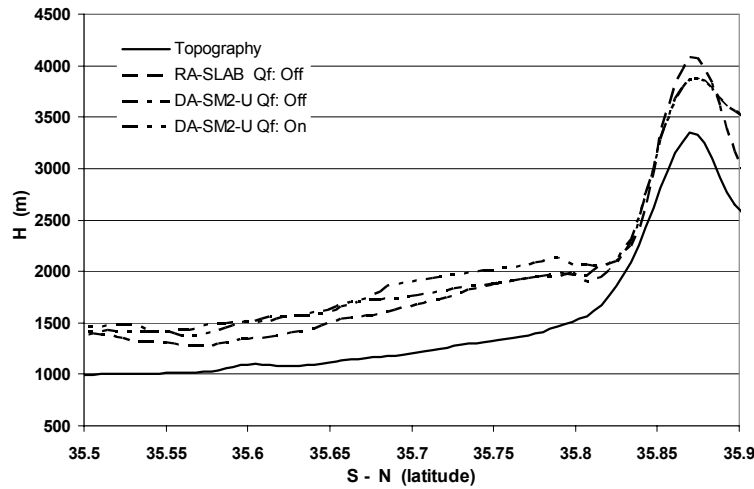
Figure 3.25: Cross section of PBL heights in south – north direction in Tehran center (longitude: 51.43 E) at 4 pm December 5th 2005 (Tehran is located between 35.58 35.82).
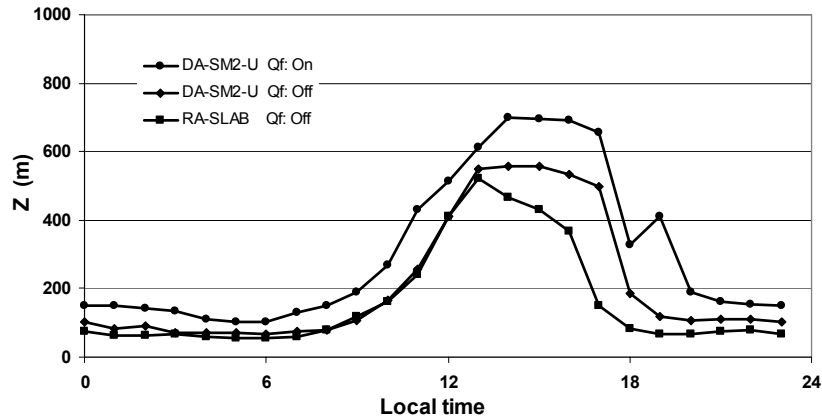
Figure 3.26: Time series of PBL height (m) at the city center during 5 December 2005.

3.4.2.5 Analyses of local circulations

A vertical cross section along the line A-A (see Figure 3.1 for location) shows the difference fields of potential temperature, vertical velocity and wind vectors in the plane of the cross section (Figure 3.27 and 3.28). The warm anomaly over the urban areas is evident, along with enhanced southerly flow aloft. There is also a cold anomaly near the Alborz Range, associated with lower values of sensible heat flux, a result of local surface energy balance differences.

As in Figure 3.27, the "RA-SLAB Q_f: Off" simulates katabatic winds stronger than other configurations and show more stability inside PBL. The local front between this regime and non local regime is evident in the left of the plane in cross section. The "DA-SM2-U

Q_f: Off" simulates katabatic winds, but those are lighter and they do not dominate the entire city. The local front is evident in the left of the plane similar to the "RA-SLAB Q_f: Off" configuration. The simulated fields by "DA-SM2-U Q_f: On", show interaction of UHI and mountain-valley flows better than other configurations, because this configuration considers urban effects much better than RA-SLAB. The katabatic winds obtained with this configuration do not enter the urban core because of the UHI forcing and a secondary front appears between upslope flow forcing by UHI and non local wind with katabatic flows. The combination of the katabatic winds from north and the upslope flow from south (Which is accompanied with a significant subsidence) with the UHI are conjoined which causes an amplified UHI in this simulation.

However, during the day (see Figure 3.28), anabatic winds dominate the city. The "RA-SLAB Q_f: Off" simulates this regime strong and continues with thickness about 300 m. The "DA-SM2-U Q_f: Off" simulates anabatic wind but they are made lighter and they do not including any sharp front. In the "DA-SM2-U Q_f: On" simulations, stronger fronts appear, the left one is located between non-local winds with flow forcing by UHI and the right one is located between regime that depends on UHI forcing and anabatic regime from suburban areas.

During the day, the wind fields simulated by RA-SLAB showed subsidence in higher altitudes of the city area and near the ground in south rural part of Tehran. The DA-SM2-U wind fields show some subsidence including wave structure in lower altitudes in the city area and near ground in the south sub-urban part of Tehran.
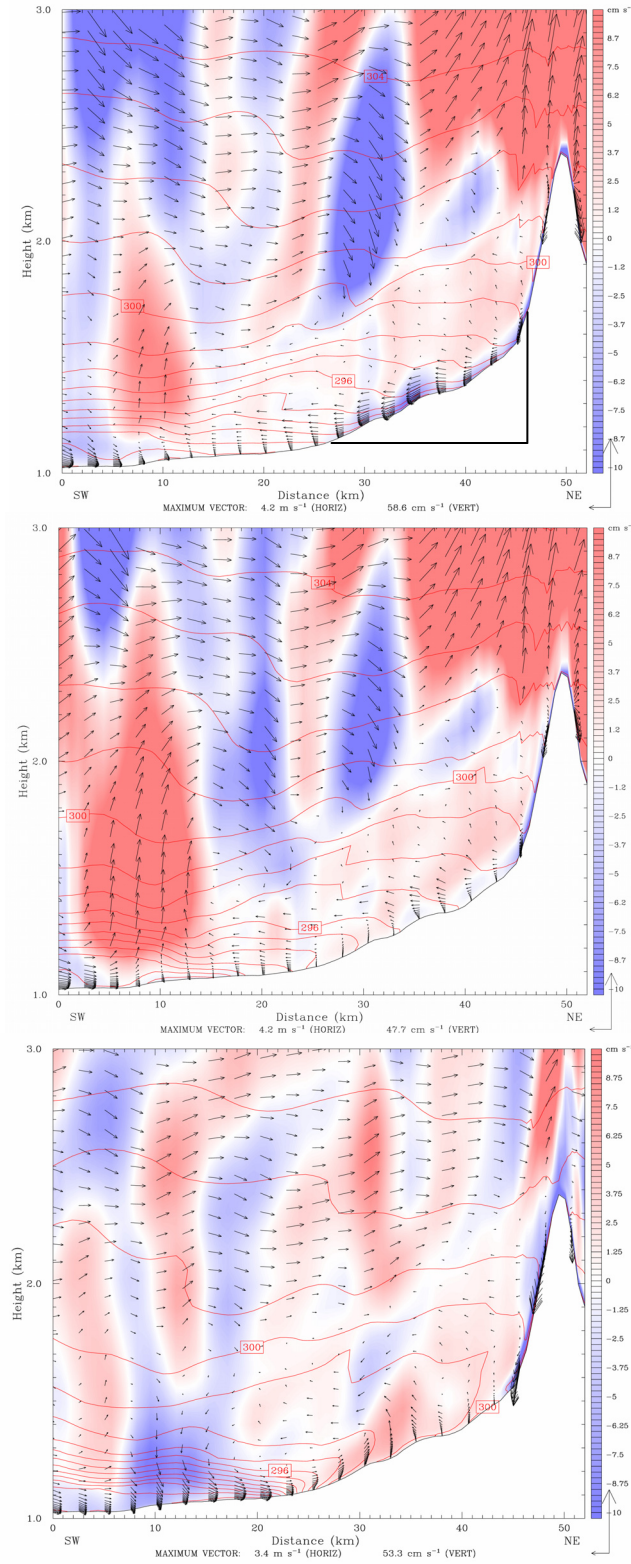
Figure 3.27: Cross section along A-A of potential temperature, vertical velocity in color shading, and wind vectors simulated by "RA-SLAB Q_f: Off" (top), "DA-SM2-U Q_f: Off "(middle) and "DA-SM2-U Q_f: On" (bottom) at 4 am December 5th 2005.
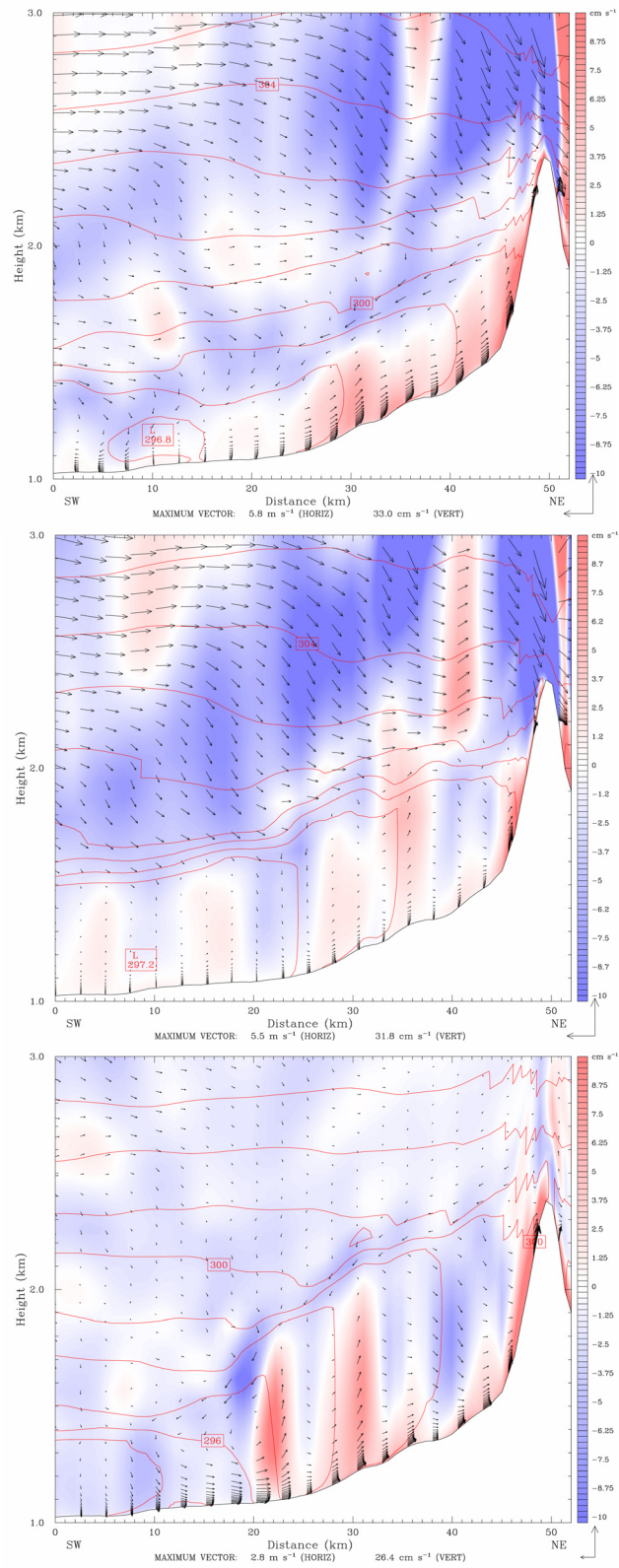
Figure 3.28: As in Figure 3.27, but in 4pm.

3.5 Conclusions

Sensitivity runs using the MM5 in a mountainous, semi-arid environment have identified urban surface characteristics and its dynamic and thermodynamic effects could be very important in simulation of local PBL structure and wind regimes.

The analysis of the dynamic, turbulent, and thermodynamic vertical profiles inside the urban RSL has shown a realistic behavior of "DA-SM2-U Q_f: On", consistent with observed data in urban. The vertical profiles of the potential air temperature in urban areas have shown that simulations using "DA-SM2-U Q_f: On" reduce the tendency toward stable stratification. They even yield a neutral layer during the night because of the anthropogenic heat fluxes and also the heat released by urban surfaces.

Within the canopies, the DA-SM2-U meteorological fields seem well simulated following the canopy morphology: decrease of the wind speed inside the dense canopies, skirting of the flow around the canopy blocks, warmer air inside the urban canopy especially during the night. By comparison with measurements, the surface air temperatures simulated with "DA-SM2-U Q_f: On" have been improved throughout the day for urban stations. However, "DA-SM2-U Q_f: On" slightly overestimates the air temperature during night that a large part of this overestimation being due to the anthropogenic heat fluxes, which are probably overestimated. Other reason for this overestimation can be from observations that are not in canopy and vicinity of anthropogenic heat sources.

Tehran PBL structure is extremely under effect of topographic and heat island flows and and show a multi layer structure. Urban Roughness and also its thermodynamics effects induce convergence and complex local circulations in this region. These local circulations could not be simulated well if model do not have capability to take into account urban forcing. The DA-SM2-U meteorological fields show that urban area have a significant forcing in thermal driving regimes in this area. We recognize that strong conclusions about interaction between local thermal diving's flows cannot be drawn from a single case study.

The results indicate that roughness approach (RA) is unsatisfactory and using a detail UCP may have significant improvements for meteorological modeling at neighborhood scales in this area.

In particular, the DA-SM2-U tends to improve simulations of temperature, wind speed, wind direction, and PBL height in and downstream of urban areas, all of which affect air-quality modeling.

References

Aniello, C., Morgan, K., Busbey, A., Newland, L., 1995. Mapping micro-urban heat islands using landsat TM and a GIS. Computers & Geosciences 21, 965–969.

Arya, S.P., 1988. Introduction to Micrometeorology. Academic Press, 307 pp.

Atkinson, B.W., 1981. Meso-scale Atmospheric Circulations. Academic Press, London, 495 pp.

Atkinson, B.W., 2003: Numerical modeling of urban heat-island intensity. Boundary-Layer Meteorology 109, 285-310.

Banta, R.M., L.S. Darby, J.D. Fast, J.O. Pinto, C.D. Whiteman, W.J. Shaw, and B.W. Orr, 2004. Nocturnal low-level jet in a mountain basin complex. Part I: Evolution and effects on local flows. Journal of Applied Meteorology 43, 1348-1365.

Bidokhti, A. A., Noroozi, M., 2004. A physical model for the layered structure of a density driven flow over a slope. 10th Asian Fluid Mechanics Congress, 17-21 May, Peradeniya, Sri Lanka.

Bornstein, R. D., 1968: Observations of the urban heat island effect in New York City. Journal of Applied Meteorology, 7, 575-582.

Bougeault, P. and Lacarrère, P., 1989, Parameterization of Orography-Induced Turbulence in a Mesobeta-Scale Model, Monthly Weather Review 117, 1872–1890.

Chen, F., and J. Dudhia, 2001: Coupling an advanced land-surface/hydrology model with the Penn State/NCAR MM5 modeling system. Part I: Model implementation and sensitivity. Monthly Weather Review, 129, 569-585.

Defant, F., 1949. Zur theorie der hangwinde, nebst bemerkungen zur theorie der berg- und talwinde. [A theory of slope winds, along with remarks on the theory of mountain winds and valley winds]. Archives for Meteorology, Geophysics, and Bioclimatology, A1, 421-450. (English translation: C. D. Whiteman, and E. Dreiseitl, 1984: Alpine meteorology: Translations of classic contributions by A. Wagner, E. Ekhart and F. Defant. Pacific Northwest Laboratory, Richland, Washington, 121 pp. [PNL-5141/ASCOT-84-3]).

de Wekker, S. F. J., 2002. Structure and morphology of the convective boundary layer in mountainous terrain. Ph.D. dissertation, University of British Columbia, 191 pp.

Draxler, R. R., 1986. Simulated and observed influence of the nocturnal urban heat island on the local wind field. Journal of Climate and Applied Meteorology 25, 1125-1133.

Dudhia, J., 1989: Numerical study of convection observed during the winter monsoon experiment using a mesoscale two-dimensional model. Journal of the Atmospheric Sciences 46, 3077–3107.

Dupont, S., 2001. Modélisation dynamique et thermodynamique de la canopée urbaine: réalisation du modèle de sols urbains pour SUBMESO, Doctoral thesis, Université de Nantes, France.

Dupont, S., Calmet, I., and Mestayer, P. G., 2002. Urban Canopy Modeling Influence on Urban Boundary Layer Simulation, in American Mathematical Society 4th Symposium on Urban Environment, Norfolk, Virginia, 20–24 May 2002, Proceedings, pp. 151–152.

Dupont, S., T.L. Otte, and J.K.S. Ching, 2004. Simulation of meteorological fields within and above urban and rural canopies with a mesoscale model (MM5). Boundary-Layer Meteorology 113, 111-158.

Dupont, S., Mestayer, P.G., 2006. Parameterization of the Urban Energy Budget with the Submesoscale Soil Model. Journal of Applied Meteorology and Climatology 45, 1744–1765.

Dupont, S., Mestayer, P.G., and Guilloteau, E., 2006. Parameterization of the Urban Water Budget with the Submesoscale Soil Model. Journal of Applied Meteorology and Climatology 45, 624- 648.

Garratt, J.R., 1990. The internal boundary layer - A review. Boundary-Layer Meteorology 50, 171-203.

Grell, G.A., Dudhia, J. and Stauffer, D.R., 1994. A description of the fifth-generation Penn State/NCAR mesoscale model (MM5). NCAR Technical Note, NCAR/TN-398+STR, 117 pp.

Grimmond, C. S. B., and T. R. Oke, 1999. Aerodynamic properties of urban areas derived from analysis of surface form. Journal of Applied Meteorology, 38, 1262-1292.

Hong, S.Y., and H.L. Pan, 1996. Nonlocal boundary layer vertical diffusion in a medium-range forecast model. Monthly Weather Review, 124, 2322-2339.

Hung, T., Uchihama, D., Ochi, S., Yasuoka, Y., 2006. Assessment with satellite data of the urban heat island effects in Asian mega cities. International Journal of Applied Earth observation and Geoinformation 8, 34–48.

Mahrt, L., 1982. Momentum balance of gravity flows. Journal of the Atmospheric Sciences 39, 2701-2711.

Mahrt, L., Sun, J., Vickers, D., MacPherson, J.I., Pederson J. R., and Desjardins, R. L., 1994. Observations of fluxes and inland breezes over a heterogeneous surface. Journal of the Atmospheric Sciences 51, 2484-2499.

Martilli, A., 2002. Numerical Study of Urban Impact on Boundary Layer Structure: Sensitivity to Wind Speed, Urban Morphology, and Rural Soil Moisture, Journal of Applied Meteorology 41, 1247-1266.

Martilli, A., Clappier, A., and Rotach, M.W., 2002. An urban surface exchange parameterization for mesoscale models. Boundary-Layer Meteorology 104, 261–304.

Mlawer, E.J., Taubman, S.J., Brown, P.D., Iacono, M.J., and Clough, S.A., 1997. Radiative transfer for inhomogeneous atmospheres: RRTM, a validated correlated-k model for the longwave. Journal of Geophysical Research 102, 16 663–16 682.

Monti, P., Fernando, H.J.S., Princevac, M., Chan, W.C., Kowalewski, T.A. and Pardyjak, E.R., 2002. Observations of flow and turbulence in the nocturnal boundary layer over a slope. Journal of the Atmospheric Sciences 59, 2513-2534.

Morris, C. J. G., Simmonds, I., and Plummer, N., 2001. Quantification of the influences of wind and cloud on the nocturnal urban heat island of a large city. Journal of Applied Meteorology 40, 169-182.

JICA project report, 1997. The Study on an Integrated Master Plan for Air Pollution Control in the Greater Tehran Area in the Islamic Republic of Iran, 816 pp.

Kastner-Klein, P., 2001. Overview of Near-Surface Turbulence Parameterizations, in Preprint COST 715 Workshop on Urban Boundary Layer Parameterizations, Zurich, May 24/25.

Kato, S., Yamaguchi, Y., 2005. Analysis of urban heat-island effect using ASTER and ETM+ Data: Separation of anthropogenic heat discharge and natural heat radiation from sensible heat flux. Remote Sensing of Environment 99, 44–54.

Kondo, H., Kikegawa, Y., 2003. Temperature variation in the urban canopy with anthropogenic energy use. Pure and Applied Geophysics 160, 317–324.

Ichinose, T., Shimodozono, K., Hanaki, K., 1999. Impact of anthropogenic heat on urban climate in Tokyo. Atmospheric Environment 33, 3897–3909.

Lacser, A., and Otte, T. L., 2002, Implementation of an Urban Canopy Parameterization in MM5, Preprints, in Fourth Symposium on Urban Environment, American Meteorological Society, Norfolk, VA, pp. 153–154.

Louka, P., Belcher, S.E., and R.G. Harrison. 2000. Coupling between Air Flow in Streets and the Well Developed Boundary Layer Aloft, Atmospheric Environment 34, 2613–2621.

Oikawa, S. and Y., Meng, 1995. Turbulence Characteristics and Organised Motions in a Suburban Roughness Sublayer. Boundary-Layer Meteorology 74, 289–312.

Oke, T. R., 1978. Boundary Layer Climates. Methuen and Co. Ltd., U.K., 435 pp.

Oke, T. R., 1982. The energetic basis of the urban heat island. The Quarterly Journal of the Royal Meteorological Society108, 1-24.

Oke, T.R., 1988. The urban energy balance. Progress in Physical Geography 12, 471–508.

Oke, T. R., 1995. The Heat Island of the Urban Boundary Layer: Characteristics, Causes and Effects. in J. E. Cermak et al. (eds.), Wind Climate in Cities, Kluwer Academic Publishers, Dordrecht, pp. 81–107.

Poulos, G.S., 1996. The interaction of katabatic winds and mountain waves. Ph.D. dissertation, Colorado State University, 399 pp. [Available from Colorado State University, Dept. of Atmospheric Sciences, Fort Collins, CO 80523.]

Prandtl, L., 1952. Essentials of Fluid Dynamics. Hafner, 452 pp.

Reisner, J., Rasmussen, R.J., and Bruintjes, R.T., 1998. Explicit forecasting of supercooled liquid water in winter storms using the MM5 mesoscale model. The Quarterly Journal of the Royal Meteorological Society 124B, 1071–1107.

Reuten, C., Steyn, D.G., Strawbridge, K.B., and Bovis, P., 2005. Observations of the relation between upslope flows and the convective boundary layer in steep terrain. Boundary-Layer Meteorology 116, 37-61.

Rife, D.L., Warner, T.T., Chen, F., and Astling, E.G., 2002. Mechanisms for diurnal boundary layer circulations in the Great Basin Desert. Monthly Weather Review 130, 921-938.

Rotach, M.W., 1993. Turbulence close to a rough urban surface Part I: Reynolds stress. Boundary Layer Meteorology 65, 1-28.

Rotach, M.W., 1995. Profiles of Turbulence in and above an Urban Street Canyon. Atmospheric Environment 29, 1473–1486.

Roth M., 2000. Review of Atmospheric Turbulence over Cities. The Quarterly Journal of the Royal Meteorological Society 126, 941–990.

Saaroni, H., Ben-Dor, E., Bitan, A., Potchter, O., 2000. Spatial distribution and microscale characteristics of the urban heat island in Tel-Aviv, Israel. Landscape and Urban Planning 48, 1–18.

Seibert, P., Beyrich, F., Gryning, S.-E., Joffre, 5 S., Rasmussen, A., and Tercier, Ph., 2000. Review and Intercomparison of Operational Methods for the Determination of the Mixing Height, Atmospheric Environment 34, 1001–1027.

Segal, M., and Arritt, R. W., 1992. Nonclassical mesoscale circulations caused by surface sensible heat-flux gradients. Bulletin of the American Meteorological Society 73, 1593-1604.

Segal, M., Garratt, J. R., Pielke, R.A., Schreiber, W.E., Rodi, A., Kallos, G., and Weaver, J., 1989. The impact of crop areas in northeast Colorado on midsummer mesoscale thermal circulations. Monthly Weather Review 117, 809-825.

Segal, M., Cramer, J.H., Pielke, R.A., Garratt, J.R., and Hildebrand, P., 1991. Observational evaluation of the snow breeze. Monthly Weather Review 119, 412-424.

Shafran, P.C., Seaman, N.L., and Gayno, G.A., 2000. Evaluation of numerical predictions of boundary layer structure during the Lake Michigan Ozone Study. Journal of Applied Meteorology 39, 412–426.

Stauffer, D.R., and N.L. Seaman, 1990. Use of four-dimensional data assimilation in a limited-area mesoscale model. Part I: Experiments with synoptic-scale data. Monthly Weather Review 118, 1250–1277.

Stauffer, D.R., and Seaman, N.L., 1994. Multiscale four-dimensional data assimilation. Journal of Applied Meteorology 33, 416–434.

Stewart, J.Q., Whiteman, C.D., Steenburgh, W.J., and Bian, X., 2002. A climatological study of thermally driven wind systems of the U.S. Intermountain West. Bulletin of the American Meteorological Society 83, 699-708.

Zhang, D.L., and Anthes, R.A., 1982. A high-resolution model of the planetary boundary layer Sensitivity tests and comparisons with SESAME-79 data. Journal of Applied Meteorology 21, 1594–1609.

Willmott, C. J., 1982. Some comments on the evaluation of model performance. Bulletin of the American Meteorological Society 63, 1309–1313.

Whiteman, C.D., 1990. Observations of thermally developed wind systems in mountainous terrain. Atmospheric Processes over Complex Terrain, Meteorological Monographs, 45, American Meteorological Society, 5–42.

Whiteman, C.D., 2000. Mountain Meteorology: Fundamentals and Applications. Oxford University Press, 355 pp.

Zumpfe, D., 2004. A case study of a strong lake-breeze front in the Salt Lake Valley. M.S. thesis, University of Utah, 72 pp.

CHAPTER FOUR

Sensitivity and Improvements of Tehran Air Quality Calculations, using different Meteorological Inputs

4.1 Introduction

Chemical transport modeling is widely used to estimate pollutant concentrations at different scales and it is recognized as an important tool in many applications such as air quality management, forecasting, evaluation of health effects and vegetation damage, and investigations of climate change. In all these applications, satisfactory precision in the modeled spatial and temporal distributions of pollutant concentrations is crucial.

Sources of error in chemical-transport modeling processes may be grouped in three main categories, (1) emissions, (2) transport (including deposition) and (3) chemistry (including phase change). At the beginning of this study the emission database over the Tehran area was improved (see chapter 2) in order to obtain better performance of air pollution modelling in this area. The errors in transport processes originate in part from uncertainty in the meteorological input fields as well as numerical approximations in the chemical transport model (CTM).

Meteorological fields are very important inputs to CTM: wind, mixing height, eddy diffusivity, radiation, temperature, precipitation, etc. (especially in the PBL) determine how pollutants are dispersed and transported over long distances. The meteorological fields also affect the chemical transformation, the production of secondary species and therefore surface concentrations. Among the various error sources affecting CTMs, meteorological input fields are recognized as a main source of uncertainty in air pollution

modelling. This uncertainty has to be minimized in complex cases such as urban areas (the regions with the larger emissions) affected by local effects such as sea breeze, topographic flows and urban heat island circulations.

Mega-cities have strong effects on the local meteorology and structure of the Planetary Boundary Layer (Bornstein et al., 1993, Oke, 1995, Saitoh et al., 1996, Martilli, 2002). In the case of Tehran, additional complexity is induced by the mountain-valley and its interaction with the urban induced flows over the area of interest. It means that the meteorological model should be capable of simulating correctly the urban effects as well as the other local effects and their interactions. In this context, meteorological simulations with detailed approaches suitable for an urban area were used and evaluated for the Tehran area (see chapter 3).

The aim of the present work is to evaluate, by means of a CTM, the effect of different approaches for modeling the transport and dispersion of pollutants in urban area, on the spatial and temporal distribution of pollutant concentrations.

Tehran is faced with air quality problems that affect more people than any other environmental problems in this region. This condition is due to the cumulative effects of rapid population growth, high population density (8.3 million inhabitants in an area of about 670 km^2), a large and old vehicle fleet (mobile sources), a large number of industrial and commercial establishments (stationary sources), geographical location (surrounded by mountains) and the ensnared condition (recirculation processes). When the synoptic forcing is small, high pollution episodes occur, especially during August, September and October.

The PBL structure with the interaction of local effects was studied during a pollution episode that occurred between December 4 and December 7 (Chapter 3). For this period, three simulations, with the mesoscale meteorological model (MM5) were performed: in the first simulation the city of Tehran was represented with the detailed urban surface exchange parameterizations, taking into account the anthropogenic heat flux (DA-SM2-U Q_f: On); in the second simulation, the same urban parameterizations were used, but without considering the anthropogenic heat flux (DA-SM2-U Q_f: Off); and in the third simulation, a simple urban parameterization based on a roughness approach available in the standard version of MM5 (RA-SLAB) was used.

The meteorological parameters (wind, temperature, turbulence, etc.) calculated by the three simulations are used here as input to a CTM, which computes dispersion, chemical reactions and depositions of air pollutants. By comparing CTM results obtained with these three different sets of meteorological inputs against measurements, we can evaluate the effect of various meteorological model parameterization, in particular the use of a detailed urban parameterization (DA-SM2-U) versus a simpler formulation (RA-SLAB). In the present chapter, after a short description of the chemical transport model and its configuration, results of simulations are analyzed and compared with observations. Then, a sensitivity analysis of CTM simulations with respect to the meteorological inputs is conducted.

4.2 Model and methods

The air quality modeling system MM5-POLYPHEMUS system was implemented and applied here to the Tehran area. MM5 and POLYPHEMUS are, respectively, the meteorological mesoscale model and the modeling platform that includes the Chemical-Transport Model POLAIR3D.

POLYPHEMUS is a modeling system that has been developed for air quality forecasts and impact assessment of new emission sources on emission reduction strategies. It has been designed as a modular system being able to host different model configurations and it is well-suited for ensemble modeling (Mallet and Sportisse, 2006a). A key focus of POLYPHEMUS is devoted to the model sensitivity with respect to emissions (Mallet and Sportisse, 2005). Many topics related to uncertainties have already been investigated by POLYPHEMUS (Mallet and Sportisse, 2006b). It has already been applied to gas-phase and aerosol modeling, through POLAIR3D over Europe, Greater Paris and East Asia respectively (Sartelet et al., 2007 ; Tombette and Sportisse, 2007 ; Sartelet et al., 2008). The POLYPHEMUS platform contains four subsets:

- Physical parameterizations and pre-processing of input fields (e.g., ground fields, meteorological fields, boundary-initial conditions and emissions) are performed within the ATMODATA library.

- Drivers have been defined in order to handle high-level use of the models, which can be viewed as black boxes, e.g., a driver for Monte Carlo simulations, a driver for ensemble forecast.

- Models (for instance the Chemiscal-Transport Model PoLAIR3D) constitute the third level of the system. Short-range models (Gaussian puff and plume models) are also available.

- Postprocessing tools, especially the Python module ATMOPY, are also available. This library (which does not depend on the previous components) performs model-to-data comparisons.

- Domains

In this study, simulations with PoLAIR3D are performed over 2 nested domains (Figure 4.1). The coarse domain covers Tehran province and the second one covers Tehran city with horizontal grid resolutions of 6 km × 6 km (0.066° × 0.054° in longitude/latitude) and 2 km × 2 km (0.022° × 0.018° in longitude/latitude), respectively. The coarse domain size includes 61×47 grid points and the second domain includes 60×61 grid point (in longitude/latitude direction). The coarse domain has 9 vertical levels (grid center points from 15 m to 2525m) and the second domain has 12 levels (grid center points from 10 m to 2400 m).

- Land-use coverage and roughness

For the land use cover, two choices area available: the Global Land Cover Facility (GLCF) dataset (14 categories) or the USGS (United States Geological Survey) land cover map (24 categories). We need to convert these land use cover data to another set such as Wesely or Zhang land use cover categories (Wesely, 1989 ; Zhang et al. 2001) in order to compute deposition velocities.

In this study, the USGS dataset is used for land use cover and it is converted to the Zhang categories to compute deposition velocities. The land use cover computed by USGS dataset is used to estimate the roughness distribution.
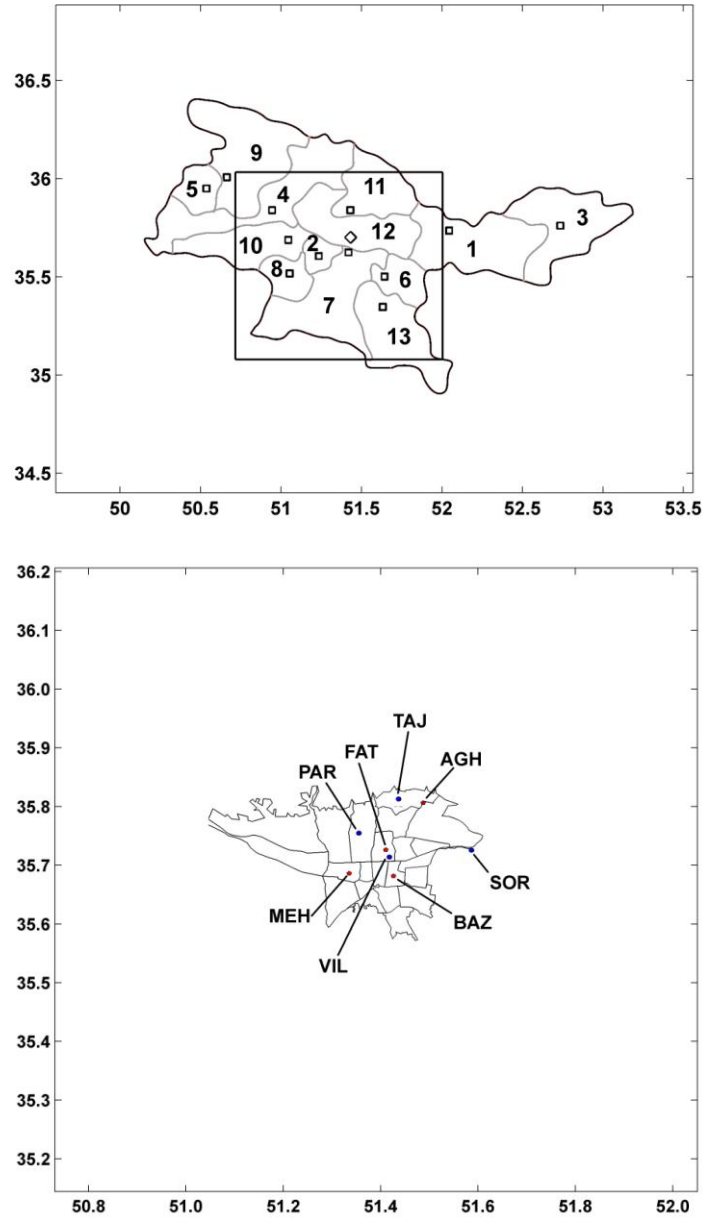
Figure 4.1 Top: Coarse domain including Tehran province and its counties (1) Damavand, (2) Eslamshahr, (3) Firouzkouh, (4) Karaj, (5) Nazarabad, (6) Pakdasht, (7) Ray, (8) Robat karim, (9) Savojbolagh, (10) Shahriar, (11) Shemiranat and (12) Tehran, (13) Varamin.
Down: nesting level 1 domain including observation network (AGH: Aghdasiyeh, BAZ: Bazar, FAT: Fatemi, MEH: Mehrabad, PAR: Pardisan, SOR: Sorkhe hesar, TAJ: Tajrish and VIL: Vila) used in this study.

- Meteorological data

In order to prepare meteorological data for the POLAIR3D simulations, one can use ECMWF (European Center for Medium-range Weather Forecasts) reanalysis or MM5 model output.

To get the complete set of input meteorological data for a the CTM, one must generate parameters such as pressure, temperature, skin temperature, wind field, Richardson number, boundary layer height, vertical diffusion coefficients, specific humidity, liquid water content, cloud attenuation coefficients, solar radiation intensity, rain intensity, convective rain intensity, cloud height, etc.

The meteorological input data were obtained with three different MM5 simulations. As describe above, in these MM5 simulations the city of Tehran is represented with different approaches in this model. In the CTM POLAIR3D, the Troen–Mahrt's parameterization (Troen and Mahrt, 1986) and the Louis's parameterization (Louis, 1979) are used to calculate the vertical diffusion coefficient within and above the PBL, respectively.

- Deposition and scavenging

For gaseous species, dry deposition velocities are calculated by using the parameterization of Zhang et al. (2003) and below-cloud scavenging (washout) is parameterized following Sportisse and Dubois (2002).

For aerosols, dry deposition is computed by a resistance approach, following Zhang et al. (2001) and below cloud scavenging (washout) and in-cloud scavenging (rainout) are parameterized as presented by Sartelet et al. (2007).

- Emissions

The anthropogenic emission module processes the selected emission inventory and generates surface and volume anthropogenic emissions according to the vertical distribution, temporal profiles for each emission sector or SNAP (Selected Nomenclature for Air Pollution) category. In this work, anthropogenic emissions are generated with the Tehran inventory dataset that was updated for 2005 (see chapter 2). This inventory includes emissions for 10 different SNAP for NO_x, SO_2, CO, non-methane volatile organic compounds (NMVOC), PM_{10} and CH_4. The NMVOC are speciated following the speciation of the Institute für Energiewirtschaft und Rationelle (IER), Stuttgart and then allocated to model species of the chemical kinetic mechanism RACM. PM_{10} are distributed among size bins. We use the chemical speciation following Tombette and Sportisse (2007). The primary PM emission is partitioned into three model species

(primary organic, black carbon and mineral dust) and the aerosol size spectrum is divided into 10 bins in the range 0.01 µm–10 µm.

The biogenic emission module computes biogenic emissions on the basis of meteorological fields and land use cover according to Simpson et al. (1999).

- Initial and boundary conditions

Preprocessing modules interpolate and generate initial and boundary conditions from available continental or global simulations such as the global model Mozart (Horrowith et al., 2003), the Goddard Chemistry Aerosol Radiation and Transport (GOCART, Chin et al., 2000) model, the global model LMDz-INCA (Hauglustaine et al., 2004) for aerosols and gases.

In this study, in order to generate initial and boundary conditions for the coarse domain run, output concentrations from Mozart 2 (Horowitz et al., 2003) are used for gas and LMDz-INCA model outputs are used for aerosol components. For the inner domain, initial and boundary conditions are interpolated from the Polair3D simulation conducted for coarse domain (see Figure 4.1).

- Gas-phase chemistry mechanism

POLYPHEMUS contains several chemistry modules, such as RACM (Regional Atmospheric Chemistry Mechanism) and RADM (Regional Acid Deposition Model). The chemical mechanism chosen for this simulation is the RACM (Stockwell et al., 1997). Photolysis rates are computed off-line, as done in the photolysis rate preprocessor JPROC of CMAQ (Roselle et al., 1999).

- Aerosol model

Two aerosol models are available in POLYPHEMUS: MAM (a Modal Aerosol Model, Sartelet et al., 2005) and SIREAM (a SIze REsolved Aerosol Model, Debry et al., 2007). Both models rely on the same parameterizations hosted by the ATMODATA library (Sportisse et al., 2006).

The SIREAM model is used for this study. In this model, thermodynamic equilibria between the gas and particular phases are simulated for inorganics (ISORROPIA v1.7;

Nenes et al., 1998) and organics (SORGAM; Schell et al., 2001), separately. Brownian coagulation is taken into account (see Debry and Sportisse, 2006b). For nucleation, binary (H_2O–H_2SO_4, Vehkamäki et al., 2002) or ternary (H_2O–H_2SO_4–NH_3, Napari et al., 2002) nucleation can be simulated. The nucleated particles are assigned to the first bin of the size discretization. Detailed cloud microphysics is not solved and is replaced by a model based on the variable size-resolved model (VSRM, Fahey and Pandis, 2001). Above a threshold in liquid water (typically 0.5 gm^{-3}), cloud condensation occurs and aqueous-phase chemistry is simulated for activated aerosols (above a fixed diameter d_{activ} = 0.7 µm). Removal of gases and particles by in-cloud scavenging is then simulated for 28 aqueous-phase and 18 gas-phase species. Moreover, the pH of cloud droplets is computed and used for a better description of the below-cloud scavenging. Following (Jacob, 2000), four heterogeneous reactions at the surface of aerosols and cloud droplets are simulated (see Tombette and Sportisse, 2007).

- Numerical approches

The numerical simulation of the aerosol general dynamic equation (GDE) (Seinfeld and Pandis, 1998) is still a challenging issue (Seigneur, 2001 for instance) and special attention must be paid to numerical algorithms.

A first-order splitting method is used with the following sequence: advection, diffusion (including dry deposition and surface emissions as boundary conditions), scavenging, gas-phase chemistry and aerosol dynamics. For the aerosol module, the sequence is: coagulation and then condensation and nucleation. In our simulations, nucleation is not taken into account because particles of diameters lower than 0.01 µm are not modeled. However, condensation evaporation and coagulation are solved.

In a size-resolved model such as SIREAM, the particle size spectrum is divided into a fixed number of sections (or bins) and sections are logarithmically distributed in the model.

Several approaches can be used for the computation of condensation/evaporation. The bulk equilibrium approach is the simplest one; it considers that mass transfer between the gas and particle phases is instantaneous and, that partitioning between both phases is determined by thermodynamic equilibrium. The dynamic approach is the most accurate

approach; it uses kinetic mass transfer between the gas and particles phases in addition to thermodynamic equilibrium at the particle surface. Usually, the timescales of mass transfer is considered to depend on particle size and small particles are assumed to reach equilibrium more rapidly than coarse ones. Therefore, a hybrid approach, between the bulk-equilibrium and the dynamic approaches is used. It consists in defining a cut-off diameter below which we apply the equilibrium approach and above which we apply the dynamic approach. The cut-off diameter is generally taken around 1 µm (Koo et al., 2003 ; Debry and Sportisse, 2006a). In our simulations, condensation is solved with the hybrid approach and the cut-off diameter is taken equal to 1.26 µm.

In order to minimize numerical diffusion, a semi-Lagrangian method is used in SIREAM for condensation evaporation. Each bin grows due to condensation and it is thereafter redistributed on the fixed grid before the transport. In this study, we used a redistribution method that ensures both mass and number conservations by solving a simple linear system (Tombette and Sportisse, 2007).

The ETR scheme is used for solving the dynamic condensation/evaporation of particles with diameters lower than 1.26 µm.

The SIREAM configurations in our simulations are similar to the simulation in Tombette and Sportisse (2007). For all three simulations, the configurations are the same. The main configurations are listed in Table 4.1 for both domains.

4.3 Case study simulations and results

The objective of this work is to study the sensitivity of gas-phase and aerosol species concentrations to meteorological inputs during a high pollution episode in a complex terrain. For the selected period, three simulations were performed for the inner domain: in the first simulation (called hereafter Run1), the meteorology was obtained from a MM5 run with the configuration DA-SM2-U Q_f: On; in the second simulation (called hereafter Run2), the meteorology was obtained from a MM5 run with the configuration DA-SM2-U Q_f: Off; and in the third simulation (called hereafter Run3), the meteorology was obtained from a MM5 run with the configuration RA-SLAB Q_f: Off. Meteorological inputs for the coarse and inner domains are presented in Table 4.2.

Table 4.1 Model configuration for coarse / inner domains.

Science Options	Configuration Coarse domain / Inner domain	Details/Comments
Simulation Periods	2005.11.26-2005.12.09 / 2005.11.28-2005.12.09	
Meteorological fields	MM5 output: RA-SLAB / RA-SLAB, DA-SM2-U	
land use coverage	Zhang categories	(Zhang et al., 2002)
vertical diffusion coefficient	Inside PBL: the Troen–Mahrt's parameterization Above PBL: the Louis's parameterization	(Troen and Mahrt, 1986) (Louis, 1979)
Horizontal Grid Mesh	6 / 2 km	
Grid dimention	$61 \times 47 / 61 \times 60$	(in longitude $\times$ latitude direction)
Vertical Grid Mesh	9 / 11 layers	
Model top	2800 / 2700 m	
Gas initial and Boundary condition	The global models Mozart / Coarse domain	(Horrowith et al., 2003)
Aerosol initial and Boundary condition	The global models LMDz-INCA / Coarse domain	
Gases dry deposition velocities	Zhang parameterization	(Zhang et al., 2003)
Aerosol dry deposition velocities	Zhang parameterization	Zhang et al. (2001)
Gas-phase chemistry	Regional Atmospheric Chemistry Mechanism (RACM)	(Stockwell et al., 1997)
Aerosol size spectrum	0.0100, 0.0200, 0.0398, 0.0794, 0.1585, 0.3162, 0.6310, 1.2589, 2.5119, 5.0119, 10.000	
Coagulation	On / On	
Condensation	On / On	
Kelvin effect	Yes / Yes	
Cut-off diameter for the dynamic resolution of condensation	1.2589 μm	(Koo et al., 2003 ; Debry and Sportisse, 2006a)
Thermodynamic module for Bulk equilibrium	Isorropia / Isorropia	
Dynamic bin condensation solver	etr / etr	
Nucleation	Off / Off	
heterogeneous reaction	Yes / Yes	
Integration Time Step	180 / 60 seconds	
Platform	Linux Intel Core 2 (4 processors)	

In order to evaluate the impact of the urban parameterizations used in the meteorological simulations on the CTM modeling in Tehran region, we conduct a preliminary evaluation with a model-to-data comparison for the episode between 2005.12.05 to 2005.12.09.

Table 4.2: Meteorological inputs for each domain during simulations (solid line: RA-SLAB Q_f: Off).

		2005.11.26 - 2005.11.28	2005.11.28 - 2005.12.05	2005.12.04 - 2005.12.09
Coarse domain		▬▬▬▬▬▬▬▬		
Inner domain	Run1		▬▬▬▬▬▬	DA-SM2-U Q_f: On
	Run2		▬▬▬▬▬▬	DA-SM2-U Q_f: Off
	Run3		▬▬▬▬▬▬	▬▬▬▬▬▬

Aghdasiyeh (AGH) and Fatemi (FAT) stations are selected among eight active stations in the study period for comparing diurnal-daily variations of pollutant concentrations, due to

their location and the availability for continuous data. The time series of observed and simulated CO, NO_2, PM_{10} and O_3 at Aghdasiyeh and Fatemi stations are given in Figure 4.2. Unfortunately, O_3 observations are available only for Pardisan (PAR) and Mehrabad stations, which are located inside the urban area where O_3 concentrations are low due to rapid titration by NO emissions. Observations at suburban and rural sites located inside urban plume would have been preferable for O_3 validation. Figure 4.3 shows time series of observed and simulated O_3 at Pardisan station. The low O_3 concentration results from the urban location as well as the wintertime conditions.

The values of observed concentrations (except for O_3) show that the level of pollution is high during this period and daily trends of concentrations show that the 6th December is the highest polluted day during this period. Simulated concentrations also show this pollution peak on the 6th December and a good correlation with observations, except for Run 3. The simulated diurnal concentrations show morning and afternoon peaks that are close to observed diurnal peaks for all pollutants in Run 1 and Run 2. The model lead to underestimation around midday especially in downtown for CO and PM10 (such as FAT station, see Figure 4.2) because of several reasons. First, the stations are near traffic sources and inside urban street canyons, which can trap pollutants; second, the model grid size for the inner domain is around 2 km and results are averaged over 4 km^2 area; third, the model always simulated more mixing during the day than suggested by observations; fourth, the model does not account for buildings explicitly, which means that emissions are dispersed in a bigger volume than the real volume of the urban canopies because part of this volume is actually occupied by buildings.
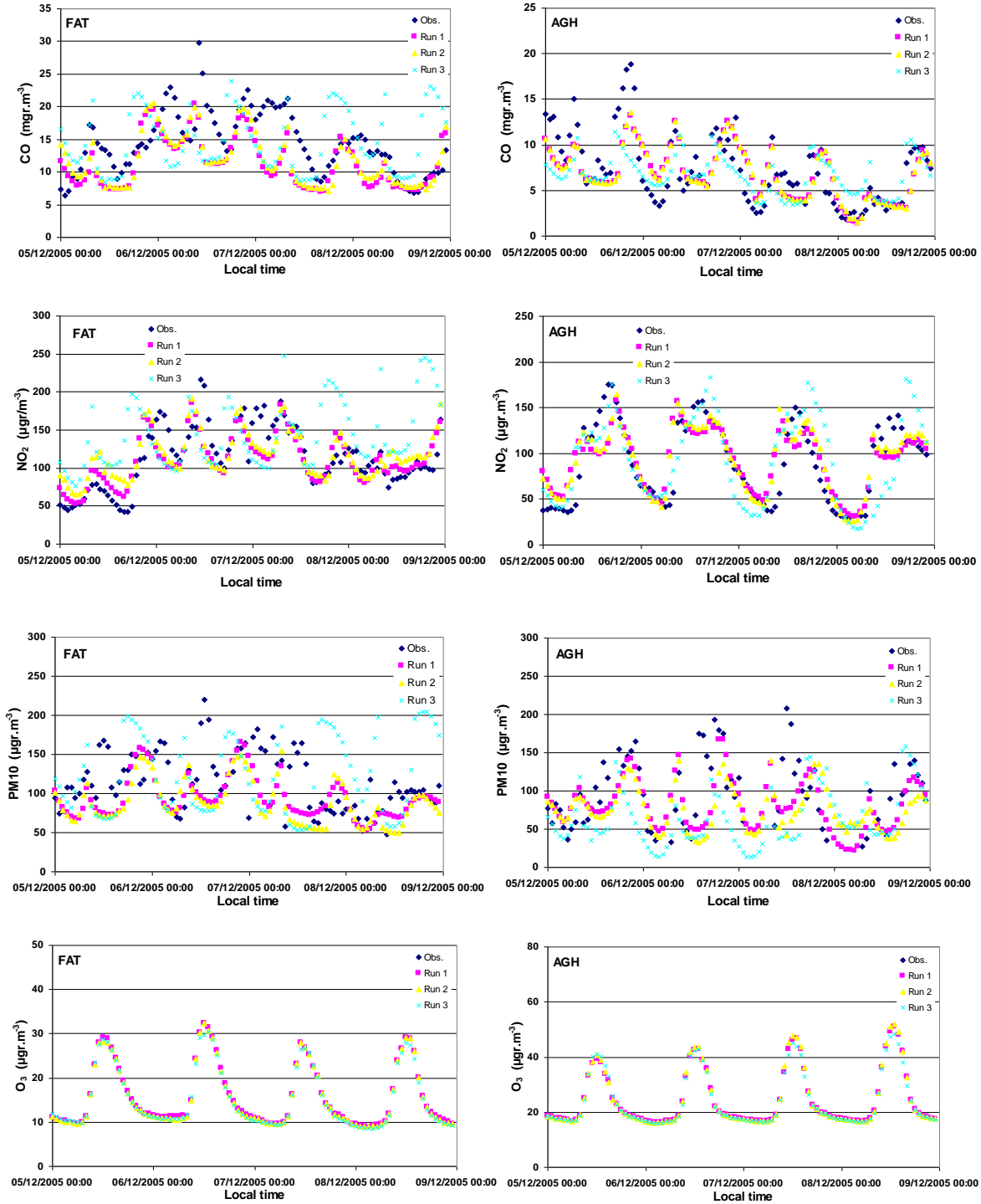
Figure 4.2: Observed and simulated time series of CO, NO$_2$, PM$_{10}$ and O$_3$ concentrations at Fatemi (left) and Aghdasiyeh (right) stations from 05/12/2005-00 until 09/12/2005-00 local time.
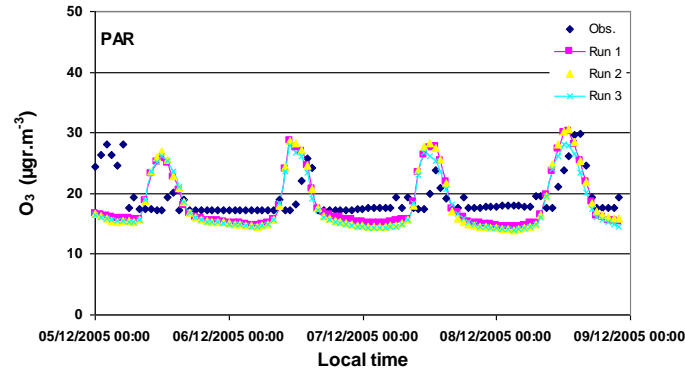
Figure 4.3: Observed and simulated time series of
O3 concentrations at Pardisan station.

Run 3 (RA-SLAB Q_f: Off) usually overestimates the morning peak concentrations (which depend on the morning traffic peak) and also predicts that peaks sooner than observations especially in downtown (such as FAT station, see Figure 4.2). This discrepancy may be due to more PBL stability, predicted in the morning with meteorological inputs from the RA-SLAB configuration. This phenomenon occurs for the evening peaks (depending on evening traffic peak) as well.

On the 9th December, Run 3 overestimates pollutant concentrations because with the "RA-SLAB Q_f: Off" option, MM5 predicts low-wind speed regime (anabatic wind) and, as a result, transport from downtown to north east is underestimated. However Run 1 shows better results. When the wind speed is low, the PBL stability becomes more important than advective transport for pollutant dispersion. The PBL stability is lower with the option "DA-SM2-U Qf: On" than "DA-SM2-U Qf: Off" and "RA-SLAB Q_f: Off", because it takes into account anthropogenic heat flux. The wind speed and direction are important for transport, which depends on interactions between local forcings in situations of low synoptical forcings, that "DA-SM2-U Qf: On" showed better results (see Chapter 3).

As shown in Figure 4.2 and Figure 4.3, the level of O_3 is low during this episode at urban locations, which is normal for these dates and locations.

The scatter plots of observed and simulated concentrations of CO, NO_2 and PM_{10} at Aghdasiyeh and Fatemi stations are given in Figure 4.4. Simulated concentrations by Run 1 and Run 2 show better correlations than Run 3. However, for high observed values, the all runs show some underestimations, as discussed above; especially around midday.

Run 3 is more scattered than other runs but with little overall bias; nevertheless, the scattered results obtained with this configuration are not satisfactory.

The model performance statistics were computed for each simulation and are presented in Table 4.3 for CO, NO_2, PM_{10} and O_3. Statistical parameters are provided below.
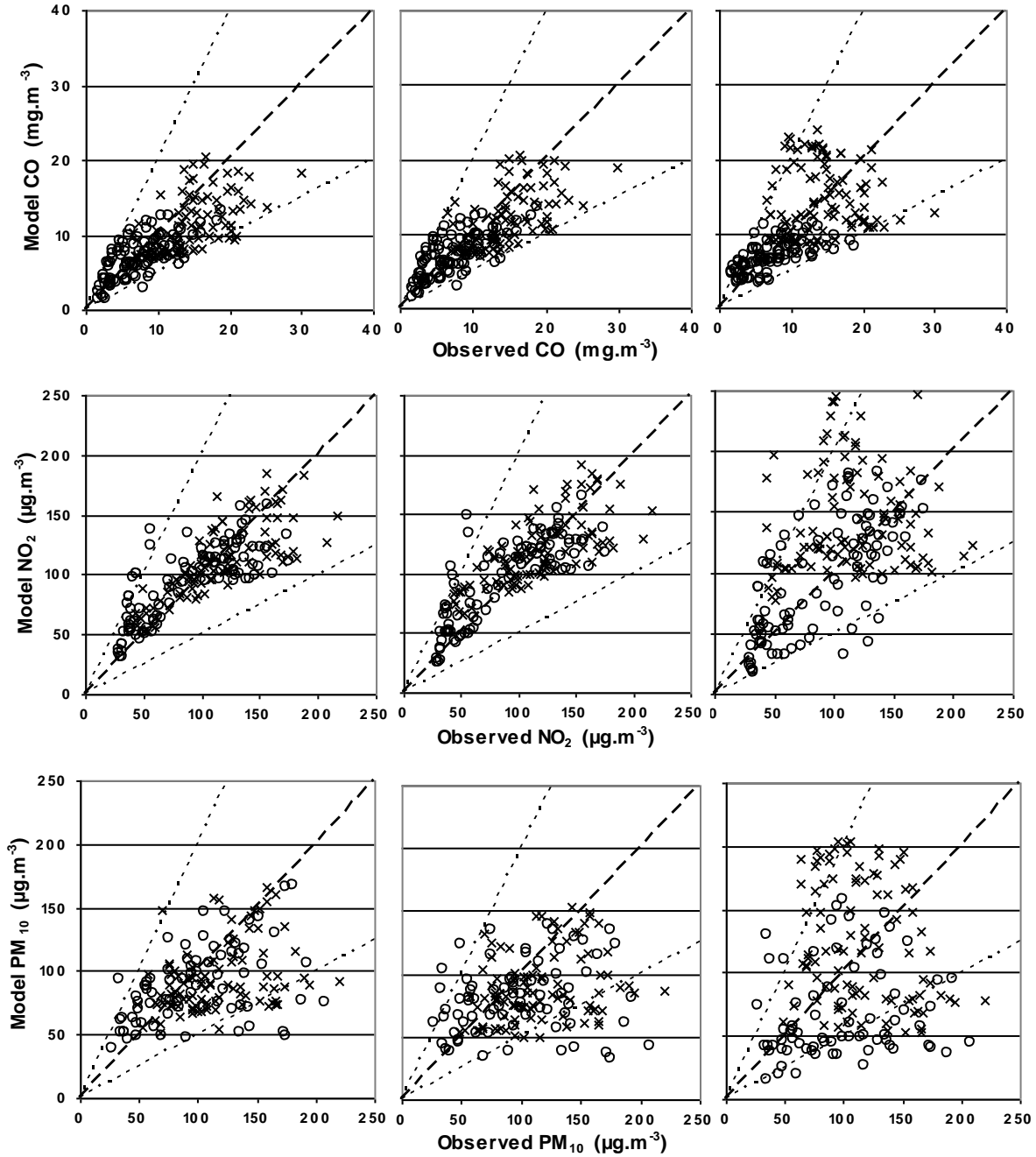

Figure 4.4: Scatter plot of observed versus simulated CO, NO_2 and PM_{10} concentrations at Fatemi (circules) and Aghdasiyeh (crosses). Left, middle and right panels relate to Run 1, Run 2 and Run 3 of POLYPHEMUS simulations, respectively.

Table 4.3: Model-to-data comparison for CO, NO$_2$, O$_3$ and PM$_{10}$ at all observational sits.

$$RMSE = \sqrt{\frac{1}{n}\sum_{i=1}^{n}(O_i - S_i)^2} \quad Correlation = \frac{\frac{1}{n}\sum_{i=1}^{n}(O_i - \overline{O})(S_i - \overline{S})}{\sqrt{\frac{1}{n}\sum_{i=1}^{n}(O_i - \overline{O})^2 \times \frac{1}{n}\sum_{i=1}^{n}(S_i - \overline{S})^2}}$$

$$BF = \frac{1}{n}\sum_{i=1}^{n}\frac{O_i}{S_i} \qquad NME = \frac{\sum_{i=1}^{n}|O_i - S_i|}{\sum_{i=1}^{n}O_i}$$

O$_i$: observed concentrations
S$_i$: simulated concentrations
n : number of observations
RMSE : root mean square error
BF : bias factor
NME : normalized mean error

CO	Sim. mean (mg.m^{-3})	RMSE (mg.m^{-3})	Correlation	BF	NME
Reference	10.92				
Run 1	9.06	4.68	0.71	1.26	0.31
Run 2	9.30	4.42	0.74	1.21	0.30
Run 3	11.35	6.88	0.51	1.15	0.46

NO$_2$	Sim. mean (µg.m^{-3})	RMSE (µg.m^{-3})	Correlation	BF	NME
Reference	134.07				
Run 1	122.29	37.2	0.82	1.08	0.20
Run 2	125.72	38.05	0.80	1.05	0.21
Run 3	137.48	62.88	0.62	1.06	0.36

O$_3$	Sim. mean (µg.m^{-3})	RMSE (µg.m^{-3})	Correlation	BF	NME
Reference	18.7				
Run 1	18.48	3.74	0.60	1.05	0.17
Run 2	18.41	4.07	0.57	1.06	0.18
Run 3	18.03	3.86	0.61	1.08	0.18

PM$_{10}$	Sim. mean (µg.m^{-3})	RMSE (µg.m^{-3})	Correlation	BF	NME
Reference	136.94				
Run 1	115.83	50.02	0.70	1.22	0.21
Run 2	108.23	59.08	0.59	1.35	0.34
Run 3	120.06	74.66	0.58	1.38	0.44

The RMSEs are significantly reduced when the model simulations take into account urban meteorological effects. Run 1 shows the lowest RMSEs, except for CO (which may due to reasons such as a low estimation of emission around midday, the absence of some stationary emissions in emission database or overprediction of mixing and instability). The correlations are significantly better for Run 1, especially for NO_2, O_3 and PM_{10}; they are all above 60%.

The bias factors are close to one but greater than one. The bias is less than 10% bias for NO_2 and O_3. It means that the model overall underestimates the level of mean concentration values. It is probable, that this underestimation is due to the absence of some stationary emissions. Normalized mean errors are lower for all considered pollutants in Run 1 and 2 than in Run 3.

These statistics show that accounting for urban effects in meteorological simulations can be very useful for increasing the accuracy of chemical transport modeling in this region.

The spatial distribution of CO, NO_2 and PM_{10} is presented with different meteorology in Figure 4.5 to Figure 4.10. They show the concentrations simulated by POLYPHEMUS at 10 and 120 m AGL, at 10 am and 10 pm. The chosen times (10 am, 10 pm) are about 3 hours after the traffic emission peak in the morning and evening, respectively.

Run 3 shows more transport of pollutants from downtown to north east and north west than other simulations at 10 am and lower concentration in downtown, due to the presence of a high-elevated slope in the north and the overestimation of the speed of anabatic winds, as well as an early starting time of the wind flow. The patterns of CO and PM_{10} concentrations are similar, because both of them are primary pollutants. In comparison, Run 2 and 3 show smaller values at 120 m level due to greater vertical diffusion and recirculation processes.

At 10 pm, Run 3 shows more transport of pollutants from downtown to south east because of the overestimation of the speed of katabatic winds and earlier starting time of this regime. At 120 m level, Run 3 shows lower concentrations due to a more stable PBL and strong horizontal advection at lower levels.

These results suggest that the meteorology of the DA approach concentrate more pollutants in downtown and does not favor long-range transport, but causes more vertical diffusion.
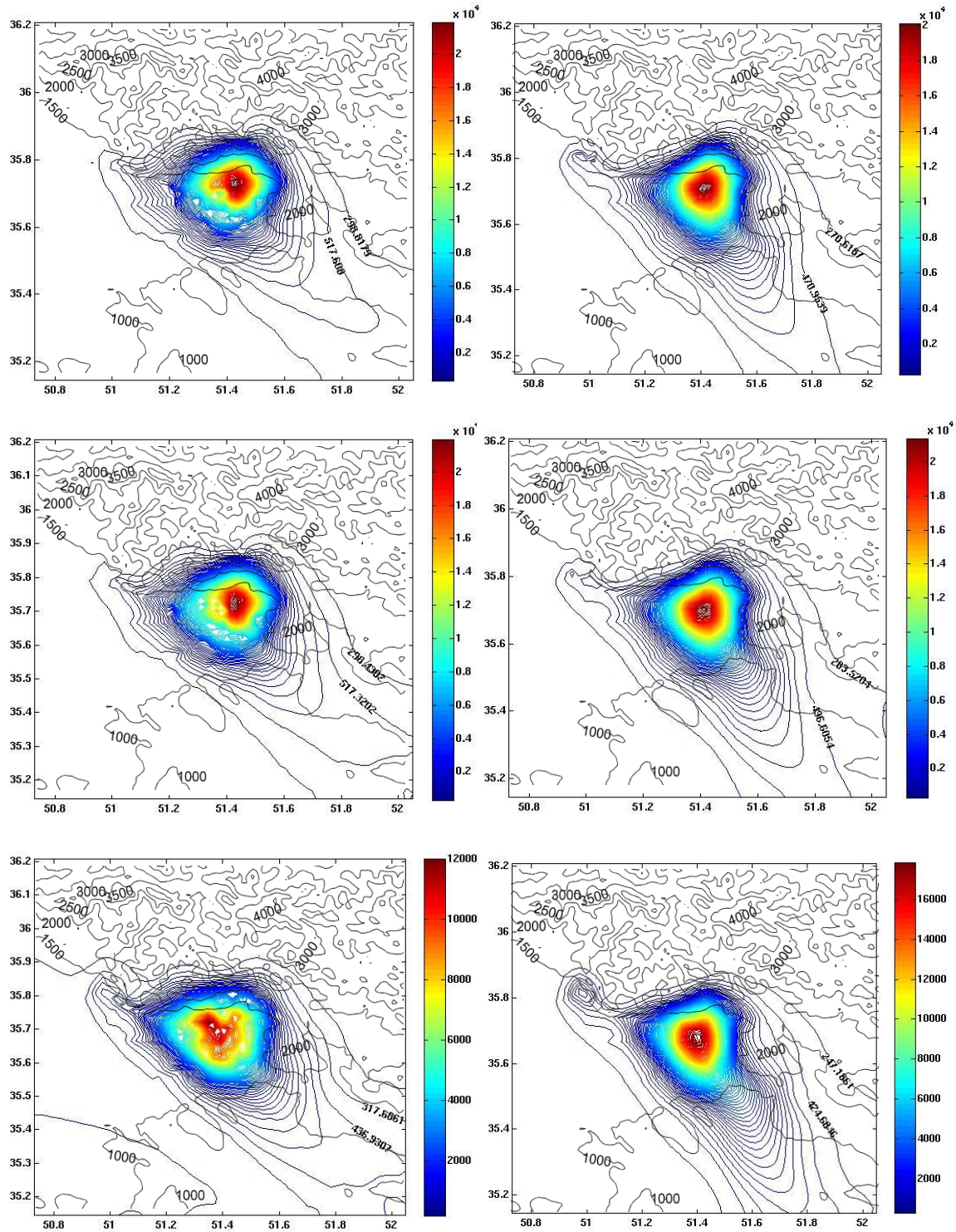
Figure 4.5: CO concentration ($\mu g.m^{-3}$) simulated by Polyphemus with meteorological fields simulated by DA-SM2-U Q_f: on (Run 1: top), DA-SM2-U Q_f: off (Run 2: middle) and RA-SLAB (Run 3: bottom) at 10 m AGL, at 10 am (left) and 10 pm (right) December 6 2005.

Figure 4.6: As in Figure 4.5, but at 120 m AGL.

Figure 4.7 : NO$_2$ concentration (μg.m^{-3}) simulated by P$_{OLYPHEMUS}$ with meteorological fields simulated by DA-SM2-U Q$_f$: on (Run 1: top), DA-SM2-U Q$_f$: off (Run 2: middle) and RA-SLAB (Run 3: bottom) at 10 m AGL, at 10 am (left) and 10 pm (right) December 6 2005.
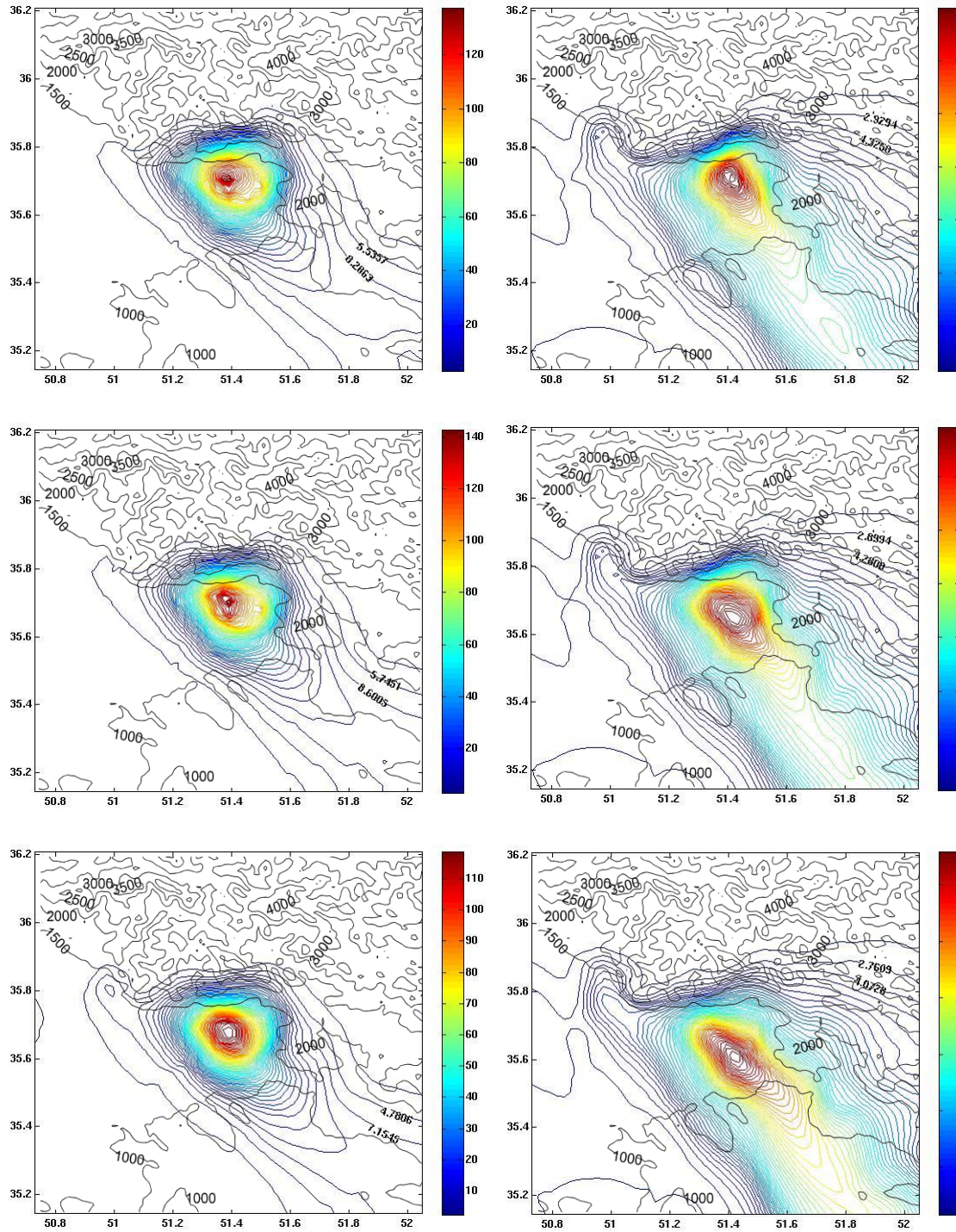
Figure 4.8: As in Figure 4.7, but at 120 m AGL.
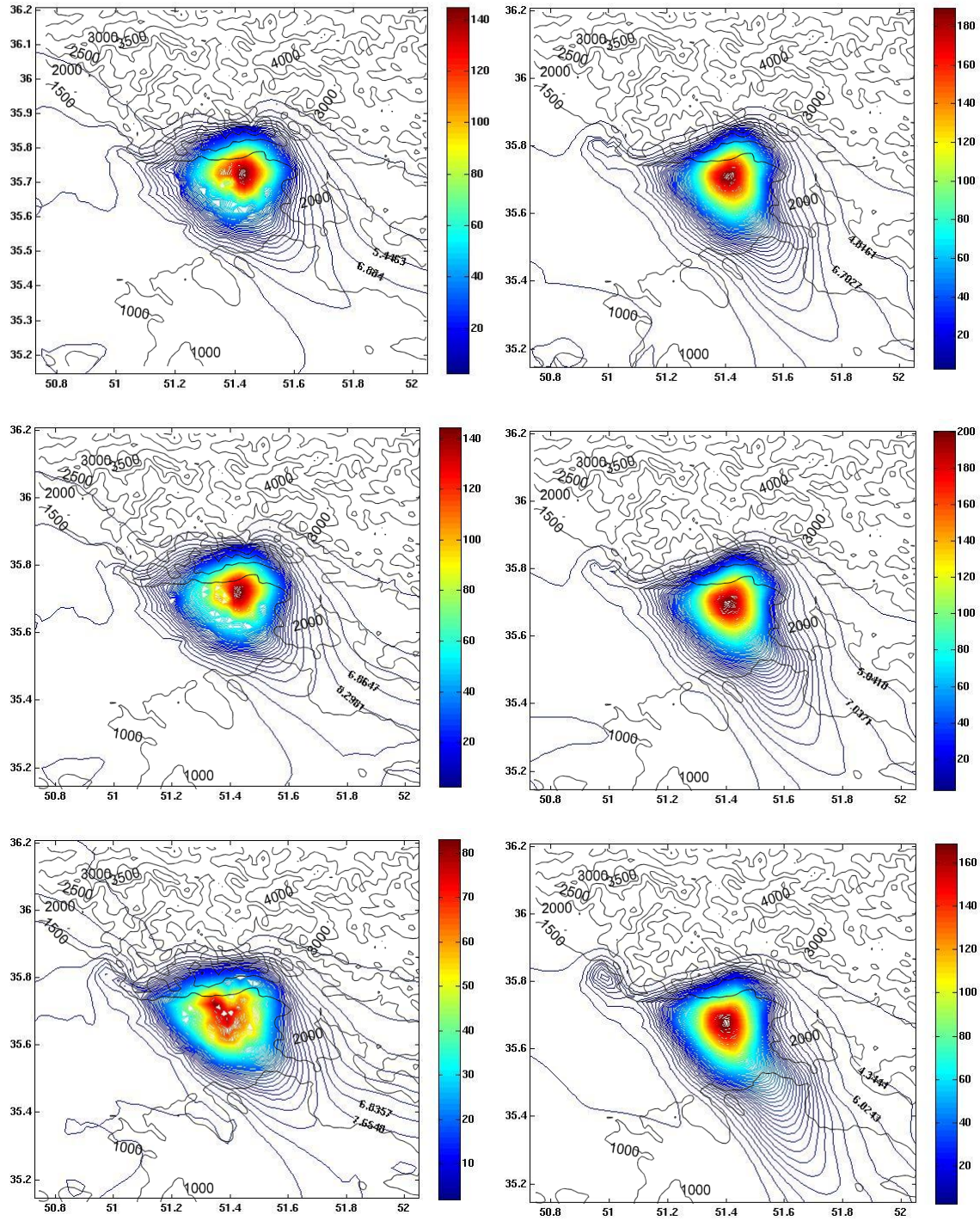
Figure 4.9: PM$_{10}$ concentration (μg.m^{-3}) simulated by P\textsc{olyphemus} with meteorological fields simulated by DA-SM2-U Q$_f$: on (Run 1: top), DA-SM2-U Q$_f$: off (Run 2: middle) and RA-SLAB (Run 3: bottom) at 10 m AGL, at 10 am (left) and 10 pm (right) December 6 2005.
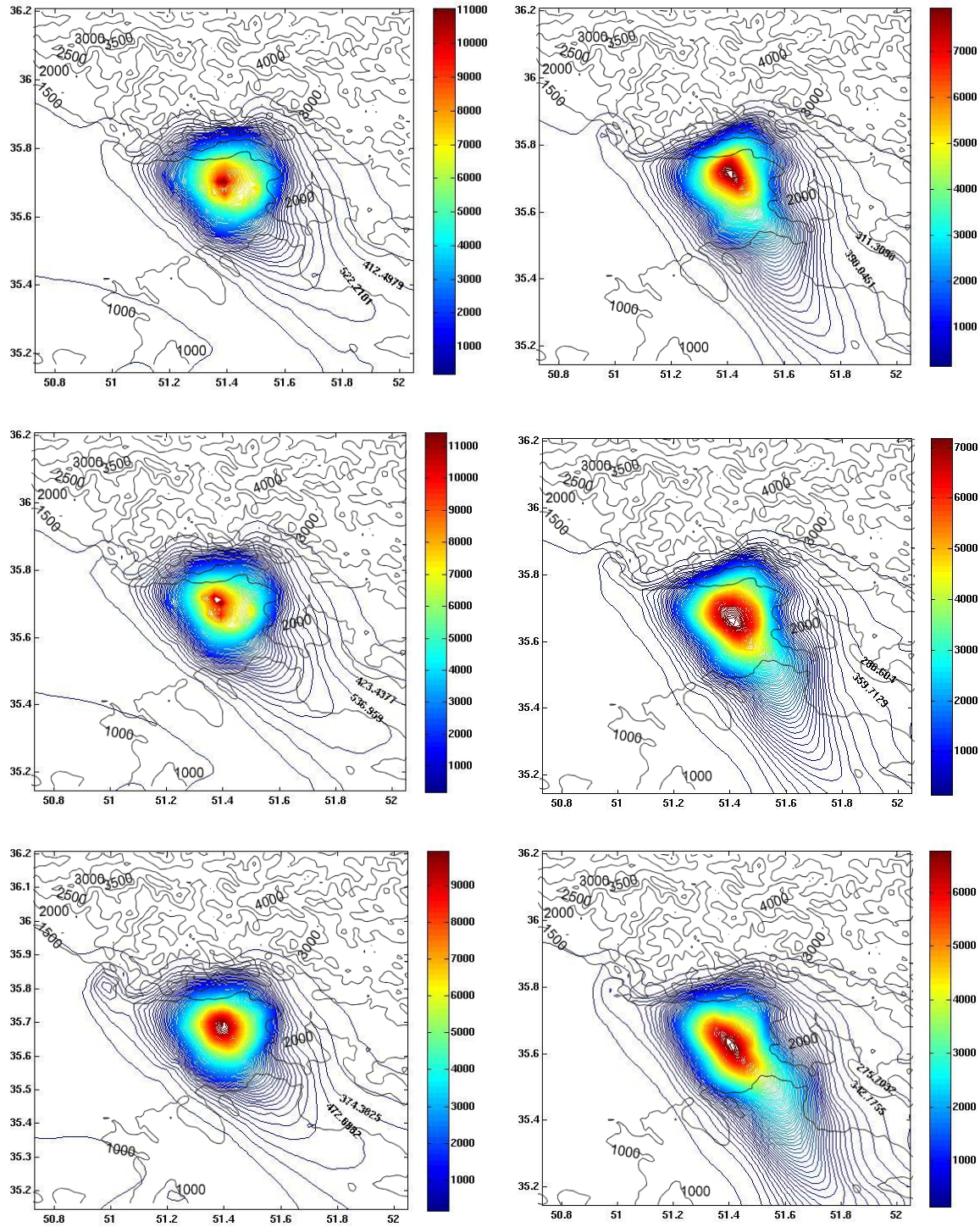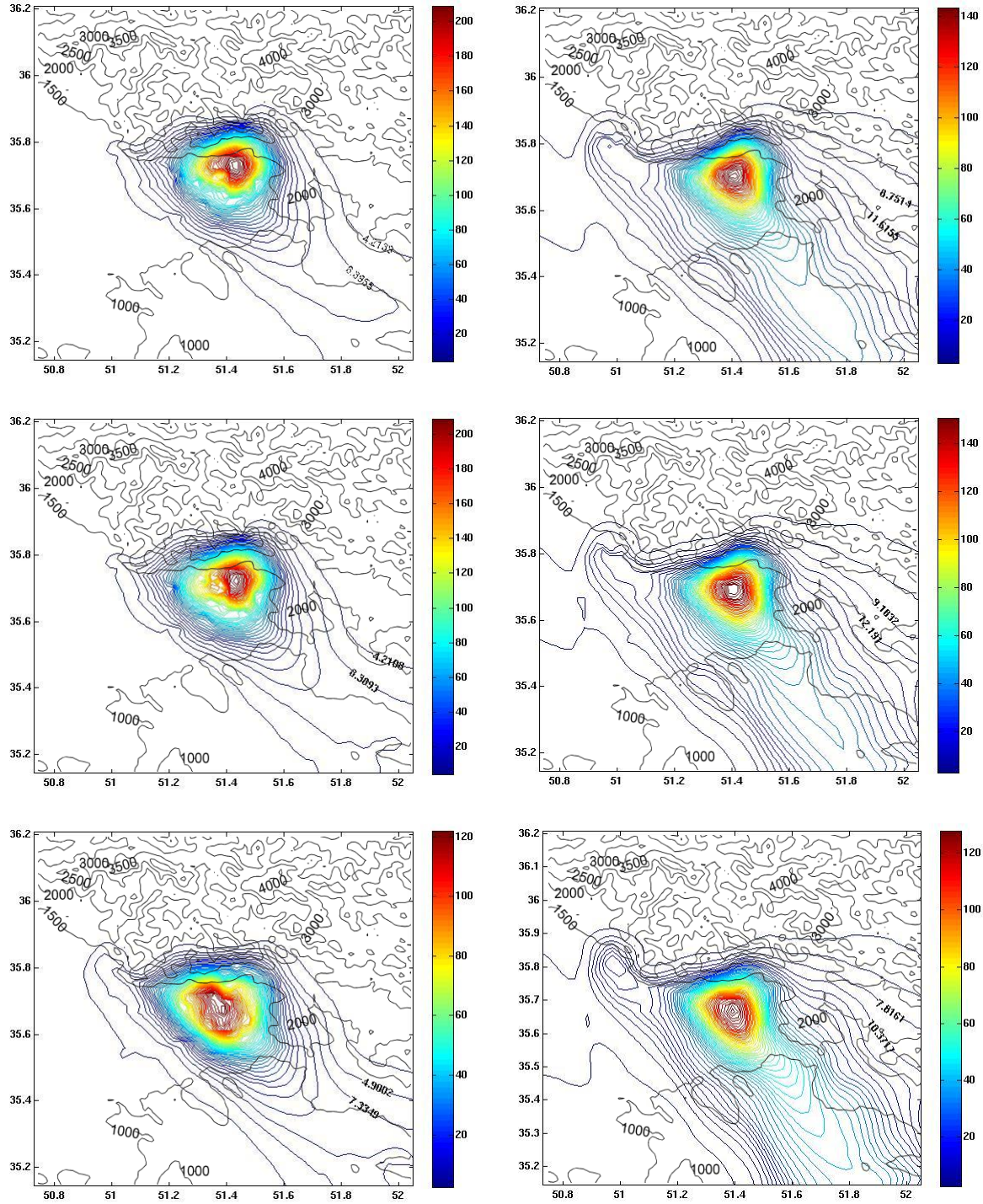
Figure 4.10: As in Figure 4.9, but at 120 m AGL.

Figure 4.11 : O_3 concentration ($\mu g.m^{-3}$) simulated by Pᴏʟʏᴘʜᴇᴍᴜꜱ with meteorological fields simulated by DA-SM2-U Q_f: on (Run 1: top), DA-SM2-U Q_f: off (Run 2: middle) and RA-SLAB (Run 3: bottom) at 10 m AGL, at 12 midday December 6 2005.

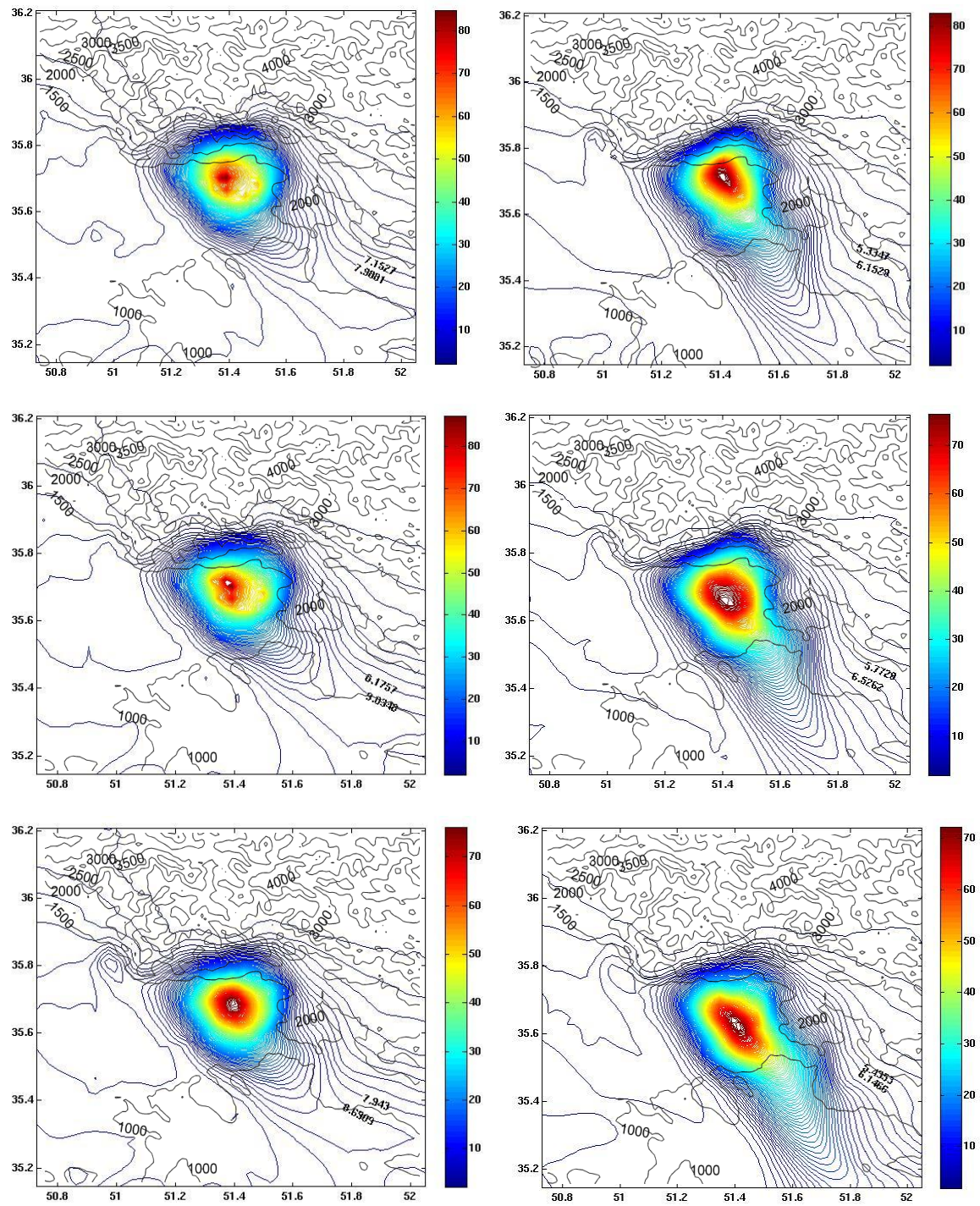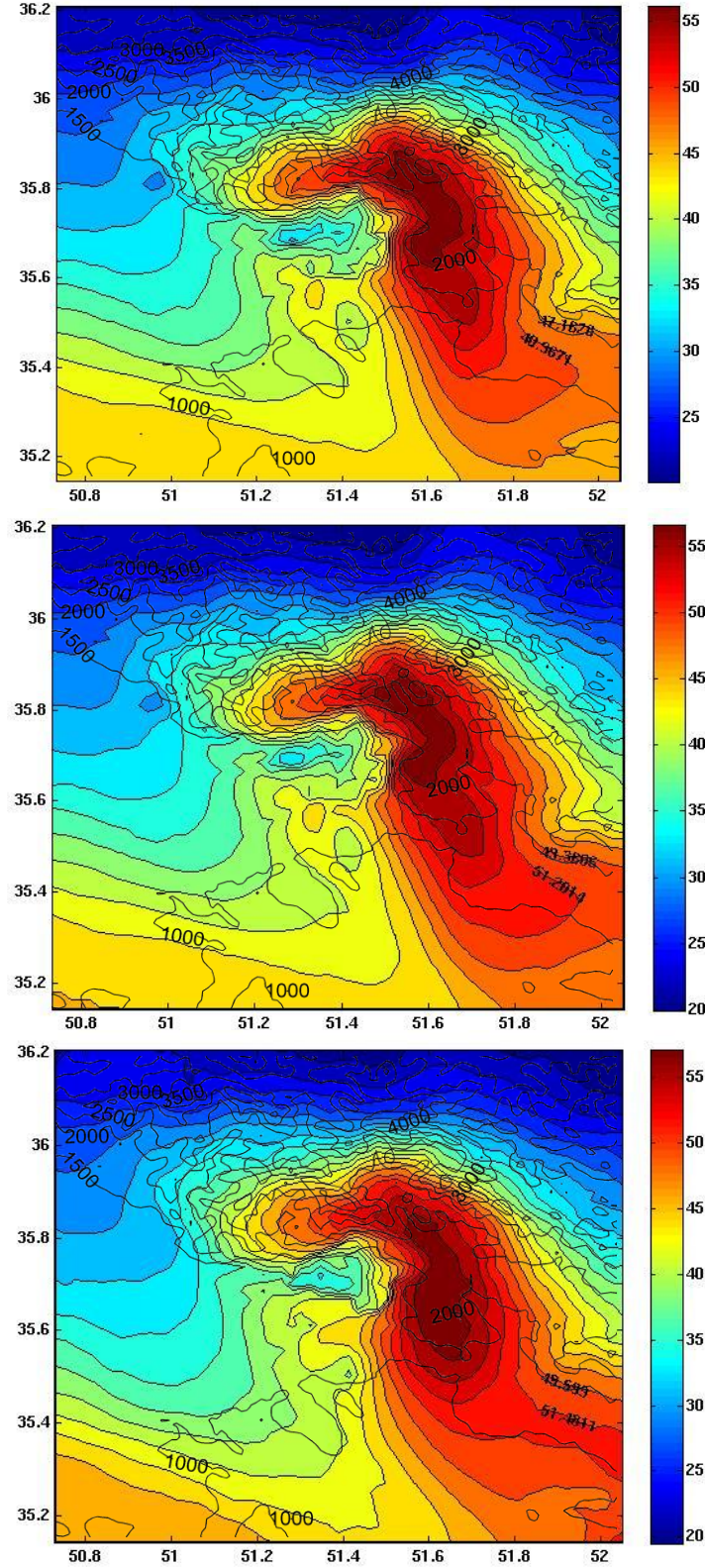The O_3 patterns at midday are presented in Figure 4.11. The O_3 peak is observed   at midday. The O3 plume is located on the north, east and south east of city. The area covered by the O_3 plume is larger in Run 3 than in Run 1 and 2, due to more transport of NO_2 and NMVOCs.

4.4 Conclusions

A preliminary simulation of a high-pollution episode over Tehran region including model-to-data comparisons was presented. The urban parameterization in the meteorological model strongly affects the results of the CTM model. A sensitivity analysis was performed to assess the sensitivity of the model outputs to the meteorological inputs.

The sensitivity analysis shows that in this area, meteorological simulations with detailed urban parameterization lead to improved CTM modeling.

A larger period of simulation (e.g. one year) is recommended to obtain better understanding of the sensitivities of air pollutant concentrations to meteorological inputs over various seasons and atmospheric conditions.

References

Bornstein, R. D., P. Thunis, and G. Schayes, 1993. Simulation of urban barrier effects on polluted urban boundary layers using three-dimensional URBMET/TVM model with urban topography. New results from NYC. Air Pollution, P. Zannetti et al., Eds., Computational Mechanics Publications, 15–34.

Chin, M., Rood, R., Lin, S.-J., Muller, J.F., Thompson, A.M., 2000. Atmospheric sulfur cycle in the global model GOCART: Model description and global properties. Journal of Geophysical Research 105 (D24, 671-24), 189–200.

Debry, E., Fahey, K., Sartelet, K., Sportisse, B., and Tombette, M., 2007. Technical Note: A new SIze REsolved Aerosol Model (SIREAM), Atmospheric Chemistry and Physics 7, 1537–1547.

Debry, E., Sportisse, B., 2006a. Reduction of the condensation/evaporation dynamics for atmospheric aerosols: theoretical and numerical investigation of hybrid methods. Journal of Aerosol Science 37, 950–966.

Debry, E., Sportisse, B., 2006b. Solving aerosol coagulation with size binning methods. Applied Numerical Mathematics 57, 1008-1020.

Fahey, K.M., Pandis, S.N., 2001. Optimizing model performance: variable size resolution in cloud chemistry modeling. Atmospheric Environment 35, 4471–4478.

Hauglustaine, D.A., Hourdin, F., Jourdain, Filiberti, L., Walters, S., J.-F. Lamarque and E.A. Holland, 2004. Interactive chemistry in the Laboratoire de Météorologie Dynamique general circulation model: Description and background tropospheric chemistry evaluation. Journal of Geophysical Research 109, D04314, doi:10.1029/2003JD003957.

Horrowith, L., Walters, S., Mauzerall, D.L., Rash, P.J., Granier, C., Tie, X., Lamarque, J.F., Schultz, M.G., Tyndall, G.S., Orlando, J.J., Brasseur, G.P., 2003. A global simulation of tropospheric ozone and related tracers: Description and evaluation of MOZART, Version 2. Journal of Geophysical Research 108 (D24, 4794).

Jacob, D., 2000. Heterogeneous chemistry and tropospheric ozone. Atmospheric Environment 34, 2131–2159.

Koo, B., Gaydos, T.M., Pandis, S.N., 2003. Evaluation of the equilibrium dynamic, and hybrid aerosol modeling approaches. Aerosol Science and Technology 37, 53–64.

Louis, J.-F. (1979). A parametric model of vertical eddy fluxes in the atmosphere. Boundary-Layer Meteorology 17, 187–202.

Mallet, V., Sportisse, B., 2005. A comprehensive study of ozone sensitivity with respect to emissions over Europe with a chemistry-transport model. Journal of Geophysical Research 110 (D22).

Mallet, V., Sportisse, B., 2006a. Ensemble-based air quality forecasts: a multi-model approach applied to ozone. Journal of Geophysical Research 111 (D18), 18302.

Mallet, V., Sportisse, B., 2006b. Uncertainty in a chemistrytransport model due to physical parametrizations and numerical approximations: an ensemble approach applied to ozone modeling. Journal of Geophysical Research 111 (D24310).

Martilli, A., Clappier, A., and Rotach, M.W., 2002. An urban surface exchange parameterization for mesoscale models. Boundary-Layer Meteorology 104, 261–304.

Napari, I., Noppel, M., Vehkamäki, H., Kulmala, M., 2002. Parametrization of ternary nucleation rates for H2SO4–NH3–H2O vapors. Journal of Geophysical Research 107 (D19).

Nenes, A., Pandis, S., Pilinis, C., 1998. Isorropia: a new thermodynamic equilibrium model for multiphase multicomponent inorganic aerosols. Aquatic Geochemical 4, 123–152.

Oke TR (1995) The heat island of the urban boundary layer: characteristics, causes and effects. In: Cermak JE, Davenport AG, Plate EJ, Viegas DX (eds) Wind Climate in Cities. NATO ASI Series E: Applied Sciences – Vol. 277, Boston: Kluwer Academic Publishers, pp 81–108.

Roselle, S., Schere, K., Pleim, J., 1999. Photolysis rates for CMAQ. Technical Report, U.S. Environmental Protection Agency, EPA/600/R-99/030 (Chapter 14).

Saitoh, T. S., T. Shimada, and H. Hoshi, 1996. Modeling and simulation of the Tokio urban heat island. Atmospheric Environment 30, 4131–3442.

Sartelet, K.N., Debry, E., Fahey, K.M., Roustan, Y., Tombette, M., Sportisse, B., 2007. Simulation of aerosols and related species over Europe with the Polyphemus system. Part I: model-to-data comparison for 2001. Atmospheric Environment, 41, 6116–6131.

Sartelet, K.N., Hayami, H., Albriet, B., Sportisse, B., 2005. Development and preliminary validation of a modal aerosol model for tropospheric chemistry: MAM. Aerosol Science and Technology 40 , 118–127.

Sartelet, K.N., Hayami, H., Sportisse, B., 2008. MICS Asia Phase II—Sensitivity to the aerosol module. Atmospheric Environment 42, 3562–3570.

Schell, B., Ackermann, I.J., Haas, H., 2001. Modeling the formation of secondary organic aerosol within a comprehensive air quality model system. Journal of Geophysical Research 106 (D22), 28,275–28,293.

Seigneur, C., 2001. Current status of air quality models for particulate matter. Journal of Air & Waste Management Association 51, 1508–1521.

Seinfeld, J.H., Pandis, S.N., 1998. Atmospheric Chemistry And Physics. Wiley-Interscience, New York.

Simpson, D., Winiwarter, W., Brjesson, G., Cinderby, S., Ferreiro, A., Guenther, A., Hewitt, C., Janson, R., Khalil, M., Owen, S., Pierce, T., Puxbaum, H., Shearer, M., Skiba, U., Steinbrecher, R., Tarrason, L., Oquist, M., 1999.Inventorying emissions from nature in Europe. Journal of Geophysical Research 104 (D7), 8113–8152.

Sportisse, B., Dubois, L., 2002. Numerical and theoretical investigation of a simplified model for the parameterization of below-cloud scavenging by falling raindrops. Atmospheric Environment 36, 5719–5727.

Sportisse, B., Sartelet, K., Debry, E., Fahey, K., Roustan, Y., Tombette, M., Albriet, B., Foudhil, H., 2006. Report of the PAM project (Multiphase Air Pollution). Modeling. Technical Report 2006-8, CEREA—ENPC.

Stockwell, W., Kirchner, F., Kuhn, M., 1997. A new mechanism for regional chemistry modeling. Journal of Geophysical Research 102 (D22),847–25,879.

Tombette, M. and Sportisse, B. (2007). Aerosol modeling at regional scale: Model-to-data com-comparison and sensitivity analysis over Greater Paris. Atmospheric Environment 41, 6941-6950.

Troen, I.B., Mahrt, L., 1986. A simple model of the atmospheric boundary layer; sensitivity to surface evaporation. Boundary-Layer Meteorology 37, 129–148.

Vehkamäki, H., Kulmala, M., Napari, I., Lehtinen, K., Timmrek, C., Noppel, M., Laaksonen, A., 2002. An improved parametrization for sulfuric acid-water

nucleation rates for tropospheric and stratospheric conditions. Journal of Geophysical Research 107 (D22) (doi:10.1029/2002JD002184).

Wesely, M.L., 1989. Parameterization of surface resistances to gaseous dry deposition in regional-scale numerical models. Atmospheric Environment 23, 1293-1304.

Zhang, L., Gong, S., Padro, J., Barrie, L., 2001. A sizeseggregated particle dry deposition scheme for an atmospheric aerosol module. Atmospheric Environment 35, 549–560.

Zhang, L., Moran, M. D., Makar, P. A., Brook, J. R., and Gong, S., 2002. Modelling gaseous dry deposition in AURAMS: a unified regional air-quality modelling system. Atmospheric Environment 36, 537–560.

Zhang, L., Brook, J., Vet, R., 2003. A revised parameterization for gaseous dry deposition in air-quality models. Atmospheric Chemistry and Physics Discussions 3, 2067–2082.

CHAPTER FIVE

Conclusions
and
Perspectives

This work was devoted to the investigation of the anthropogenic air pollutant emissions, heat emission, meteorology (including urbanization effects) and air quality (including sensitivity of air quality dispersion patterns to urban meteorological parameterizations) in the Tehran region. The analysis presented was based on the study of an air pollution episode which took place in this region on 5 - 9 December 2005. These results may be considered as a starting point for a better understanding of the local terrain and urban effects on the atmosphere in this region, and they provide a new opportunity to improve air quality through a scientifically-based approach. This chapter presents the general conclusions of this thesis. Future aspects are also discussed and some directions are suggested to enter in more details in each part of this work.

The first step to act on air pollution and its mitigation consists in accurately quantifying the amounts of pollutants released to the atmosphere. An emission inventory of air pollutants and an inventory of heat generation were developed and updated for 2005 in this work using available database (chapter 2). The mobile source emission inventory was investigated in greater detail and it can be considered more satisfactory than the inventory of stationary emissions. Emissions from on-road motor vehicles are a major portion of the emission inventory and play the most important role in terms of contributions of air pollutants to the atmosphere in Tehran. The contribution of vehicles categories changes rapidly, due to replacing old cars with new cars, therefore, it was necessary to update the car fleet and corresponding emission factors; such updates will need to be conducted at least every year. For the stationary emission inventory, only emissions from larger industries, power plants and the Tehran refinery were estimated. Unfortunately, this aspect of emission inventory is

not resolved, because it has not been well studied by the responsible agencies in Tehran until recently. Another aspect that can influence the accuracy of air quality modeling in this area is the absence of a reliable continental emission inventory in order to model air quality at the continental scale. In order to improve future modeling results, we strongly suggests, that new versions of the emission inventory should cover a larger area (including at least northern Iran) and include other stationary sources, which have not yet been taken into account.

Furthermore, data assimilation techniques are recommended in order to improve and optimize the emission rates, especially at continental scale. Such an approach seems necessary, because there are some uncertainties associated with the statistics, emission factors, temporal allocation profiles, and grid allocation factors used in bottom-up emission inventories.

The inventory of heat generation in Tehran region was investigated and it found that wintertime Q_f is larger than summertime Q_f, which reflected the importance of heating emissions from buildings and traffic during cold and warm period respectively.

The second part of this thesis addresses high resolution meteorological modeling over the region of Tehran (Chapter 3). The validation of meteorological simulations is very important in order to minimize errors originating from meteorological variables in the air quality modeling, which includes transport, diffusion and in production of secondary chemical species. Therefore, this part was investigated in a comprehensive manner.

The influence of building drag and anthropogenic heating on the meteorology of the Tehran mega-city (TMC) was particularly significant. The dominant influences on the structure of the planetary boundary layer (PBL) in these meteorological simulations in the Tehran basin were found to be the Alborz range (including valleys that enter this basin) and urbanization effects.

During weak synoptic forcing periods, the area located north and north-east of Tehran was strongly affected by mountain and valley winds, but the area west and south showed lower frequency of topographic flows. The observations generally showed weak and variable winds with complex circulation patterns and also semi-periodic oscillations during both night and day with periods typically longer than 40 minutes that could be attributed to internal waves induced by drainage flows at night and instability of the upslope flow during the day. The observed vertical profiles of temperature and wind observations showed some discontinuity originating from local

circulations. The anabatic flow was found to be thicker but with lower headwinds aloft. The morning and evening transitions were characterized by low speed and highly variable winds. Layers of different temperature and wind speed/direction characterize the vertical structure of the flow. The formation of such layers in TMC may occur due to different air masses of disparate densities originating at slopes of different orientations surrounding the air basin.

Next, the mesoscale model with different urban parameterizations, was used as a tool to investigate the modifications induced by the presence of an urban area on the PBL structure in the area of interest. It was found that the drag-force approach coupled with an urban soil model (DA-SM2-U) is preferable to the roughness approach (RA-SLAB), for local meteorological simulations. The comparisons among three configurations of the mesoscale model indicated that the most important features of the wind, temperature and turbulent fields in urban areas are well reproduced by the DA-SM2-U configuration with the anthropogenic heat flux being take into account (DA-SM2-U Q_f: On). The potential air temperature vertical profiles in the urban area showed a reduction in the tendency toward stable stratification. Within the urban canopy, the DA-SM2-U meteorological fields seem well simulated and they follow the canopy morphology with a decrease of the wind speed inside the dense canopy, skirting of the flow around the canopy blocks and warmer air inside the urban canopy, especially during the night. The urban heat island patterns simulated by this configuration were found to be strong that include more forcing on topographic flows. The turbulent mixing was generally under-estimated by the RA-SLAB configuration inside the canopy because of the limitation of K-theory. The DA-SM2-U configuration is capable of generating the turbulent kinetic energy budget component, turbulent length and eddy diffusivity with a better representation in the urban canopy and roughness sub-layer. These prognostic variables for atmospheric and air quality modeling are important because they control the vertical mixing of meteorological and pollutant quantities.

A PBL depth analysis showed that the urban canopy parameterization plays a very important role in determining the boundary layer depth. In the RA-SLAB configuration, the PBL rapidly collapsed shortly after reaching its peak value, and in the urban core, it was generally 100 –300 m smaller than those simulations with the "DA-SM2-U Q_f: On" configuration during night and day, respectively.

Tehran's wind pattern is not only influenced by the physiographic of the plateau and surrounding mountains, but also by urban roughness-drag and buoyancy forces along with the topographic flows. The run with the "DA-SM2-U Q_f: On" configuration indicated that interaction between the urban heat island and the topography is complex and can play a significant role in the atmospheric circulations observed over the Tehran basin. The comparison between " DA-SM2-U Q_f: Off" and "RA-SLAB Q_f: Off" simulations in the city showed that the presence of urban canopy effects reduces the intensity of the katabatic regime. Consequently, the katabatic regime can not be dominant in whole of Tehran city. The anabatic regime of " DA-SM2-U Q_f: Off" configuration showed lower intensity too. During the day, the wind fields simulated by RA-SLAB showed subsidence in higher altitudes of the city area near the ground in south rural part of Tehran. The DA-SM2-U wind fields showed some subsidence in lower altitudes in the city area and near ground in the south sub-urban part of Tehran. During the night, wind fields simulated by the " DA-SM2-U Q_f: On" configuration, generated some heat island circulation, forming warm plumes downwind during the katabatic regime from north and synoptic winds from west and south west.

The comparisons and validation demonstrated that a new configuration of the mesoscale model used here is a clear improvement as compared to default methods generally used to represent urban surfaces in mesoscale models. Nevertheless, several points will require more attention in the future. In order to continue to improve modeling results and to develop a better understanding of the local meteorology, we strongly recommended the following points:

-Performing standard intensive meteorological field campaigns over Tehran
From these experiments, one will expect to obtain valuable information about local winds, urban heat island effects, and the turbulent structure both of the Urban Roughness Sub-layer and of the entire Planetary Boundary Layer with a more complete space and time coverage than available for this study. Such data are necessary in order to conducted future validation of urban simulations and develop improved parameterizations and model configuration.

-Detailed analyses of landuse and surface
The detailed urban parameterizations require accurate information about surface characteristics (roughness length, albedo, emissivity, thermal conductivity, volumetric

heat capacity, etc), urban and vegetation canopy morphology (height, plane area density, frontal area density, etc). Coupling satellite images processing and local observations can lead us to a high resolution dynamic database that would be extremely useful for the purpose of detailed urban parameterizations.

-Performing long term simulations

The episode investigated in this study represents a common critical situation, which can occur during the fall and winter in Tehran. A study of long term simulations can be very useful for investigating the interaction between different forcing effects on local meteorology as they evaluate with seasonal validations.

-Impact of land cover change

The implications of land cover change on atmospheric processes depend on the nature of the change and the climatic context in which it occurs. Sensitivity studies, in which the effects of various land cover scenarios on boundary layer development will be compared, should be conducted. One anticipates that the results will show grater urbanization and agricultural development effects in the Tehran area and due to local terrain and mesoscale effects greater along the Tehran basin.

-Application of Building Energy Models (BEM)

The coupling of a Building Energy Model (BEM) with the Urban Canopy parameterization (UCP) in mesoscales model is another tool that takes into account the diffusion of heat through walls, roofs, and floors, the natural ventilation, the generation of heat from occupants and equipments, and the consumption of energy through air conditioning systems. BEM is able to accurately simulate the basic heat transfer phenomena, and to reproduce the heat fluxes exchanged between buildings and the atmosphere with more details. This approach should be compare with the one presented here under the same condition.

-Anthropogenic heat comparison

The anthropogenic heat flux estimated from emission inventories should be compared with values estimated from experiments. An experimental method based on the residual term of the SEB equation (Surface energy balance) at the local scale around measurement sites could be use to provide such observations of heat flux.

-Effect of Tehran plume on local meteorology

Exceptionally high values of aerosol optical depth can be observed during high polluted episodes in mega-cities. Radiative transfer modules that take into account aerosol particles effects on the atmospheric energy budget can be used to drive a dynamic model of the PBL. During high polluted episodes, the height of the PBL can significantly decrease due to the warming of the aerosol particles inside the PBL , which creates a stabilizing effect within the PBL. It will be interesting to evaluate, by means of a radiation transfer model, the impact of the presence of aerosol on the radiation and consequently, on the PBL evolution and the urban energy budget.

The final part of study was dedicated to high resolution chemical transport modeling (CTM) (Chapter 4). In this part, the numerical CTM was used to investigate the impact of the different urban parameterization on the dispersion of pollutants over the Tehran region. Results show that applying DA approaches lead to significant improvement in simulated spatial and temporal distribution of pollutant concentrations in the city area and on the size of the urban plumes.

The "DA-SM2-U Q_f: On" configuration for meteorological inputs caused more vertical diffusion and less transport of pollutants. The RA approach for meteorological input overestimated morning peak concentrations and also predicted peak earlier than observation, especially in downtown. These results are due to more PBL stability in this meteorological simulation and more advection from the northern part of the city by a katabatic regime. This phenomenon occurred for evening peaks too. During night, recirculation processes induced by urban heat island circulation and sub-circulation caused more persistence of pollution over Tehran. As a general result, the presence of the city enhances the transport of pollutants to rural area through a reservoir layer aloft and recirculation processes.

In order to improve chemical transport modeling over Tehran, several aspects need to be improved over Tehran region. In order to improve modeling results and our understanding of air quality in Tehran, we strongly recommend the following points:

-Improvement of the air quality observation network

The air pollution monitoring system has to have a significant development, for assessing local, regional and global concentrations of ground air pollutants. Recently, the Tehran observation network was augmented with new stations (16 active stations), but the spatial distribution is not sufficient to study the validation of the interactions

between the scale of the city and the mesoscale in order to have a complete understanding of the processes governing the dispersion and transport of the primary pollutants emitted in the city, and the secondary pollutants (like ozone) formed on mesoscale. Another problem is network maintenance and data validity, because some stations are maintained by DoE (Department of the environment) team and others by AQCC (Air quality control company). This leads to difference in the observations because of the difference maintenance and also difference in technology of stations. Therefore, we recommend that a harmonization of the network be conducted with identical monitoring protocols being used at all stations.

-Improvement of emission inventory and module for generating 4D emissions

Air quality models need detailed information about emissions in the area studied. Even when a box model is applied (i.e., without considering spatial features of the emissions), the hourly time profile is required for all pollutants. In addition, information on particulate matter size spectrum and chemical composition of the emission are necessary, when dealing with PM and ozone modeling. For example, suitable speciation profiles of emitted volatile organic compounds (VOCs) is a requirement for modeling photochemical processes in the atmosphere. Therefore, information on chemical speciation and PM size fractions of selected sectors and sub-sectors in the Tehran area are essential to improve air quality of Tehran mega-city.

-Model development and optimized configuration

Several sensitivity analyses should be conducted in order to develop optimized configuration for chemical transport modeling over Tehran.

Two points that should be investigated are analyses of different vertical turbulence parameterization schemes and algorithms accounting for building volumes within the canopy layer.

-Performing long term simulations

The episode investigated in this study represents a critical situation, which can occur during fall and winter in Tehran. Long term simulations would be very useful for investigating the interactions between the scale of the city and the mesoscale. Such simulations will allow us to better understand the dispersion of the primary pollutants

and the formation of secondary pollutants during different meteorological conditions throughout the year.

-Testing of emission reduction strategies

Air quality modeling can be a very useful tool for evaluating emission scenarios in future years and prioritizing actions to mitigate pollution in Tehran. Various emissions scenarios can be implemented within Tehran, such as in the on-road vehicle fleet, the quality of the fuel, industrial sources, etc. Additionally, abatement strategies should be examined under different meteorological conditions in order to formulate definitive conclusions.